Computed Tomography elucidates ontogeny within the basal therapsid clade Biarmosuchia

Aliénor Duhamel [Corresp., 1, 2, 3], **Julien Benoit** [2], **Michael Day** [2, 4], **Bruce Rubidge** [2], **Vincent Fernandez** [4, 5]

[1] ENS de Lyon, CNRS UMR 5276 LGL-TPE, Université Claude Bernard (Lyon I), Villeurbanne, France

[2] Evolutionary Studies Institute, University of the Witwatersrand, Johannesburg, South Africa

[3] School of Geosciences, University of Witwatersrand, Johannesburg, South Africa

[4] Department of Earth Sciences, Natural History Museum, London, United Kingdom

[5] European Synchrotron Radiation Facility, Grenoble, France

Corresponding Author: Aliénor Duhamel
Email address: alienor.duhamel@ens-lyon.org

Biarmosuchia is a clade of basal therapsids that includes forms possessing plesiomorphic 'pelycosaurian' cranial characters as well as the highly derived Burnetiamorpha which are characterised by cranial pachyostosis and a variety of cranial bosses. Potential ontogenetic variation in these structures has been suggested based on growth series of other therapsids with pachyostosed crania, which complicates burnetiamorph taxonomic distinction and thus it is essential to better understand cranial ontogeny of the Burnetiamorpha. Here, three new juvenile biarmosuchian skulls from the late Permian of South Africa are described using X-ray micro computed tomography (CT tomography). We found that juvenile biarmosuchians are distinguished from adults by their relatively large orbits, open cranial sutures, and incomplete ossification of the braincase and bony labyrinth. Also, they manifest multiple centres of ossification within the parietal and preparietal bones. CT examination reveals that the holotype of *Lemurosaurus pricei* (BP/1/816), previously alleged to be a juvenile, shows no evidence of juvenility and is thus probably an adult. This suggests that the larger skull NMQR 1702, previously considered to be an adult *L. pricei,* may represent a new taxon. This study provides, for the first time, a list of characters by which to recognise juvenile biarmosuchians.

Computed Tomography elucidates ontogeny within the basal therapsid clade Biarmosuchia.

Aliénor Duhamel[1,2,3], Julien Benoit[2], Michael Oliver Day[2,4], Bruce Sidney Rubidge[2], Vincent Fernandez[5,6]

[1]Univ Lyon, Université Lyon 1, ENS de Lyon, CNRS UMR 5276 LGL-TPE, F-69622 Villeurbanne, France.

[2]Evolutionary Studies Institute, University of the Witwatersrand, PO Wits, 2050, Johannesburg, South Africa.

[3]School of Geosciences, University of the Witwatersrand, PO Wits, 2050, Johannesburg, South Africa.

[4]Department of Earth Sciences, Natural History Museum, Cromwell Road, SW7 5BD London, United Kingdom.

[5] Imaging and Analysis Centre, Natural History Museum, Cromwell Road, SW7 5BD London, United Kingdom.

[6]European Synchrotron Radiation Facility, 71 Avenue des Martyrs, 38000, Grenoble, France.

Corresponding author:
Aliénor Duhamel
Evolutionary Studies Institute, University of the Witwatersrand, Johannesburg, Gauteng, 2001, South Africa
Email address: alienor.duhamel@ens-lyon.org

Abstract

Biarmosuchia is a clade of basal therapsids that includes forms possessing plesiomorphic 'pelycosaurian' cranial characters as well as the highly derived Burnetiamorpha which are characterised by cranial pachyostosis and a variety of cranial bosses. Potential ontogenetic variation in these structures has been suggested based on growth series of other therapsids with pachyostosed crania, which complicates burnetiamorph taxonomic distinction and thus it is essential to better understand cranial ontogeny of the Burnetiamorpha. Here, three new juvenile biarmosuchian skulls from the late Permian of South Africa are described using X-ray micro computed tomography (CT). We found that juvenile biarmosuchians are distinguished from adults by their relatively large orbits, open cranial sutures, and incomplete ossification of the braincase and bony labyrinth. Also, they manifest multiple centres of ossification within the parietal and preparietal bones. CT examination reveals that the holotype of *Lemurosaurus pricei* (BP/1/816), previously alleged to be a juvenile, shows no evidence of juvenility and is thus probably an adult. This suggests that the larger skull NMQR 1702, previously considered to be an adult *L. pricei,* may represent a new taxon. This study provides, for the first time, a list of characters by which to recognise juvenile biarmosuchians.

Introduction

Largely because of the small numbers of complete specimens, the Biarmosuchia is a poorly-understood group of mid-late Permian therapsids in terms of phylogeny, ontogeny, locomotion (paucity of post-crania) and paleobiology (Hopson & Barghusen, 1986; Rubidge & Sidor, 2001; Kemp, 2006). Broom (1913) was the first to describe a member of this clade,

45 *Ictidorhinus martinsi*, from South Africa. Over the past two decades several new biarmosuchian
46 specimens have been described and historical specimens have been re-assessed (Rubidge &
47 Kitching, 2003; Sidor, 2003; Rubidge, Sidor & Modesto, 2006; Sidor & Rubidge, 2006; Kruger
48 et al., 2015; Day, Rubidge & Abdala, 2016; Kammerer, 2016; Benoit et al., 2017b; Day et al.,
49 2018; Kulik & Sidor, 2019), but the systematics of the group remains uncertain as all described
50 genera are monospecific and most species are represented by only one specimen (cranial
51 material). Even though the Biarmosuchia is considered a monophyletic group (Rubidge & Sidor,
52 2001; Liu, Rubidge & Li, 2009; Day et al., 2018), taxonomic diversity and phylogenetic
53 positions of genera are not yet well understood as some published phylogenetic analyses are still
54 contradictory (Day, Rubidge & Abdala, 2016; Kammerer, 2016; Day et al., 2018).
55 Thirty-one biarmosuchian genera have been described, mainly based on cranial material,
56 from different regions of Pangea (Malawi, Zambia, Tanzania, Zimbabwe, and Russia). However,
57 some of these are not considered valid or diagnosable. Twelve valid genera are from the main
58 Karoo Basin of South Africa (Rubidge & Kitching, 2003; Sidor, 2003; Sidor & Welman, 2003;
59 Sidor, Hopson & Keyser, 2004; Rubidge, Sidor & Modesto, 2006; Smith, Rubidge & Sidor,
60 2006; Sidor & Smith, 2007; Kruger et al., 2015; Kammerer, 2016; Day et al., 2018) where they
61 have been recovered from all Permian tetrapod-defined biozones of the Beaufort Group except
62 the *Eodicynodon* Assemblage Zone (AZ) (Day, Rubidge & Abdala, 2016).
63 One of the best-represented biarmosuchian subclades, both in numbers of specimens and
64 quality of preservation, is the Burnetiamorpha. This group includes *Lemurosaurus pricei* as the
65 basal-most taxon (Sidor & Welman, 2003; Sidor & Smith, 2007; Kruger et al., 2015; Kammerer,
66 2016; Kammerer & Sidor, 2021) and the Burnetiidae is the most derived subclade (Rubidge &
67 Kitching, 2003; Sidor, 2003; Sidor & Welman, 2003; Sidor, Hopson & Keyser, 2004; Rubidge,

Sidor & Modesto, 2006; Smith, Rubidge & Sidor, 2006; Sidor & Smith, 2007; Kruger et al., 2015; Kammerer, 2016; Day et al., 2018; Kammerer & Sidor, 2021). Most burnetiamorph genera are represented by a single specimen, which limits understanding of ontogenetic development and sexual dimorphism (Sigogneau, 1970; Sidor & Welman, 2003; Kruger et al., 2015; Kulik & Sidor, 2019).

Previous research on ontogenetic series of some non-biarmosuchian therapsid taxa provided insight on their palaeobiology. Allometric studies have been undertaken on various therapsid groups to evaluate and study ontogenetic patterns (Huttenlocker & Abdala, 2015; Jasinoski, Abdala & Fernandez, 2015; Jasinoski & Abdala, 2017a; Krone, Kammerer & Angielczyk, 2019). Using allometric and multivariate analyses Jasinoski and Abdala (2017a) identified ontogenetic modifications and sexual dimorphism in the cynodont *Galesaurus planiceps* and found that a few craniomandibular features, including the shape of the sutures, change during ontogeny. Moreover, the discovery of juvenile specimens of *Thrinaxodon liorhinus, Galesaurus planiceps*, and *Kayentatherium wellesi* in association with adult individuals enabled research on anatomical features linked to ontogeny and led to the conclusion that both species provided parental care (Jasinoski & Abdala, 2017b; Hoffman & Rowe, 2018, but see Benoit, 2019). Ontogenetic studies on South African and Russian dinocephalians also revealed allometric growth in the length of the skull compared to the diameter of the orbit, and some specimens like *Stenocybus* and *Sinophoneus* are likely to be part of the same ontogenetic series (Ivakhnenko, 2003, 2008; Kammerer, 2011; Kruger, Rubidge & Abdala, 2017). It has also been demonstrated that cranial ornamentation developed during postnatal development in *Biarmosuchus* and several dinocephalians such as *Estemmenosuchus* (Ivakhnenko, 2008). Understanding burnetiamorph cranial ontogenesis would thus possibly provide a path to

understand their elusive palaeobiology.

To investigate biarmosuchian ontogeny we studied two new, apparently juvenile, biarmosuchian specimens (CGS MJF 22 and SAM-PK-K11126), and three already described putative juvenile specimens: the holotype of *Rubidgina angusticeps* (RC 55), *Lende chiweta* (MAL290), the holotype of *Lemurosaurus pricei* (BP/1/816), and a specimen (NMQR 1702) previously considered to represent a more mature specimen of *L. pricei* (Sidor & Welman, 2003). Micro CT was undertaken to determine histological and anatomical clues to characterise ontogenetic stages in this clade. Our results support the non-juvenile status of BP/1/816 and the taxonomic status of *Lemurosaurus pricei* is revised accordingly.

Materials and Methods

The specimens described in this paper were chosen either because they have been described as juveniles, or because they have not yet been described and exhibit characters suggesting that they are juveniles.

New material

CGS MJF 22 is an almost complete skull, collected in 1980 on the farm Amsterdam, in the Victoria West district of the Northern Cape, in strata that appear on the geological map (Geological Survey, 1989) as belonging to the Poortjie Member (presumably the *Lycosuchus-Eunotosaurus* Subzone of the *Endothiodon* AZ) of the Teekloof Formation (Day & Smith, 2020). The biostratigraphic provenance of this specimen remains uncertain as associated material is fragmentary and uninformative, and the lithostratigraphic units as mapped in the Victoria West

112 area are not necessarily consistent with the biostratigraphic relationships established in their type
113 areas (Day & Rubidge, 2019).

114 Specimen SAM-PK-K11126 includes a snout with an almost complete palate, a fragment
115 of the pineal region, a fragment of the occiput around the foramen magnum, and fragments of the
116 lower jaw. Eleven vertebrae (dorsal and sacral) and the pelvis are preserved in articulation. The
117 proximal epiphysis of a femur, one indeterminate long bone diaphysis, and three indeterminate
118 bony fragments are also preserved. Only the cranial material is described here for comparison;
119 the postcranium will be the subject of a future study. Specimen SAM-PK-K11126 was collected
120 in 2012 by Zaituna Skosan on the farm Reiersvlei, in the Beaufort West district of the Western
121 Cape. It was found in the upper part of the Poortjie Member (*Endothiodon* AZ) sensu (Day &
122 Smith, 2020).

123 **Previously-described material**

124 Specimen RC 55 comprises an almost complete skull. It was collected in 1940 by a party
125 lead by Croonie Kitching on the farm Wellwood in the Graaff-Reinet district of the Eastern
126 Cape, from rocks of the Balfour Formation, likely *Cistecephalus* AZ, ~ 256 Ma (Day et al.,
127 2015). It was described by Broom (1942) as the holotype of *Rubidgina angusticeps*, initially
128 considered a gorgonopsian, and later assigned to the "Ictidorhinidae" by Sigogneau (1970). Most
129 recently, RC 55 was identified as a potential juvenile of the non-burnetiamorph biarmosuchian
130 *Herpetoskylax hopsoni* (Sidor & Rubidge, 2006).

131 BP/1/816 is a relatively complete skull and lower jaw, collected in 1948 by James
132 Kitching on the farm Dorsfontein in the Graaff-Reinet district in the lower Balfour Formation
133 (*Cistecephalus* AZ). It was described by Broom (1949), who designated it as the holotype of
134 *Lemurosaurus pricei* and was later part of Sigogneau's (1970) PhD dissertation. *Lemurosaurus*

pricei was also placed among Ictidorhinidae by Sigogneau (1970) but was considered as a possible juvenile burnetiamorph by Sidor & Welman (2003).

Specimen NMQR 1702 is a well-preserved skull and lower jaw collected in 1974 by a team from the National Museum, Bloemfontein, on the farm Petersburg in the Graaff-Reinet district. Although the precise locality of the find is not known and the farm Petersburg straddles the escarpment and a significant stratigraphic thickness, the specimen most likely comes from the lower Balfour Formation (*Cistecephalus* AZ) (Sidor & Welman, 2003). The specimen was described and referred to *L. pricei* by Sidor & Welman (2003).

Specimen MAL290 (holotype of *Lende chiweta*) is a well-preserved skull and lower jaw collected in the Chiweta Beds of Malawi dated from the same period as the South African *Cistecephalus* AZ. The specimen was described by Kruger et al. (2015) and classified as a derived burnetiamorph.

Preparation

Specimen CGS MJF 22 was prepared mechanically at the Evolutionary Studies Institute by Charlton Dube using a compressed air driven air-scribe equipped with specially adapted and sharpened tungsten carbide tips. Paraloid diluted with acetone was used as an adhesive. For SAM-PK-K11126, partial preparation was previously undertaken at Iziko Museum in Cape Town. Specimen RC 55 had been previously prepared using a vibro-tool fitted with gramophone needles.

Scanning

To enhance understanding of internal cranial morphology and sutural patterns, CGS MJF22 and BP/1/816 (holotype of *L. pricei*) were scanned at the ESI using X-ray microCT with a Nikon Metrology XTH 225/320 LC (scanning parameters: 0.0445 mm, 185 kV, 185 μA and 0.050 mm, 110 kV, 150 μA respectively). Specimen SAM-PK- K11126 was scanned during two sessions at the same CT facility. The skull roof, occiput, and lower jaw were scanned during the first session and the snout during the second one (scanning parameters: 0.034 mm, 155 kV, 235 μA, and 0.03448 mm, 155 kV, 235 μA for each respective session). Specimens RC 55 and MAL 290 were also scanned at the ESI using the following scanning parameters: 0.0545 mm, 70 kV and 160 μA; and 0.08 mm, 105kV and 160 μA respectively. Specimen NMQR 1702 was scanned at the ID17 beamline of the European Synchrotron Radiation Facility (ESRF, Grenoble, France), using propagation phase contrast synchrotron X-ray micro computed tomography. The beamline setup consisted of a monochromatic beam of 130 keV (Si 111 double bent Lauë monochromator); filtration with 4 mm of aluminium and 1 mm of copper; a sample-detector distance of 10.9 m; an indirect detector (2 mm thick LuAG scintillator, 0.26x optical magnification and a FReLoN-2k camera), recording imaging with an isotropic pixel size of 0.054 mm. The data acquisition was done following the so-called attenuation protocol (Carlson et al. 2011), placing the specimen in a plastic tube filled with aluminium balls 5 mm in diameter, and consisted of 4998 projections recorded over a rotation of 360°, an exposure time of 0.6 s each. Additionally, the centre of rotation was shifted to increase the reconstructed horizontal field of view. Given the limited vertical size of the X-ray beam (~8 mm), 71 scans were necessary to cover the full length of the skull, moving the specimen by 5 mm between each acquisition. The CT reconstructions were done with the software PyHST2, using the single-distance phase retrieval approach (Paganin et al., 2002; Mirone et al., 2014). The resulting 32-bit data were

179 converted to a stack of 16 bits tiff using 0.02% saturation values from the 32-bit 3D histogram
180 generated by PyHST2.

181 Three-dimensional reconstructions and visualization of CT data of all specimens were
182 generated using AVIZO 9.0 (FEI VSG, Hillsboro OR, USA). Three-dimensional renderings were
183 obtained using manual segmentation with AVIZO 9.0 (FEI VSG, Hillsboro OR, USA).

184

185 **Institutional abbreviations–AMNH**, American Museum of Natural History, New York, USA;
186 **BP**, Evolutionary Studies Institute (formerly the Bernard Price Institute for Paleontological
187 Research), University of the Witwatersrand, Johannesburg, South Africa; **CGS**, Council for
188 Geosciences, Pretoria, South Africa; **MAL**, Malawi Department of Antiquities Collection,
189 Lilongwe and Nguludi, Malawi; **NHCC**, National Heritage Conservation Commission, Lusaka,
190 Zambia; **NMQR**, National Museum, Bloemfontein, South Africa; **PIN**, Paleontological Institute,
191 Moscow, Russia; **RC**, Rubidge Collection, Graaff-Reinet, South Africa; **SAM**, Iziko South
192 African Museum, Cape Town, South Africa.
193
194 **Anatomical Abbreviation–ang**, angular; **art**, articular; **aso**, anterior extension of the
195 supraoccipital; **bo**, basioccipital; **c**, caniniform tooth; **co**, occipital condyle; **cor**, coronoid; **d**,
196 dentary; **ect**, ectopterygoid; **eo**, exoccipital; **f**, frontal; **fe**, temporal fenestra; **fm**, foramen
197 magnum; **i**, incisiform tooth; **j**, jugal; **l**, lacrimal; **m**, maxilla; **n**, nasal; **o**, orbit; **op**, opisthotic; **p**,
198 parietal; **pa**, anterior portion of the parietal; **pac**, caudal portion of the parietal; **pal**, palatine; **pal**
199 **t**, palatal teeth; **pao**, paroccipital process; **part**, pre-articular; **pbs**, parabasisphenoid; **pc**,
200 postcanine; **pf**, postfrontal; **pif**, pineal foramen; **pl**, lateral portion of the parietal; **pm**,

premaxilla; **po**, postorbital; **pp**, postparietal; **prf**, prefrontal; **pro**, prootic; **prp**, preparietal; **pt**, pterygoids; **ptf**, post-temporal fenestra; **q**, quadrate; **qj**, quadratojugal; **rt**, replacement tooth; **sb**, supraorbital boss; **scl**, sclerotic ring; **smx**, septomaxilla; **so**, supraoccipital; **spl**, splenial; **st**, stapes; **sq**, squamosal; **sur** surangular; **t**, tabular; **v**, vomer.

Description

This section presents a full updated anatomical description of three of the five above mentioned skulls. Specimens NMQR 1702, BP/1/816 and MAL290 are not fully redescribed here as i) sufficiently detailed descriptions of their external cranial anatomy are already available in the published literature (Sigogneau, 1970; Sidor & Welman, 2003; Kruger et al., 2015; Benoit et al., 2017b) and ii) the CT images did not enable isolation all the bones using digital segmentation and therefore do not significantly add to previous descriptions. Only new observations enabled by CT scanning are discussed in this paper.

BIARMOSUCHIA Sigogneau-Russell, 1989

BIARMOSUCHIA gen. et sp. indet.

Material – RC 55, the holotype of *Rubidgina*, comprises a nearly complete laterally compressed skull. The specimen was considered a possible juvenile of *Herpetoskylax hopsoni* by Sidor and Rubidge (2006). RC 55 can be identified as a biarmosuchian by the presence of a squamosal with a long ventral ramus and an elongated zygomatic process under the orbit, but we consider it indeterminate within this clade because of its juvenile condition and lack of diagnostic characters.

224

225

226 **Description** – This specimen is an almost complete skull with lower jaws (Fig. 1). The orbit is
227 relatively large (3 cm diameter) in comparison to the skull length (7.5 cm), and the skull roof is
228 flat and does not show any sign of bosses, ridges, or pachyostosis (Duhamel et al., 2016;
229 Duhamel, Benoit & Rubidge, 2018; Kulik & Sidor, 2019), consistent with a juvenile status or a
230 basal phylogenetic position (Sidor & Rubidge, 2006). In lateral view, the skull has a triangular
231 outline (Fig. 1). The specimen is poorly preserved, being laterally compressed with the left side
232 eroded. The anterior snout has been eroded such that the premaxilla, septomaxilla, part of the
233 maxilla, incisors, and a large part of the nasals are damaged (Fig. 1). As a result of diagenesis,
234 most occipital bones are crushed, and the posterior margin of the right temporal fenestra is
235 missing while the left is distorted (Fig. 1). Because sutures are difficult to recognise and many
236 bones are concealed by matrix, the following description is mostly based on the 3D renderings.
237 As a result of the poor visibility of the sutures, the postparietal, supraoccipital, tabular,
238 opisthotic, prootic, parabasipshenoid and stapes could not be separated digitally but are definitely
239 preserved on the specimen as seen on the "unsegmented bones" section (Fig. 1-C). Both lower
240 jaw rami are present and articulated to the skull (Fig. 1).

241 **Skull**

242 The anterior portion of the skull is damaged, including the premaxilla and septomaxilla.
243 The full extent of the maxilla is difficult to evaluate but despite its weathered surface it is clear
244 that it is the largest bone of the lateral surface of the snout (Figs. 1 and 2). Posterodorsally, the
245 maxilla has a long and oblique sutural contact with the lacrimal on the anterior orbital rim.
246 Posteroventrally, the maxilla extends on the zygomatic arch as a long and thin process that

reaches the anterior end of the jugal at the level of the dentary/surangular suture (Figs. 1-A and 2). The medial surface of the maxilla is excavated by a triangular maxillary sinus (Fig. 2-B). The facial area of RC 55 is crushed, and it is thus difficult to position the prefrontal, lacrimal and jugal sutures with accuracy. The following description is based on an interpretation that we estimate to be the most probable, however a possible second interpretation is shown in Fig. 1-A and 2-A. The lacrimal, as preserved, is a thin strip-like bone limited to the anteroventral margin of the orbit (Figs. 1 and 2) but, because the facial process is damaged, it is difficult to estimate the anterolateral extension of the bone. Dorsally the lacrimal has a short contact with the prefrontal (Figs. 2-A and B). Posteroventrally, at the base of the zygomatic arch, the lacrimal meets the jugal and the maxilla in a tripartite suture (Fig. 2-A). Medially, the lacrimal has a sutural contact with the palatine within the orbit (Fig. 1-B). Two nasolacrimal foramina are present on the lacrimal: one medially positioned (Fig. 2-F) and the second is on the lateral surface (Fig. 2-A).

The prefrontal is a small bone forming the anterodorsal margin of the orbit (Fig. 2-A and B). Although the right prefrontal has a flat anterodorsal extension (Fig. 2-A and B), this unusual morphology could be the result of deformation or an artefact of segmentation. In dorsal view, the left prefrontal is triangular with posterolateral and posteromedial extensions (Fig. 2-D). The anterior margin of the frontal is positioned between these two small extensions (Fig. 1-D).

The frontal is a long and thin bone forming the anterior half of the dorsal margin of the orbit (Fig. 1). It sutures with the prefrontal anteriorly, the prepariental posteromedially, the postfrontal posterolaterally, and the parietal posteriorly (Figs. 1 and 3-C). The suture with the nasal is not preserved. In lateral view, a posterolateral process of the frontal extends lateral to the postfrontal on the orbital rim (Fig. 3-B). Another thin process separates the postfrontal and the

prepariental and meets the parietal posteriorly with a short contact in line with the anterior margin of the pineal foramen (Fig. 3-C). As in most biarmosuchians, a longitudinal depression on the frontal separates the low orbital rim from a rounded midline ridge (Figs. 3-E and F). Given the lateral compression of the specimen, the depth of this depression might have been exaggerated by post-mortem damage. In ventral view (Fig. 3-D), the frontal bears a thick longitudinal ridge that curves medially and (on the left frontal) continues posteriorly onto the parietal where it disappears caudally (Fig. 3-D).

The prepariental is a small unpaired and almost rectangular bone located on the dorsal-most point of the skull roof, above the posterior half of the orbit (Fig. 3-A). No midline suture is visible (Figs. 1 and 3-C). It has sutural contact with the frontal rostrally and the parietal caudally (Fig. 1 and 3). Its posterior margin is slightly elevated and contributes to the pineal boss and the anterior margin of the pineal foramen (Figs. 3-A and C).

In lateral view the postfrontal is a prominent bone that has a vertical orientation (Figs. 1-A, 1-B and 3). This vertical orientation might be exaggerated by lateral compression. The postfrontal sutures with the frontal anteromedially, the parietal posteromedially, and the postorbital posterolaterally (Fig. 3).

The paired parietal bones are separated by a distinct midline suture (Fig. 3-C) and the chimney-like pineal foramen is completely included within the parietals (Fig. 3-C). Because of compression, the sutural contacts of the parietal are unclear on the left side. However, it is evident that the parietal contacts the prepariental anterolateral to the pineal foramen through a tripartite connection between the frontal, prepariental, and the parietal. Laterally, the parietal contacts the postfrontal, and extends anteriorly to form another tripartite suture between the postfrontal, the frontal, and parietal (Figs. 3-C and D). Finally, the lateral margin of the parietal

293 is overlapped by the postorbital (Figs. 3-D and F), with a small posterolateral cleavage above the
294 postorbital (Fig 3-F).

295 The right jugal of RC 55 forms the posterior half of the ventral and the posteroventral
296 margins of the orbit (Fig. 1 and 2). It is an anteroposteriorly elongated bone that contacts the
297 lacrimal and the maxilla anteriorly (Figs. 2-A, B and F), and the postorbital posteriorly (Fig. 1-
298 A). The suture with the squamosal is unclear because of poor preservation (Fig. 1-A). The left
299 jugal has been displaced vertically and rotated counter clockwise such that the dorsal portion of
300 the displaced bone is actually the posterior portion of the jugal (Fig. 2-B). Its two extremities are
301 vertically flat and V-shaped for articulation with the maxilla anteriorly and the squamosal
302 posteriorly. This gives it a double-wrench overall outline. Medially, the long shaft of the jugal is
303 slightly concave for insertion of the masseter muscle.

304 The postorbital is a T-shaped bone. Its ventral extension forms the postorbital bar and
305 marks the posterior margin of the orbit and the anterior border of the temporal fenestra (Figs. 1
306 and 3), but the nature of the contact with the squamosal and jugal is uncertain (Fig. 1-A). The
307 postorbital contacts the squamosal dorsomedially and forms the dorsal and posterior margin of
308 the temporal fenestra in lateral view (Figs. 1-B and C). Anterodorsally the postorbital contacts
309 the postfrontal and frontal; and the parietal posterodorsally (Fig. 3). Medially, the ventral process
310 of the postorbital has a caudally curved ridge that extends from the postfrontal/postorbital suture
311 to the possible jugal/postorbital contact (Figs. 1-A, 1-B and 3-B).

312 The squamosal is a crescent-shaped bone forming the posterior and ventral margins of the
313 temporal fenestra (Fig. 4-A) and is best preserved on the left side. It possibly sutures with the
314 postorbital on the zygomatic arch below the anterior margin of the temporal fenestra (Fig. 1-A).
315 In occipital view, the squamosal overlies the quadrate dorsally (Figs. 4-A, B, E, and F). In medial

316 view (Fig. 4-B), the squamosal cradles the posterior side of the dorsal process of the quadrate.
317 Anteroventrally the squamosal has a triangular fossa at the base of the zygomatic process (Fig. 4-
318 B), which may represent the facet for the now displaced jugal.
319 Both quadrates of RC 55 are well preserved (Fig. 4). This bone is vertically flattened and
320 looks almost rectangular in occipital view. It is positioned on the anteromedial side of the
321 squamosal (Figs. 4-C and D). In occipital view (Fig. 4-E) the ventral articulatory margin of the
322 quadrate, comprising the lateral and the medial condyles, slopes ventrolaterally and has a smooth
323 surface that articulates with the articular (Figs. 1-C, 1-E and 4-E). Dorsal to the lateral condyle,
324 the quadrate has a small fossa (Fig. 4-F) where it contacts the small quadratojugal. On the right
325 side, the quadrate appears to share a contact with the angular (Figs. 1-A).
326 The quadratojugal is a small ovoid bone surfacing on the lateral side of the quadrate
327 (Figs. 4-A and E) and, like in other synapsids, participates in the jaw articulation with the
328 quadrate on the skull, and the articular and the angular on the lower jaw (Figs. 1-A, B, and E).
329 This tiny quadratojugal constitutes the dorsolateral part of the jaw articulation. Only the left
330 quadratojugal is preserved (Fig. 4), and it articulates solely with the quadrate on its dorsal,
331 medial, and ventral borders (Figs. 4-E and F).
332
333
334 **Occiput and basicranium**
335 The occiput has a roughened surface and lateral compression has resulted in the occiput
336 having a square outline in posterior view. The occipital surface is poorly preserved, most of the
337 bones are crushed and could not be differentiated during segmentation (Figs. 1-C and E).
338 However, the jaw articulation is complete and well preserved in RC 55.

339 The small triangular exoccipital bone is preserved lateral to the foramen magnum (Figs.
340 4-B and E) and its medial margin meets the basioccipital (Figs. 4-B and E).
341 The basioccipital, which is roughly cylindrical, is poorly preserved (Fig. 4). The condyle
342 is rounded in occipital view and extends ventrolaterally into a broken basioccipital tubera (Figs.
343 4-E and F). In dorsal view, the basioccipital is concave medially, probably for the pituitary fossa
344 (Fig. 4-D) but, because of poor preservation this could not be confirmed from the CT data. In
345 ventral view, a midline ridge extends from the middle of the basioccipital to the anterior border
346 of the occipital condyle (Fig. 4-C).
347 Three unidentified bones are positioned ventral to the basioccipital (Figs. 4-A, E and F).
348 Although they cannot be identified with certainty, they may represent fragments of the prootic,
349 opisthotic, basioccipital tubera, and/or stapes.
350
351 **Palate**
352 The palate has been damaged as a result of lateral compression. The vomers and the
353 ectopterygoids are missing, and some sutures are unclear, especially the one between the
354 parabasisphenoid and pterygoid (Fig. 1-E). Because of their fragmentary nature (Fig. 1-E), it was
355 not possible to digitally segment and isolate the posteriormost palatal bones and those of the
356 basicranium, such as the parabasisphenoid. The right side of the palate is best preserved and is
357 thus the basis of this description.
358 The anterior extension of the palatine extends posteriorly along the alveolar margin from
359 the last postcanine to the posterior margin of the palatine boss (Fig. 5-C), which in turn is in
360 contact with the pterygoid boss. Only the right palatine is preserved in RC 55 and contacts the
361 maxilla anteriorly and anterolaterally (Fig. 1-B), and the pterygoid posteriorly and

posterolaterally (Fig. 5). The dentigerous palatine boss bears eleven teeth arranged in a single U-shaped row. In medial view (Fig. 5-B), the palatine has a dorsal process that projects vertically from the anterior ramus of the palatine (Figs. 1-B and 5-B) and reaches the level of the dorsal margin of the maxilla (Fig. 1-B) to form the posteroventral margin of the maxillary sinus. A small vertical lamina present on the palatine also contributes to the lateral wall of the sinus. In lateral view, the ascending process sutures with the maxilla and is excavated by an ovoid concavity (Fig. 5-A). Medially and ventrally, the palatine shares a diagonal suture with the pterygoid along the lateral margin of the palatine boss (Figs. 5-B and 5-C).

In all Biarmosuchia, the pterygoid is a tripartite, paired bone, comprising the anteromedial process (or pterygoid corpus), the transverse process, and the quadrate ramus, the last of which forms the posterolateral part of the pterygoid (Rubidge & Sidor, 2002; Sidor & Welman, 2003; Rubidge & Kitching, 2003; Sidor, Hopson & Keyser, 2004; Kammerer, 2016; Day et al., 2018). On RC 55, the palatine ramus expands anteriorly between the maxilla laterally and the palatine medially (Fig. 5-C). A low longitudinal ridge is present on the lateral margin of the palatine ramus (Fig. 5-C). A high vertical lamina extends anterodorsally from the dorsal surface of the palatine ramus and reaches the level of the posteromedial border of the lacrimal dorsally (Figs. 1-B and 5-B). Posteromedial to the palatine ramus, the right pterygoid boss bears six teeth which are circular in cross-section. The right transverse process forms a 90° angle with the rest of the pterygoid in ventral view (Fig. 5-C) and three palatal teeth are preserved on the left transverse process but there are none on the right. A posteromedially oriented ridge marks the transition between the transverse process and the quadrate ramus (Fig. 5-C). The latter is divided into a thick posteromedial process and a thinner posterolateral process which is directed toward the quadrate (Fig. 5-F).

385

386 **Lower jaw**

387 Both mandibular rami are damaged anterior to the level of the canine (Figs. 1 and 6) and
388 the right ramus is missing the canine and incisors, but the canine and two incisors are preserved
389 on the left (Fig. 1).

390 Only the posterior part of the dentary is preserved in RC 55. It is a long and thin bone on
391 the dorsolabial surface of the lower jaw and has ten tooth sockets on the left and five on the right
392 ramus (Figs. 6-A and B). The dorsal margin of the dentary thickens posterodorsally to form a
393 low coronoid process at the highest point of the lower jaw, where the dentary, the coronoid and
394 the surangular meet (Fig. 6-B). Posteromedially, the dentary has a straight vertical contact with
395 the prearticular and the splenial (Figs. 6-A, B and D).

396 The splenial is a delicate elongated bone on the medial side of the dentary and is not
397 visible in lateral view (Fig. 6). Posterodorsally it has a sutural contact with the angular (Fig. 6-D)
398 and anteriorly it is broken at the level of the 9th postcanine.

399 A small coronoid is positioned on the dorsal part of both lower jaw rami (Fig. 6) and is
400 present between the dentary anteriorly and the surangular posteriorly (Figs. 6-A and B). On the
401 left lower jaw ramus, the coronoid cradles the anterior margin of the upper mandibular fenestra
402 (Fig. 6-B).

403 The angular is a large flat bone that forms a third of the posteroventral part of the lower
404 jaw on the medial side (Figs. 6-A and B) and is damaged along its ventral edge as a result of
405 post-mortem weathering (Figs. 6-A and B). The elongated and thin anterior portion is positioned
406 ventromedial to the dentary (Fig. 6-A). This portion of the angular contacts the splenial
407 anteriorly and the coronoid and the surangular dorsally (Figs. 6-A and B). The posterior portion

of the angular is broad with a damaged posteroventral margin (Figs. 6-A and B) and contacts the prearticular posteriorly. Postmortem damage resulted in an opening between the angular and the surangular on the left ramus (Fig. 6-B). Ventral to this opening the angular bears the reflected lamina that is preserved on the left ramus (Fig. 6-B). The reflected lamina of RC 55 consists of a thin ridge curving dorsally, that extends along the the ventral margin of the angular (Fig. 6-B). As this ventral margin has been weathered away, it is possible that the ventral-most part of the reflected lamina is not preserved on RC 55.

The poorly preserved surangular makes up the posterodorsal part of the lower jaw, posterior to the coronoid, anterior to the angular, and dorsal to the prearticular (Fig. 6-B). The surangular of RC 55 is badly preserved, however it is clear that the surangular forms most of the dorsal margin of an opening, bordered anteriorly by the coronoid, and is due to possible post-mortem damages (Fig. 6-B).

The prearticular is a small bone of the lower jaw located posteriorly, and exposed mainly on the medial side of both rami (Fig. 6-A and D). It is better preserved on the left ramus and surrounds the anterior margin of the articular posteriorly (Fig. 6-B), while sharing only a short contact with the articular on the right ramus (Fig. 6-A). The prearticular contacts the surangular posterodorsally and the medial side of the angular anteriorly (Fig. 6-A and D).

In RC 55, the articulation surface of the articular is concave and positioned posteromedially (Fig. 6-D). In posterior view (Figs. 6-D and E) the articular has two ventral processes separated by a deep notch (Figs. 6-D and E).

Dentition

The anterior dentition of RC 55 is not preserved because of incomplete preservation of the anterior end of the lower jaws and snout (Figs. 1 and 7). Despite this, CT imagery has, for the first time, revealed the presence of three small upper and two lower incisors (Fig. 7). The last upper incisor seems to have a caniniform morphology but is too poorly preserved to ascertain. One sharp caniniform is present on the lower jaw, and the upper canine has suffered post-mortem deformation. As in SAM-PK-K11126, a replacement upper canine is positioned posterior to the functional one. The upper postcanines are small and are poorly preserved such that it is not possible to determine their morphology. In contrast, the lower jaw has ten well-preserved conical postcanines (Fig. 7).

The remaining palatine boss bears ten teeth which are circular in cross-section and arranged in a U-shaped single row (Figs. 1-E and 5-C). The six teeth on the pterygoid boss are smaller and randomly distributed. Three medially positioned teeth are present on the transverse process (Figs. 1-E and 5-C).

BIARMOSUCHIA Sigogneau-Russell, 1989

BURNETIAMORPHA Broom, 1923

BURNETIAMORPHA gen. et sp. indet.

Material – CGS MJF 22, an almost complete skull with the lower jaw. The anterior part of the snout and dentary are missing. It can be recognized as a burnetiamorph on the basis of a median ridge on the skull roof and a supraorbital boss; the palatal process of premaxilla is long and

453 laterally bounds the anterior portion of vomer; and the surangular bears a deep fossa laterally.
454 The genus cannot be determined because of its juvenile condition.
455
456 **Description** – Specimen CGS MJF 22 (Fig. 8) comprises an almost complete skull and occluded
457 lower jaw. On specimen CGS MJF 22, the roof of the snout and part of the left side are damaged.
458 Superficially the skull is broadly triangular in lateral view (Fig. 8-A). The right side of the skull
459 is relatively well preserved, allowing most bones to be digitally segmented (Fig. 8). Similarly,
460 the right ramus of the lower jaw is well-preserved except for the anterior tip of the dentary,
461 which is missing. The left lower jaw is badly weathered and preserves only the anterior portion
462 of the dentary. The large orbit makes up about 70 % of the lateral surface of the skull (orbit
463 diameter is 30 mm and basal skull length is 77 mm). It forms an almost perfect circle and at least
464 six sclerotic plates from the posterodorsal region of the sclerotic ring are preserved in the right
465 orbit. As the left side is poorly preserved, this description is based mostly on the right side. The
466 palate is well preserved and much of the anatomy is visible, including the palatal teeth. The
467 medial portion of the occiput is well preserved, but the left side is missing and the right side is
468 weathered, which prevents accurate description.
469 **Skull**
470 The anterior tip of the skull is weathered away, and it is not possible to determine the
471 morphology of the premaxilla, the septomaxilla, and the arrangement of the external nares. The
472 right lateral surface of the maxilla is well preserved. It is a smooth and triangular bone (Fig. 8-A)
473 that covers most of the lateral surface of the snout. The long, straight alveolar margin bears one
474 canine and eight postcanines, the last of which is unerupted and has been revealed by CT (Fig. 8-
475 A). Along its posterior margin, the maxilla shares a suture with the lacrimal and sends out a thin

476 strip-like posterior process that tapers below the jugal ventrally. This process probably shares a
477 short contact with the squamosal on the zygomatic arch below the orbit, but the contact is not
478 visible.

479 The lacrimal is a quadrangular bone, forming most of the anterior margin of the orbit
480 (Fig. 8-A) and contacts the jugal ventrally, the maxilla anteriorly, and the prefrontal dorsally but
481 the anterior part of the prefrontal is not preserved. A vertical ridge extends up the lacrimal along
482 the anterior border of the orbit. The lacrimal is excavated by an ovoid depression anterior to the
483 orbit, close to the suture between the maxilla and jugal.

484 The jugal comprises almost the entire ventral margin of the orbit and forms a small part
485 of the anteroventral margin of the temporal fenestra (Fig. 8-A). Anterodorsally it shares a
486 horizontal sutural contact with the lacrimal and meets the maxilla anteroventrally, the squamosal
487 posteroventrally, and the postorbital posterodorsally. The suborbital portion of the zygomatic
488 arch formed by the jugal is thin and not pachyostosed. The small triangular temporal fenestra is
489 less than one third the size of the orbit and is positioned posteroventral to the orbit. It is bordered
490 anteriorly by the postorbital and the jugal, and posteriorly by the squamosal.

491 The narrow postorbital bone slopes posterodorsally at an angle of 45° to the horizontal
492 and forms practically the entire postorbital bar (Fig. 8-A). Anterodorsally it meets the postfrontal
493 at the posterior margin of the orbit, has a long sutural contact with the postfrontal on the skull
494 roof, and meets the parietal posteromedially such that the postorbital has extensive exposure on
495 the skull roof (Fig. 8-C).

496 The squamosal is a comparatively large bone forming the ventral and posterior borders of
497 the temporal fenestra. It shares a suture with the tabular on the occiput, and ventrally it contacts

498 the quadrate and quadratojugal (Figs. 8-A and C). Anteriorly, the squamosal tapers into a long
499 process that sutures with the posterior process of the maxilla (Figs. 8-A and C).
500 As many of the skull roof bones are slightly pachyostosed (Fig. 8-B), their sutural
501 contacts are not readily visible and were identified using CT data. The orbital rim bears a
502 conspicuous supraorbital boss that reaches its highest point halfway above the orbit and is
503 formed mainly by the frontal and the postfrontal. A large domed boss surrounds the circular
504 pineal foramen (Fig. 8-B) which is positioned posteromedial to the orbit. The pineal tube extends
505 anteroventrally at an angle of about 70° relative to the skull axis (Fig. 8-A). Only a small portion
506 of the posterior end of the right prefrontal is preserved. It constitutes the anterior-most part of the
507 supraorbital boss and forms the anterodorsal rim of the orbit (Fig. 8-B). Although the degree of
508 pachyostosis of the supraorbital boss is low in CGS MJF 22, the CT data revealed the presence
509 of radial structures in coronal cross-section (Fig. 8-B), which are considered to be radial vascular
510 structures linked to the possibly juvenile status of the specimen (see discussion).
511 The paired frontals have a smooth dorsal surface with no midline ridge (Fig. 8-B). Each
512 frontal contributes a large portion of the supraorbital part of the skull roof, participates in the
513 dorsal margin of the orbit, and tapers posterolaterally between the prepparietal and postfrontal.
514 The posterior tip of the frontal forms a pointed contact with the parietal at the level of the
515 anterior margin of the pineal foramen.
516 The prepparietal is a relatively large, roughly triangular, paired bone positioned between
517 the two supraorbital bosses (Fig. 8-B) with the apex of the prepparietal tapering anteriorly
518 between the frontals. Posteromedially, the prepparietal contributes to the border of the pineal
519 foramen, and posterolaterally it shares an oblique sutural contact with the parietal. A midline
520 suture is present in the prepparietal (Fig. 8).

521 The parietal contributes to the lateral margin of the pineal foramen and extends onto the
522 lateral and posterior sides of the pineal boss (Fig. 8-B). In dorsal view, it contacts the preparietal
523 anteromedially, shares a short contact with the frontal and postfrontal anterolaterally, with the
524 postorbital posterolaterally, and the postparietal posteriorly on the occiput (Fig. 8-C). In addition,
525 the postfrontal forms a posteriorly directed process between the frontal and the postorbital. Based
526 on the CT images it appears that the parietal is divided into two separate bones (Fig. 8-B), a
527 rostrolateral part and a posteromedial part radiating posteriorly from the pineal foramen (Fig. 8),
528 which may indicate two distinct centres of ossification (see Discussion). The midline suture
529 between the paired parietals, posterior to the pineal foramen, is not fused (Fig. 8).
530 Most of the left side of the occiput of CGS MJF 22 is missing and the right side is badly
531 weathered (Fig. 8-C). However, the central portion is preserved. The postparietal is a large
532 unpaired rectangular bone that forms the dorsal half of the occiput. Ventrally it shares a
533 horizontal suture with the supraoccipital and touches the parietal dorsally. Because of extensive
534 post-mortem damage, the lateral suture with the tabular is impossible to determine. However, a
535 short dorsolateral contact with the right squamosal is evident. A vertical midline ridge, the
536 external occipital ridge, extends ventrally from the postparietal to the foramen magnum (Fig. 8-
537 C) and is more rounded on the supraoccipital than on the postparietal.
538 The unpaired supraoccipital is not well preserved, and the left side is the most complete
539 (Fig. 8-C). It forms the dorsal margin of the foramen magnum and extends laterally and ventrally
540 to contact the exoccipital ventrally, and the opisthotic ventrolaterally. Dorsally it shares a long
541 horizontal contact with the postparietal.
542 The opisthotic is mostly weathered, its exact shape cannot be determined, and it is only
543 partly preserved on the left side of the occiput (Fig. 8-C). It contacts the supraoccipital

dorsomedially, the exoccipital medially, and the basioccipital ventromedially. On the ventral side (Fig. 8-D), the opisthotic is oriented posterolaterally and shares a sinusoidal medial contact with the basioccipital. The opisthotic contacts the parabasisphenoid anteromedially, and bears the fenestra ovalis anteriorly. This fenestra is partially crushed laterally and has a straight sutural contact with the opisthotic medially (Fig. 8-D).

A small, oval exoccipital forms the lateral border of the foramen magnum (Fig. 8-C). Ventrally, it contacts the basioccipital, dorsally the supraoccipital, and the opisthotic laterally. The right exoccipital is not preserved.

The midline basioccipital forms the ventral and ventrolateral margin of the foramen magnum and the occipital condyle (Fig. 8-C). It contacts the exoccipital dorsolaterally and the opisthotic laterally. Only a small portion of the left basioccipital condyle is preserved ventrally. In palatal view (Fig. 8-D), the basioccipital contacts the opisthotic laterally and the parabasisphenoid anteriorly.

Palate

Generally, the ventral side of the skull is well preserved except for the posterior part close to the basicranium (Fig. 8-D). Anteriorly, the vomer is a thin midline bone which has not been extensively prepared because it is too delicate. From the CT data, it appears that the vomer is an unpaired structure with a medial trough flanked by two thin vertically oriented lateral flanges. Posteriorly, the vomer forms a large expanded vomerine plate (Fig. 8-D). The lateral flanges of the vomers converge posteriorly to form a midline ridge that extends posteriorly onto the vomerine plate (Fig. 8-D) which has posterior contact with the palatines. The horizontal suture

566 between the vomerine plate and the palatine is more dorsally positioned than the rest of the
567 palate.

568 The palatine and pterygoid form most of the palate (Fig. 8-D). The palatine bears a long
569 anterior tongue-like process that forms the lateral margin of the internal naris and extends
570 anteriorly to the level of the caniniform tooth. A prominent palatine boss protrudes ventrally and
571 bears numerous nubbin-like teeth arranged in a U-shaped pattern (Figure. 8-D). Twenty small
572 teeth are present on the right palatine boss and are arranged in two rows (Fig. 8-D). The left
573 palatine boss is not well preserved. A midline trough separates the paired palatine and pterygoid
574 bosses. Posteriorly, the palatine shares a reverse V-shaped suture with the pterygoid and meets
575 the ectopterygoid posterolaterally (Fig. 8-D).

576 The ectopterygoid (Fig. 8-D) is preserved on the right side. It is an anteroposteriorly long
577 and flat bone that constitutes the lateral aspect of the palate. Anteriorly and anteromedially it has
578 a long sutural contact with the palatine and posteriorly contacts the pterygoid.

579 The tripartite paired pterygoid comprises the pterygoid boss anteriorly, the transverse
580 process, and the quadrate ramus caudally (Fig. 8-D). The pterygoid boss is in continuity with the
581 palatine boss and also bears small nubbin-like teeth (Fig. 8-D). On the right pterygoid boss,
582 about 25 teeth are clustered randomly, but because of the poor preservation of the left side, the
583 exact number of teeth is uncertain (both on the specimen and the CT data). The transverse
584 process is robust and positioned halfway along the pterygoid, at the level of the anterior margin
585 of the orbit. On the medial side of the right transverse process, are four teeth arranged in a single
586 row. As a result of post-mortem damage, it is not possible to determine whether teeth are present
587 on the left transverse process and metallic inclusions prevent clear identification on the CT data.
588 Posterior to the transverse process, the pterygoid corpus is excavated by a long slit-like

589 interpterygoid vacuity (Fig. 8-D). The raised margins of the interpterygoid vacuity are in
590 continuity with the transverse processes. A long quadrate ramus extends back from the lateral
591 side of the pterygoid corpus, posterior to the transverse process (Fig. 8-D).
592 Posteromedially, the pterygoid corpus meets the parabasisphenoid (fusion of the
593 parasphenoid and basisphenoid), which is slightly offset dorsally (Fig. 8-D). On its ventral
594 surface, this bone bears an elongated medial mound. Lateral to this mound, the parabasisphenoid
595 forms a small shelf (Fig. 8-D). Posterior to the mound, the suture with the basioccipital is
596 unclear, but a very slight depression is present between the two basal tubera. Posterolaterally, the
597 parabasisphenoid meets the opisthotic and forms the anteromedial border of the fenestra ovalis
598 (Fig. 8-D).
599 The quadrate forms the jaw articulation with the articular, and only the right quadrate is
600 preserved (Fig. 8-D). The ventral side of the quadrate is rectangular, mediolaterally elongated,
601 and presents a medial crest. This crest is probably a result of the fusion between the two quadrate
602 condyles as already observed in other biarmosuchian taxa (Sidor & Rubidge, 2006). The
603 quadrate contacts the quadrate ramus of the pterygoid anteromedially and the quadratojugal
604 posterodorsally (Fig. 8-D). In lateral view, the quadrate has a small exposure at the
605 posteroventral extremity of the skull (Fig. 8-A), but in occipital view the dorsal process is broad
606 and attaches to the anterior side of the squamosal ventral flange (Fig. 8-C). It is in close contact
607 with the articular such that its anterior aspect is not visible.
608 The quadratojugal is a small, thin, and vertically flat bone that is visible in lateral,
609 occipital, and ventral views (Figs. 8-A, C, D respectively) on the right side. On its lateral aspect,
610 the rectangular quadratojugal contacts the quadrate dorsal to its lateral articular condyle (Fig. 8-
611 A). In occipital view the quadratojugal contacts the quadrate below the small quadratojugal

foramen and the squamosal dorsally (Fig. 8-C). In palatal view, the quadratojugal contacts the lateral quadrate condyle and has an articular contact with the angular anteriorly (Fig. 8-D).

Lower jaw

The right dentary is reasonably well preserved in comparison to the left, but the ventral surface has been weathered away. In lateral view, the dentary forms the anterior half of the mandible (Fig. 8-A). Posteroventrally, the dentary contacts the angular with a posterodorsally oriented suture. The exact nature of the contact is unclear because of damage to the ventral part of the mandible from this point forward. The dentary meets the surangular and continues posterodorsally as a process that overlies the surangular and forms the dorsal margin of the mandible. Below the orbit, the dentary is mediolaterally compressed into a low coronoid process (Fig. 8-A). The lateral surface of the dentary is relatively flat and smooth, as is typical in biarmosuchians (Rubidge & Kitching, 2003; Sidor, 2003; Sidor & Welman, 2003; Sidor, Hopson & Keyser, 2004; Rubidge, Sidor & Modesto, 2006; Smith, Rubidge & Sidor, 2006; Sidor & Smith, 2007; Kruger et al., 2015; Kammerer, 2016). The posterodorsal margin of the dentary forms a laterally projecting ridge that extends posteriorly, dorsal to the surangular. This structure originates dorsal to the contact of the dentary and angular, initially swelling into a round ridge but flaring caudally so that it is very thin as it projects over the surangular (Fig. 8-A). The splenial is visible as a long, thin ribbon-like bone on the medial side of the jaw. It extends anteriorly from the ectopterygoid to the tip of the mandible (Fig. 8-D).

In lateral view, the surangular has a small exposure on the posterodorsal side of the mandible, where it forms the curved posterodorsal edge of the coronoid process. It bears a prominent laterally projecting longitudinal ridge (Fig. 8-A). On its ventral side, the surangular

has a long horizontal sutural contact with the angular and contacts the dentary dorsally (Fig. 8-D).

The angular forms the posterolateral portion of the lower jaw extending posteriorly from below the anterior margin of the orbit (Fig. 8-A). The extensive reflected lamina bears a prominent oblique ridge that curves posterodorsally. In lateral view, the angular contacts the surangular dorsally and the dentary anteriorly (Fig. 8-A). On the medial side it contacts the dentary anterolaterally and posteriorly reaches the two articular condyles (Fig. 8-D). The anterior contact with the splenial cannot be determined because of poor preservation.

The poorly preserved articular is located posterior to the angular as is usual in Biarmosuchia (Sidor, Hopson & Keyser, 2004). Medially the articular bears two condyles, one lateral and one medial (Fig. 8-D). The articular articulates with the quadrate posteriorly to form the jaw joint.

Dentition

As the tip of the snout and mandible is eroded, no pre-canine teeth are preserved on the upper and lower jaw. On the maxilla, the weathered alveolus of the right caniniform tooth extends dorsally almost as far as the dorsal margin of the maxillary bone (Fig. 8-A). CT data reveal the presence of an unerupted tooth posterior to the erupted caniniform socket that might be a replacement caniniform tooth (Fig. 8-A). The scan also reveals eight marginal postcanines in the right maxilla, but no teeth are visible on the left side. The anterior-most three postcanines have serrations on their posterior edge, whereas the four posterior-most ones bear serrations on both the anterior and posterior edges (Fig. 8-A). It was not possible to determine the serration pattern on the fourth postcanine.

No pre-canine or caniniform teeth are preserved on the lower jaw. Eight postcanines are visible on the right lower jaw (Fig. 8-A). They all share a similar, conical morphology, and decrease in size posteriorly. No serrations are visible on the anterior-most post-canine tooth, but the second, third, and fourth teeth have serrations on the anterior side. The fifth post-canine tooth has serrations on both sides, the sixth does not have visible serrations, and the seventh and eighth post-canines have serrations on both sides. These seemingly random variations could be the result of over-preparation or differential weathering due do rapid dental replacement in this juvenile individual.

BIARMOSUCHIA Sigogneau-Russell, 1989

BURNETIAMORPHA Broom, 1923

cf. *Lophorhinus willodenensis* Sidor and Smith (2007)

Material –Specimen SAM-PK-K11126, a broken potential juvenile specimen which preserves a partial snout and palate, the pineal region, the occiput, a partial lower jaw, posterior dorsal and sacral vertebrae attached to a pelvis, a distal part of a femur and some indeterminate bones. SAM-PK-K11126 can be identified as a burnetiamorph because of the presence of a median ridge-like structure on the skull roof and a long palatal process of the premaxilla laterally bounding the anterior portion of the vomer. We think it to be likely referrable to *Lophorhinus willodenensis* because of the presence of a long palatal process of the premaxilla that laterally bounds the anterior part of the vomer (Sidor & Smith, 2007) and similarities in the shape of the vomer in SAM-PK-K11126 and SAM-PK-K6655 (holotype of *Lophorhinus willodenensis*).

680 **Description** –The description of the skull fragments of SAM-PK-K11126 is mostly based on CT
681 data, as the delicate nature of its bones prevents further preparation. Description of the
682 postcranial material will be the subject of a future paper. Bone sutures are readily visible making
683 segmentation of individual bones relatively easy to accomplish (Figs. 9-13).
684
685 **Snout fragment**
686 On the left side, most of the maxilla and the complete premaxilla are preserved as well as
687 part of the jugal (Fig. 9-A). The right side is severely damaged, and this description is thus based
688 mostly on the left lateral side of the specimen.
689 The premaxilla is a short and thin bone on the anterior aspect of the snout (Fig. 9-A) and
690 accommodates six incisiform teeth. It has sutural contacts with the maxilla posterior to the last
691 incisiform tooth, and with the vomer posteromedially through the vomerine process. In palatal
692 view, the vomerine process of the premaxilla extends posteriorly to the level of the first
693 caniniform tooth (Figs. 9-B and 10-B). Because of the presence of many crushed bones inside
694 the snout, the morphology of the anterior part of the vomerine process of the premaxilla is
695 uncertain (Figs. 9-B and 10-B). In lateral view, the premaxilla tapers posterodorsally into an
696 elongated caudal process (Fig. 9). As the nasals are not preserved, it is not possible to evaluate
697 the sutural contact of the premaxilla with these bones.
698 In lateral view the maxilla is a large bone that makes up most of the face of the isolated
699 snout, but the bone is very thin and bears many fractures. At its anterior end, it overlaps the
700 posterior margin of the premaxilla (Fig. 9-A). Two caniniform teeth and eight postcanines are
701 preserved on the left side (Fig. 9-A). Posterodorsally the maxilla has an oblique sutural contact
702 with the jugal which begins dorsally below the anterior margin of the orbit and continues

posteroventrally to the broken zygomatic arch (Fig. 9-A). In ventral view, the thin elongated maxilla has short sutural contacts with the palatine and a long contact with the ectopterygoid posteromedially (Fig. 9-B).

Palate

The anterior part of the palate is relatively well preserved on the snout, up to the posterior border of the ectopterygoid, and segmentation enabled description of the internal anatomy (Fig. 10). Because of deformation and the thin nature of some bones (particularly the dorsal lamina), some sutures were not discernible in the CT data. We present here our interpretation of the palate of SAM-PK-K11126 with some uncertainties.

The vomer is a long unpaired bone that extends almost half of the length of the palatal surface of the snout fragment (Fig. 10-A). It has a longitudinal midline trough bordered by lateral ridges that join anteromedially to form a midline ridge at the level of the last incisiform, just posterior to the suture with the premaxilla (Figs. 10-A and B). The resulting medial ridge continues anteriorly onto the premaxilla. The midline trough extends posteriorly as far as the level of the third postcanine. Posteriorly the vomer contacts the palatine and separates the palatine bosses ventrally (Fig. 10-A). On its dorsal side, the vomer forms a long thin septum that separates the nasal chamber into two bilateral cavities (Figs. 10-B and C). In lateral view, the dorsal margin of this septum slopes at a 30° angle (Fig. 10-C). Posteriorly, the suture between the vomer and the palatine cannot be determined with certainty due to post-mortem damage, but it appears that the vomer thins to form a wedged contact between the two palatine bones (Fig. 10-A).

725 The posterior half of the palatal surface comprises the paired palatine and pterygoid
726 bones (Fig. 10-A). As the right palatine bone is poorly preserved and incomplete, the description
727 is based on the left side. The maxillary process of the palatine is triangular. It extends anteriorly
728 along the tooth row (Fig. 10-B) and tapers against the maxilla at the level of the first postcanine
729 tooth (Fig. 9-B). The palatine bosses are separated by a midline suture and a medial trough. The
730 palatine contacts the pterygoid posteroventrally and medially (Fig. 10-A). Laterally the palatine
731 shares a long and oblique suture with the ectopterygoid. (Fig. 10-A). Dorsally, a thin and high
732 septum extends from the level of the ectopterygoid to the vomerine septum caudally (Fig. 10-B,
733 C and D). This septum may belong, at least in part, to the pterygoid, though the quality of
734 preservation does not allow the definitive identification of a suture in CT data. Posterodorsally,
735 the palatine overlies the pterygoid bosses (Fig. 10-C).
736 In ventral view the ectopterygoid is a rectangular and longitudinally elongated edentulous
737 bone located anterolateral to the lateral process of the pterygoid (Figs. 10-A and B). The left
738 ectopterygoid is best preserved and shows that it contacts the palatine boss medially and the
739 maxilla laterally. Its contribution to the medial septum dorsally is uncertain (Fig. 10-C).
740 Posteromedially, the ectopterygoid borders the pterygoid boss (Fig. 10-A and B).
741 In SAM-PK-K11126 only the corpus and quadrate ramus of the pterygoid are preserved.
742 The quadrate ramus is visible on the occipital fragment as a thin process that contacts the
743 quadrate posteriorly (Fig. 11-D) and curves anteromedially toward the anterior margin of the
744 parabasisphenoid (Fig. 11-D). On the palatal side of the snout, the anterior part of the pterygoid
745 corpus is damaged; however, it is clear that the pterygoid boss overlaps the palatine (Fig. 10-C).
746 The anterior end of the pterygoid corpus is separated from its counterpart by the palatine. On the

747 left side, the pterygoid contacts the ectopterygoid laterally (Fig. 10-B). The transverse process is
748 not preserved in SAM-PK-K11126.
749
750 **Pineal region fragment**
751 This fragment comprises the supraorbital and pineal region of the skull roof (Fig. 12). The
752 dorsal rim of the left orbit is preserved and has no pachyostosis or supraorbital boss. The left side
753 preserves no sutures and most of the bones could not be identified. Accordingly, the
754 segmentation and description are mostly based on the right side (Fig. 12).
755 The frontal is a paired bone with a smooth dorsal surface and forms a large part of the
756 interorbital region (Fig. 12-A). A low ridge is present on the midline between the two frontals
757 and extends posteriorly on the prearietal, and up to the pineal boss (Fig. 12-A). Because the
758 anterior portion of the frontal is not preserved, the frontal appears as a triangular bone. It tapers
759 caudally and extends laterally to the pineal foramen as a thin caudal process contacting the
760 parietal and prearietal medially, the postfrontal laterally, and the postorbital posteriorly (Fig.
761 12-A). The suture between the frontal and the postfrontal appears ridged, but CT data reveal that
762 this is due to post-mortem displacement of the frontal to artificially overlap the postfrontal (Fig.
763 12-A). In ventral view, the frontal bears a longitudinal, medially curved ridge extending from the
764 level of the middle of the prearietal to the anterior part of the frontal (Fig. 12-B).
765 The postfrontal forms the posterodorsal margin of the orbit in dorsal view (Fig. 12-A) and
766 shares a sinuous suture with the postorbital posterolaterally (Fig. 12-C). In ventral view, the
767 posterior end of the postfrontal has a short posteromedial contact with the parietal (Fig. 12-B).
768 Only a small fragment of the postorbital is present in this skull roof fragment, posterior to the
769 postfrontal (Fig. 12) and makes up a very short part of the posterior margin of the orbit (Fig. 12-

C). Anteriorly, the postorbital mostly contacts the postfrontal and also shares a short suture with the caudal process of the frontal. The postorbital has sutural contact with the parietal medially (Fig. 12-B) and posterolaterally the rim of the postorbital is inset by the dorsal margin of the temporal fenestra. The squamosal is not preserved.

The prepariетal is an unpaired and relatively small diamond-shaped bone on the skull roof that forms the anterior margin of the pineal foramen and tapers anteriorly between the two frontals (Fig. 12). It has a long oblique anterior sutural contact with the frontal and a short, slightly curved suture with the parietal posteriorly (Fig. 12-A).

The pineal foramen is relatively large and surrounded by a prominent pineal boss formed by the prepariетal anteriorly and the parietal laterally and caudally (Fig. 12-A and B). The parietal is a paired bone that contacts the prepariетal anteriorly and anterodorsally, extends onto the frontal laterally, and is overlapped by the postorbital posterolaterally (Fig. 12-B). Based on CT images, it appears that the parietal comprises three parts separated by distinct sutures radiating from the pineal foramen: an anterior part, a lateral part, and a caudal part behind the pineal foramen (Fig. 12). The implications of these subdivisions are addressed in the discussion.

Occipital fragment

The occipital part of the skull, and some of the basicranial elements are preserved on a single fragment (Fig. 11). The supraoccipital is a relatively large and unpaired bone, contributing 40% of the surface on the occiput fragment, and forming the dorsal margin of the foramen magnum (Fig. 11-A). Dorsolaterally, the supraoccipital has a short contact with the remains of the postparietal (Fig. 11-A). The anterior extension of the supraoccipital forms a cavity on the ventral surface to accommodate part of the brain (Fig. 11-C). Ventrolaterally, the supraoccipital

forms the dorsal margin of the post-temporal fenestra. Lateral and medial to the fenestra, it shares sutures with the opisthotic (Fig. 11-A). Laterally the supraoccipital has a diagonal contact with the medial margin of the tabular, ventrally with the dorsal process of the basioccipital (Fig. 11-A and B). The supraoccipital appears to surround the ovoid exoccipital (Fig. 11-A) and that the supraoccipital is positioned anterior to the exoccipital. Their exact position in relation to the supraoccipital and the basioccipital cannot be accurately determined (Fig. 11-A).

A broken piece of the tabular is present on the right side of the occiput in association with part of the squamosal and the quadrate (Figs. 11-A and B). The tabular extends dorsoventrally from the top of the supraoccipital to the ventral margin of the opisthotic. It shares an anteromedial contact with the supraoccipital and contacts the opisthotic along its ventromedial margin (Fig. 11-A). On its anterior side, the tabular has a slight depression to fit the anterior depressed surface of the squamosal (Fig. 11-B).

Part of the dorsal process of the squamosal is positioned anterior to the tabular and the opisthotic (Figs. 11-A, B, and C). The squamosal contacts the stapes posteromedially and the quadrate anteromedially.

The opisthotic is positioned on the ventrolateral side of the occiput and is shaped like a horizontal hourglass (Fig. 11-A). Its dorsal concavity constitutes the ventral border of the post-temporal fenestra while its ventral concavity forms the dorsal margin of the fenestra ovalis. The opisthotic contacts the basioccipital medially, and the supraoccipital dorsomedially. Laterally, the opisthotic has a flat contact with the squamosal and is overlapped by the tabular dorsolaterally (Figs. 11-A and B).

The basioccipital is an unpaired midline bone forming the lateral and ventral edges of the foramen magnum, and comprises the single occipital condyle (Fig. 11-A). The two dorsolateral

parts of the basioccipital are ovoid and in contact with the exoccipital dorsomedially, the supraoccipital medially, and the opisthotic laterally. The ventral part of the basioccipital contacts the parabasisphenoid anteriorly (Fig. 11-B).

The prootic is positioned between the basioccipital and the parabasisphenoid (Figs. 11-B and D) and shares a contact with the stapes and the supraoccipital (Fig. 11). The prootic on SAM-PK-K11126 is a tripartite bone, with a median posterior process at the level of the occipital condyle, and two lateral processes. The right lateral process is oriented toward the supraoccipital (Figs. 11-B and D).

Only the posterior part of the quadrate is preserved on the occipital fragment (Fig. 11). Dorsally, it is in sutural contact with the opisthotic. A curved suture runs dorsolaterally along the left quadrate and separates it from the stapes (Fig. 11-A). On the right quadrate, only the ventral side reaches the stapes. In right lateral view (Fig. 11-B) it is evident that the quadrate underlies the squamosal and extends anterodorsally along the anterior margin of the squamosal (Fig. 11-B). Anteromedially, the left quadrate contacts the quadrate ramus of the pterygoid (Figs. 11-A and D).

The stapes is a small dumbbell-shaped bone that contacts the ventral margin of the fenestra ovalis (Fig. 11-A). This description is based on the right stapes as it is the best preserved. The stapes is positioned lateral to the ventral process of the basioccipital and the prootic (Figs. 11-A and D) and shares a sutural contact with the basioccipital and the prootic medially and the quadrate and the tabular laterally. No stapedial foramen is present.

The laterally displaced parabasisphenoid is visible on the ventral side of the fragment. Anteriorly it divides into two processes (Figs. 11-B and D).

839 **Lower jaw**

840 A small posterior portion of the left lower jaw is preserved attached to the occiput fragment
841 (Fig. 11). No sutures could be identified but as it is articulated to the quadrate, this part of the
842 lower jaw is probably the angular with a piece of articular (Figs. 11-A and D). In addition to the
843 posterior piece of left lower jaw, a small portion of the right lower jaw ramus is also preserved
844 and bears the four distal-most postcanine teeth (Fig. 13). In dorsal view, the CT data clearly
845 show a vertical suture extending along the three teeth sockets and the suture between the dentary
846 and splenial (Fig 13-B).

847

848 **Dentition**

849 On the ventral side of the snout, it is evident that six incisiform teeth are present in the
850 premaxilla, two prominent caniniform teeth are rooted anteriorly in the maxilla, and eight
851 postcanines are positioned caudally on the maxilla (Figs. 9 and 14-A). A replacement tooth at the
852 third incisiform position is preserved on each side (Fig. 14-A). All the incisiform teeth are
853 elongated and slender. The caniniform teeth are well exposed (Figs. 9 and 14) and have,
854 serrations on the posterior face. The canines are curved and laterally compressed, with the distal
855 side sharper than the mesial side. Two replacement teeth are visible medial to the caniniforms
856 (Fig. 14). Eight postcanines are arranged in a single row on the left maxilla, while the right side
857 shows only six poorly preserved postcanines (Figs. 9 and 14).

858 Posteromedially, on the body of the palatine, the prominent, anteriorly rounded, dentigerous
859 palatine boss (Fig. 10-A) bears twenty-four nubbin-like teeth arranged in a U-shaped manner
860 along the anterior edge of the boss (Fig. 14-A). On the lateral edge they are arranged in two
861 parallel rows, but there is only a single row on the medial edge (Fig. 14-A).

862 Nubbin-like teeth arranged in a V-shape are also present on the pterygoid boss with the apex
863 of the V-oriented posteriorly (Fig. 10-A). Fourteen teeth are visible on the CT data of the left
864 boss, and twenty-three on the right boss.
865
866 BURNETIAMORPHA Broom, 1923
867 Genus *LEMUROSAURUS* Broom, 1949
868 *LEMUROSAURUS PRICEI* Broom, 1949
869 **Material** – BP/1/816 (holotype of *L. pricei*), NMQR 1702 (Sidor & Welman, 2003) and
870 BP/1/818 (cf. *Lemurosaurus*, referred as BPI 353 in Sigogneau (1970))
871
872 **Holotype** – BP/1/816, complete skull and lower jaw.
873
874 **Description** – Sigogneau (1970) provided a full description of BP/1/816 pointing out that the
875 skull is small (basal skull length of 71 mm) and complete with a lower jaw. The relatively large
876 orbit (21 mm) is suggestive of a juvenile status. The specimen has been previously considered to
877 be possibly a juvenile specimen when NMQR 1702 was described (Sidor & Welman, 2003). The
878 ratio of the diameter of the orbit to skull length is 0.3. This small specimen has pachyostotic and
879 relatively large supraorbital bosses (Fig. 15). CT data (Fig. 15-A) show thick and dense tissue
880 inside the supraorbital boss instead of a thin and porous skull cap. The pineal boss is a domed
881 structure and a round boss is present on the posterior part of the zygomatic arch. The braincase is
882 fully formed and its walls are thick and well ossified (Benoit et al., 2017a). The two
883 orbitosphenoids are long and fused in the midline to form a gutter that cradled the anteriormost
884 part of the tubular brain (Benoit et al., 2017a). The orbitosphenoid sutures with the prootic

caudally to close the lateral wall of the braincase. The bony labyrinth is completely separated from the brain cavity (Benoit et al., 2017a). The same degree of ossification of the braincase and bony labyrinth walls are also found in the alleged adult specimen NMQR 1702, whereas it is absent in the above-described juveniles. In CGS MJF 22, SAM-PK-K11126, and RC 55, no bony labyrinth could be segmented out because of the lack of fusion between the opisthotic and prootic and the absence of a medial wall on the inner ear capsule, and no ossified orbitosphenoid or epipterygoid are preserved. In addition, the supraorbital boss of NMQR 1702 is comparatively thinner and less developed than that of the *Lemurosaurus* holotype, despite the former being the larger specimen (Fig. 16). Sidor and Welman (2003) considered the differences between NMQR 1702 and the holotype (BP/1/816) to be the result of either intraspecific or ontogenetic variation. They gave preference to the ontogenetic explanation because of the great differences in cranial length and the comparatively larger orbit of the smaller specimen (BP/1/816), implying that BP/1/816 is a juvenile of the same species as NMQR 1702 (Sidor & Welman, 2003). From our observations and CT assisted re-assessment of these two specimens, it appears more likely that BP/1/816 and NMQR 1702 are at a similar stage of development and that BP/1/816 cannot be referred to a juvenile of the taxon represented by NMQR 1702.

Discussion

What are the reliable indicators of juvenility in Biarmosuchia?

Here we discuss characters that can be or have been considered in the literature as indicators of juvenile status, and their relevance in the context of biarmosuchian ontogeny at a suborder level.

Orbit size

908 Specimens CGS MJF 22 and BP/1/816 have large orbits relative to their skull lengths. This
909 character is commonly considered a juvenile characteristic in therapsids (Abdala, Flores &
910 Giannini, 2001; Giannini et al., 2010; Jasinoski & Chinsamy-Turan, 2012; Kruger et al., 2015;
911 Kruger, Rubidge & Abdala, 2017). In *Biarmosuchus*, the orbit remains similar in absolute size
912 during growth from the juvenile to adult stage but reduces in size relative to skull length
913 (Ivakhnenko, 1999, 2008). Recently, specimen BP/1/816 (*Lemurosaurus pricei*) was re-
914 identified as a juvenile specimen because of its comparatively large orbit and overall small size
915 (Sidor & Welman, 2003); however, as shown above, BP/1/816 displays many other traits that are
916 indicative of a maturity. This casts doubt on the reliability of relative orbit size as an indicator of
917 juvenility in biarmosuchians.
918 In extant species, a large eye diameter compared to skull length characterizes nocturnal
919 species, as it enhances sensitivity to light in low light conditions (Hall, 2008; Heesy & Hall,
920 2010; Schmitz & Wainwright, 2011). In extinct species, the dimensions of the eyeball can be
921 inferred from those of the sclerotic ring (optical ratio) (Hall, 2008; Schmitz & Motani, 2011).
922 The calculation of the optical ratio (a proxy to determine the light sensitivity of the eye) in
923 synapsids enabled Angielczyk and Schmitz (2014) to determine the diel activity pattern of many
924 species, including biarmosuchians. They concluded that most biarmosuchians had eyes adapted
925 to either a scotopic or mesopic environment, and were thus likely not diurnal. If nocturnality was
926 common in biarmosuchians, it is expected that many species may have developed larger orbits to
927 accommodate larger eyeballs, and it is reasonable to hypothesize that *Lemurosaurus pricei* may
928 be one of them. As such, a large orbit alone is not a reliable indicator of juvenility in
929 biarmosuchians as it could be related to specific diel activity, and should be backed with other
930 anatomical clues before concluding on a possible juvenile condition (see below).

931

932 **Tooth replacement**

933 Specimens SAM-PK-K11126 and RC 55 have erupting caniniforms positioned lingually and
934 posteriorly relative to the main row of teeth (Fig. 7 and 14). Until the present description
935 replacement canines had never been observed in biarmosuchians. In dinocephalians, *Moschops,*
936 *Tapinocaninus* and *Agnosaurus* show a pattern of tooth replacement (Boonstra, 1962; Whitney &
937 Sidor, 2019; Neumann, 2020). In dicynodonts, the presence of a supernumerary tusk is
938 considered pathological (Fröbisch, 2005; Jinnah & Rubidge, 2007; Fröbisch & Reisz, 2008). In
939 theriodonts (Gorgonopsia, Therocephalia and Cynodontia), replacement canines are found late in
940 ontogeny but are not found in the largest specimens (Kermack, 1956; Hopson, 1964; Van den
941 Heever, 1980; Norton, 2020; Norton et al., 2020) except for *Thrinaxodon* (Abdala, Jasinoski &
942 Fernandez, 2013). As such, double canines are expected to be found in, but are not exclusive to,
943 juveniles. Specimen CGS MJF 22, and the holotypes of *Lende chiweta* and *Lemurosaurus pricei*
944 do not show a replacement caniniform and as such, are better interpreted as mature specimens
945 compared to SAM-PK-K11126 and RC 55 (see Norton, 2020; Norton et al., 2020).

946 Notably SAM-PK-K11126 has two functional upper caniniforms, which is unusual among
947 Biarmosuchia (Sidor & Welman, 2003; Sidor & Rubidge, 2006; Day et al., 2018). In SAM-PK-
948 K11126 (Fig. 14), it is likely that the two caniniform teeth might have been functional at the
949 same time to some degree given that the two labial teeth are totally or partially erupted. One row
950 of replacement teeth is positioned posterolingually to the corresponding functional caniniform
951 (Fig. 14). The presence of two erupted maxillary caniniforms is considered a plesiomorphic
952 condition in synapsids as sphenacodontians present continuous replacement with two functional

maxillary caniniforms (Romer & Price, 1940; Van den Heever, 1980; Sigogneau-Russell, 1989; Norton, 2020; Norton et al., 2020).

Cranial bosses and pachyostosis

Pachyostosis is a non-pathological augmentation of the volume of the bone by an increase of deposit of periosteal cortices (de Buffrénil & Rage, 1993). Among biarmosuchians, cranial pachyostosis is present in burnetiamorphs, particularly on the cranial roof (Kulik and Sidor, 2019). In CGS MJF 22, SAM-PK-K11126, and RC 55, cranial ornamentation and pachyostosis are weakly developed (Figs. 1, 8, and 12). Low development of cranial ornamentation and pachyostosis have been linked to an early ontogenetic stage in various groups of therapsids, including dinocephalians and burnetiamorphs (Estes, 1961; Van Heerden, 1972; Ivakhnenko, 2008; Horner & Goodwin, 2009; Kammerer, 2011; Liu, 2013; Cassini, Flores & Vizcaíno, 2015; Kruger, Rubidge & Abdala, 2017; Kulik & Sidor, 2019). Ivakhnenko (2008) and Kruger, Rubidge & Abdala (2017) showed that in *Titanophoneus potens* and *Anteosaurus magnificus* the fronto-nasal ridge, supraorbital bosses, and pachyostosis developed between the juvenile and the adult conditions. The formation of cranial bosses in the anteosaurian genus *Sinophoneus* was also noted as a postnatal development (Liu, 2013). A similar ontogenetic development was observed for the bosses of *Estemmenosuchus uralensis* (Ivakhnenko 2008). In tapinocephalids, cranial pachyostosis develops while the relative size of the orbit and temporal fenestra shrinks during growth (Gregory & Broom, 1926; Boonstra & Broom, 1936; Boos et al., 2015; Neumann, 2020). Compared to the juvenile specimens studied here, adult burnetiamorphs show a higher degree of pachyostosis and cranial ornamentation (Figs. 15, 16 and 17). A low degree of pachyostosis thus appears to be linked to juvenility, whereas the higher degree of pachyostosis in MAL 290 and

976 BP/1/816 (Figs. 15 and 17), as well as the presence of well-formed cranial bosses (Fig. 16 and
977 17) suggest that these specimens are a lot more mature. However, pachyostosis and cranial
978 bosses are known to vary with phylogeny, as basal biarmosuchians display lower degree of
979 cranial pachyostosis and smaller cranial bosses than derived burnetiamorphs (Sidor & Rubidge,
980 2006; Day et al., 2018). Sexual dimorphism may also result in differences in cranial boss and
981 pachyostosis development (Lande, 1980; Kraaijeveld, Kraaijeveld-Smit & Komdeur, 2007;
982 Benoit et al., 2016; Gates, Organ & Zanno, 2016), although this has not been documented in
983 biarmosuchians. As such, cranial pachyostosis should not be considered in isolation as a means
984 to determine whether a biarmosuchian specimen is a juvenile.
985
986 **Radial vasculature pattern**
987 In pachycephalosaur dinosaurs, the presence of radial vasculature in the bones of the
988 pachyostotic cranial dome is indicative of juvenile status at the time of death, and overall
989 vascularization decreases with ontogeny and the growing of pachyostosis (Schott et al., 2011).
990 Radial vascular patterns in the cranial bones of dicynodonts have been interpreted similarly
991 (Jasinoski & Chinsamy-Turan, 2012) and similar radially arranged vascular canals are also
992 visible on CT images in the supraorbital bosses of CGS MJF 22 (Fig. 8-B). Using thin sections
993 and CT data, Kulik and Sidor (2019) also observed radial vasculature in the skull caps of some
994 juvenile and sub-adult burnetiamorphs. The presence of these patterns could not be confirmed in
995 SAM-PK-K11126 and RC 55 because their supraorbital bosses are not well preserved.
996 A radial vascular pattern has been interpreted as an adaptation to resist tensile constraints in
997 (Lee, 2004) but we find this an unlikely explanation in the case of CGS MJF 22 because the
998 supraorbital boss is not an attachment point for any muscle that could have generated such

tensile constraints (Benoit et al., 2016). Instead, because it occurs in combination with other characters (e.g., orbit size, a low degree of pachyostosis and other juvenile features), we interpret the radial vasculature patterns observed in CGS MJF 22 to be linked to the immature status of specimen. In MAL 290, NMQR 1702, and BP/1/816 (Figs. 15, 17 and 18), the supraorbital bosses are thick and dense, with no sign of a radial vasculature pattern, which suggests that their bosses were fully grown at the time of death.

Braincase and bony labyrinth ossification

In CGS MJF 22, SAM-PK-K11126, and RC 55 individual cranial bones are disarticulated as most sutures are wide open, which is commonly interpreted as a juvenile trait (Estes, 1961; Kermack, 1984; Rieppel, 1992; Schaefer et al., 2009; Giere et al., 2010; Sekiya & Dong, 2010). CT images through the braincase and bony labyrinth of CGS MJF 22 (not preserved in SAM-PK-K11126 and RC 55) reveal that these anatomical structures are not well ossified as the orbitosphenoid is absent (and was likely still cartilaginous), and the prootic and opisthotic are not fused (Fig. 19). An epipterygoid was not found in any of the juvenile specimens either. This contrasts with adult burnetiamorphs in which these structures are well co-ossified and solidly sutured to each other (Fig. 15; Benoit et al, 2017). In mammals the capsule of the bony labyrinth and the orbitosphenoid ossify early in ontogenetic development (Jeffery & Spoor, 2004; Ekdale, 2010; Koyabu et al., 2014; Spiekman & Werneburg, 2017; Sánchez-Villagra & Forasiepi, 2017), but in sauropsids this happens later and more slowly, if at all (Ngwenya et al., 2013; Neenan et al., 2019). The lack of ossification of these structures in CGS MJF 22 suggests that the development of the braincase and bony labyrinth had not yet reached maturity. The braincases of

1021 BP/1/816, MAL 290 and NMQR 1702 are fully ossified (Figs. 15, 17 and 18; Benoit et al, 2017),
1022 which is suggestive of cranial maturity.
1023
1024 **Fusion of the preparietals and internal parietal sutures**
1025 Adult biarmosuchians have an unpaired prepariental (Rubidge & Kitching, 2003; Rubidge,
1026 Sidor & Modesto, 2006; Sidor, 2003; Sidor, Hopson & Keyser, 2004; Smith, Rubidge & Sidor,
1027 2006; Sidor & Smith, 2007; Sidor & Welman, 2003; Marilao, Kulik & Sidor, 2020). This
1028 character is present in RC 55 and SAM-PK-K11126 (Figs. 3 and 12), but not in CGS MJF 22
1029 where the bone is paired (Figs. 8-B and 20). In addition, all juvenile specimens studied here
1030 share the presence of intraparietal sutures (except, maybe RC 55, in which this condition is
1031 unclear Fig. 3-A). The parietal of CGS MJF 22 is not only paired but comprises four parts (Figs.
1032 8-B and 20), while the parietal of SAM-PK-K1126 is made of six parts (Figs. 12 and 21). Based
1033 on their spatial configuration, none of these additional parts are homologous to the bones usually
1034 encountered in therapsids. As these sutures are symmetrical, they are unlikely cracks resulting
1035 from post-mortem damage (Figs. 20 and 21). From histological studies, Kulik & Sidor (2019)
1036 also observed this in the skull cap of a subadult burnetiamorph from Zambia (NHCC LB373)
1037 where the right parietal comprises two distinct bones.
1038 Supernumerary cranial bones (called wormian bones) have been reported in adult human
1039 skulls (Bellary et al., 2013) and are formed by the addition of extra ossification centres (da Mata,
1040 da Mata & Aversi-Ferreira, 2010; Bellary et al., 2013). Veterinary studies have also reported
1041 wormian bones in dogs (Linton, 1906). However, recent studies on adult and juvenile human
1042 skulls suggest that wormian bones are more likely due to congenital pathological conditions
1043 rather than ontogenetic variation (Marti et al., 2013; Nikolova et al., 2014a). In addition,

anomalous parietal sutures have been recognised in some modern human individuals (Hrdlička, 1903; Shapiro, 1972). These sutures, found on adult individuals, are perpendicular to the interparietal suture, and appear to be an anomalous rather than a juvenile feature (Shapiro, 1972). Unlike what would be expected in the case of wormian bones or post-mortem breakage, the condition in CGS MJF 22 and SAM-PK-K11126 is perfectly bilaterally symmetrical and radiates from the pineal foramen (instead of being perpendicular to the interparietal suture, or randomly distributed). As such, they are unlikely to be pathological or post-mortem damage.

Extra cranial bones have been observed in the skull of various juvenile dicynodonts and lycosuchid therocephalians (Estes, 1961; Van den Heever, 1980; Jasinoski et al., 2014; Kulik & Sidor, 2019; Marilao, Kulik & Sidor, 2020). For example, some supernumerary bones found in the nasal of a small-sized *Lystrosaurus* specimen have been tentatively homologized to the anterior process of the frontal and been hypothetically linked to their juvenile condition (Jasinoski et al., 2014). Amongst the Cynodontia, two small specimens of *Thrinaxodon liorhinus* (UCMP 42878 and UCMP 42877) possess a divided interparietal (Estes, 1961; Van Heerden, 1972). The extra intraparietal bones of CGS MJF 22 and SAM-PK-K11126 resemble the Os Incae (or Inca bones) that are present in a small fraction of modern human populations (Shapiro & Robinson, 1976; Hanihara & Ishida, 2001; Wu et al., 2011; Thanapaisal et al., 2013; Nikolova et al., 2014b). This condition usually results in a non-symmetrical division of the supraoccipital in humans; however, in some rare cases, this division can be symmetrical and results in radiating sutures, just like in CGS MJF 22 and SAM-PK-K11126 (Hanihara & Ishida, 2001: Figs. 2b and 5). In humans the presence of an interparietal is the result of the persistence of the Mendosal fontanel in adults (Wu et al., 2011) which supports the contention that the condition observed in CGS MJF 22 and SAM-PK-K11126 is a juvenile feature. The Inca bones, which in mammals

normally fuse to form the interparietal bone (e.g. artiodactyls, hyracoids) or fuse to either the supraoccipital (e.g. humans) or parietal (e.g. possum, sirenians), comprises two to four pairs of ossification (Wu et al., 2011; Koyabu, Maier & Sánchez-Villagra, 2012; Nikolova et al., 2014b,a); which is reminiscent of the condition in the parietal of CGS MJF 22.

Accordingly, we interpret the presence of intraparietal sutures and the absence of interparietal fusion as a manifestation of the juvenile status of our specimens, each resulting bone probably being an independent centre of ossification of the parietal bone normally observed in adult specimens (Figs. 20, 21). That this phenomenon is a real anatomical feature, and not the result of some taphonomic processes or CT scanning artefact, is demonstrated by the study of the histological sections made by Kulik & Sidor (2019:Fig. 1-I), who found the same results as the present work. The variable number of centres of ossifications is not abnormal given the diversity of Inca bone patterns observed in modern humans (Hanihara & Ishida, 2001; Wu et al., 2011). It appears that this condition is relatively common in juvenile burnetiamorphs (and perhaps biarmosuchians in general), but has not previously been observed in other therapsids with the the exception of the few specimens recently studied by Kulik & Sidor (2019) and Marilao, Kulik & Sidor (2020).

Conclusion on ontogenetic characters

It is important to point out that the characters presented in this discussion cannot be considered on their own, but rather that a combination of morphological features should be considered in a specimen to assess its ontogenetic status. The general size of the specimen and its orbit diameter in comparison to the basal skull length is often a good sign of juvenility, but can also reflect the lifestyle of the animal (eg. nocturnality). In modern mammals, the presence of

replacement teeth is usually an indication of immaturity. By contrast, non-mammalian therapsids were likely replacing their teeth throughout their life, although it is possible that some taxa, such as *Galesaurus*, might have experienced replacement of the canine only up to the subadult stage. This variability of tooth replacement pattern between genera and species might have occurred in Biarmosuchia. The degree of development of cranial bosses and pachyostosis is traditionally interpreted as ontogenetic, but can vary between lineages and within species (eg. sexual dimorphism). The degree of ossification of the braincase region is rather a strong argument to assess the ontogenetic stage of the specimen, but like in extant species, the timing of ossification of the different internal bones is taxon dependant. The presence of intra-bone sutures is rarely observed in extinct and extant species, especially on the parietal, but, when not pathological, this has been observed in immature specimens only.

A hypothetical biarmosuchian ontogenetic series

As demonstrated above there are a number of clues from cranial morphology that, when considered together, enable recognition of a juvenile burnetiamorph: the presence of two caniniform teeth on the upper jaw; incomplete cranial fusion; low degree of pachyostosis and cranial ornamentation (bosses and ridges small or absent); and the presence of a paired preparietal and subdivisions of the parietal. A sizable orbit relative to skull length and a relatively short snout are not reliable juvenile characters on their own as they can be the result of interspecific allometry.

Here we propose a hypothetical ontogenetic sequence of the Biarmosuchia based on the anatomical data from the actual specimens studied and literature presented above (Fig. 22). It is

challenging to build a complete ontogenetic series of an extinct higher ranked taxon as the order of closure of the sutures is likely to be variable among the lower ranked taxa. As such, our hypothetical model focuses on the occurrence of different centres of ossification, the presence and relative size of cranial bosses and ridges, and the overall proportions of the different parts of the skull. Two ontogenetic directions are reconstructed depending on whether the species considered is a burnetiamorph or a non-burnetiamorph biarmosuchian (Fig. 22). In green are reconstructed stages that we postulate for all biarmosuchians and in red are ontogenetic stages that would pertain only to burnetiamorphs.

Beginning with a hypothetical juvenile stage (stage 0 on Fig. 22; sutures visible within the parietal, preparietal paired, no cranial ornamentation visible, replacement caniniforms present as in CGS MJF 22), we identified two different juvenile stages before the adult stage. In stage 1 (Fig. 22), the preparietal fuses, and the supraorbital bosses and naso-frontal ridge then begins to grow (only in burnetiamorphs). This stage is exemplified by SAM-PK-K11126. In stage 2 (Fig. 22), the intraparietal sutures may fuse, and cranial ornamentation becomes larger (in burnetiamorphs only). According to the model, this stage corresponds to the status of RC 55. Finally, the possible adult stage (stage 3 in Fig. 22) is be marked by the absence of replacement caniniforms, significant elongation of the snout and enlargement of the temporal fenestra. In burnetiamorphs cranial ornaments lose their radial vasculature, the skull roof is fully pachyostotic, and the braincase and bony labyrinth become completely ossified. According to this model, the development of cranial pachyostosis occurs after complete ossification of the preparietal and parietal, which concurs with the conclusions made by Kulik & Sidor (2019).

This hypothetical series could be tested in the future by the discovery of a single species ontogenetic series.

Reconsideration of *Lemurosaurus* Broom, 1949?

In contrast to the situation in the juvenile specimens described above, both the braincase and the bony labyrinth of BP/1/816 (holotype of *Lemurosaurus pricei*) are well ossified (Fig. 15; Benoit et al., 2017) and they are even more extensively ossified than in the largest specimen (NMQR 1702) attributed to *Lemurosaurus pricei* (Fig. 19; Benoit et al., 2017b). Most cranial sutures of the holotype are completely fused and cannot be determined, even on the CT images (Fig. 15). In contrast to the juvenile biarmosuchian specimens described above, the supraorbital bosses are well developed, show no radial vasculature (Figs. 15 and 16-A). More importantly, no replacement canine is present, which is only found otherwise in the most mature (such as the holotype of *Lende chiweta*), and largest specimens in other therapsid taxa (Norton, 2020). This supports the idea that the holotype of *Lemurosaurus pricei* (BP/1/816), despite having very large orbits and a relatively short snout, is an adult (contra Sidor and Welman 2003). As stated above, the large size of the orbit is not a reliable indicator of juvenility in biarmosuchians. The only characters left supporting that BP/1/816 may be a juvenile are thus its small cranial length and short snout, two characters that are also expected to occur in dwarf species of a given taxon (Reynoso & Clark, 1998). As such, given the comparatively large amount of evidence suggesting that BP/1/816 is an adult, the juvenile hypothesis is untenable. Specimen NMQR 1702, one of the best preserved biarmosuchian specimens, comprises a large skull with lower jaw that were described as an adult specimen of *Lemurosaurus pricei* by Sidor & Welman (2003). Compared to the holotype of *Lemurosaurus* (BP/1/816), NMQR 1702 has a much longer snout (115 mm) and the size of the orbit is smaller (35 mm) relative to skull length, with an orbit to basal skull length ratio of 0.3 (Fig. 16). In contrast to BP/1/816, which has six postcanines, the maxilla of

NMQR 1702 bears only three or four teeth (Sidor & Welman, 2003). If BP/1/816 is a juvenile representative of the same taxon as NMQR 1702, this would imply that the number of post-canine teeth decreasd during ontogeny, whereas jaw length increased. Though counterintuitive, such a reduction has been anecdotally hypothesized in gorgonopsians (Sigogneau (1970), who, in contrast, found that the dental formula remains constant) but dedicated studies are lacking. Two zygomatic bosses are present in NMQR1702, whereas there is only one in BP/1/816 (Fig. 16). The supraorbital boss of NMQR 1702 is comparatively thinner and less developed than that of the *Lemurosaurus* holotype (Fig. 16). In the holotype the highest point on the skull roof is above the centre of the orbit, whereas the highest point in NMQR 1702 is behind the orbit (Fig. 16). The skull roof of NMQR 1702 has a long midline crest extending from the nasal to the parietal foramen, whereas the holotype of *Lemurosaurus pricei* has only a little boss at the level of the orbit (Fig. 16). The pineal boss of NMQR 1702 is a well-defined chimney, whereas that of the *Lemurosaurus* holotype is a smooth dome-like structure (Fig. 16).

In occipital view, the external occipital ridge of NMQR 1702 extends ventrally across the postparietal and supraoccipital from the skull roof to the foramen magnum. In the holotype, this ridge is confined to the postparietal. In addition, NMQR 1702 possesses a nubbin-like boss on the dorsal apex of the lateral temporal fenestra; a low-developed boss on the anteroventral margin of the temporal fenestra, and two bosses on the zygomatic bar; characters that are absent on the holotype.

Considering the number and nature of the anatomical differences between BP/1/816 and NMQR 1702, and given that BP/1/816 might be an adult individual, it is unlikely that these differences represent intraspecific variation and it is more likely that NMQR 1702 represents a

different taxon, distinct from *Lemurosaurus pricei*. The creation of a new nomenclatorial combination for NMQR 1702 might be taken into consideration in the future.

Similarly, MAL 290, the holotype of *Lende Chiweta*, which has relatively large orbits in comparison to the skull length, was previously identified as a possible juvenile (Kruger et al., 2015). However, it displays well-developed cranial ornamentation and no visible replacement caniniforms, which are probably indicative of an adult, very mature age (Fig. 17). Along with BP1/816, MAL 290 suggests that a paedomorphic cranial morphology (large orbit, short snout) might have been common among adult burnetiamorphs. As discussed above, large orbits may have been an adaptation to a nocturnal lifestyle in biarmosuchians (Angielczyk & Schmitz, 2014), but further study will be necessary to better understand the cause of such dramatic interspecific allometry.

Conclusion

The discovery of new immature biarmosuchian cranial material and its study has lead to a better understanding of ontogenetic variation within the clade. We found that the presence of multiple centres of ossification in the bones of the skull roof is unique to juvenile biarmosuchians and a reliable indicator of an immature individual in addition to the presence of a replacement canine, poorly developed cranial ornamentation and pachyostosis, and poorly ossified braincase and bony labyrinth. In contrast, the reliability of other previously recognised possible juvenile characters, such as the presence of relatively large orbits, is questioned. Some of these juvenile features are currently used in character matrices for phylogenetic analysis and need to be reconsidered in light of the ontogenetic and intraspecific variations highlighted in this contribution.

Acknowledgements

We acknowledge the assistance of Charlton Dube and Sifelani Jirah with preparation, Kudakwashe Jakata for performing the scans, and the Council for Geosciences in Pretoria, the National Museum in Bloemfontein, the Rubidge Collection and the Iziko South African Museum for the loan of specimens. We express our gratitude for financial assistance to the National Research Foundation (NRF), South Africa; the Paleontological Scientific Trust (PAST) and its Scatterlings of Africa program; the African Origins Program (AOP) of the National Research Foundation (NRF), South Africa, and the University of the Witwatersrand, Johannesburg, South Africa. We are grateful to Paul Tafforeau at the European Synchrotron Radiation Facility (ESRF), Grenoble, France, for providing assistance in using beamline ID17. We acknowledge Gilles Cuny, Jérémy Martin, Nour-Eddine Jalil and Christian Sidor for their constructive comments on the study and the manuscript. We thank Christian Kammerer, Luisa Pusch, Claudia Marsicano, Jörg Fröbisch and an anonymous reviewer for editing and reviewing the manuscript.

References

Abdala F, Flores DA, Giannini NP. 2001. Postweaning ontogeny of the skull of *Didelphis albiventris*. *Journal of Mammalogy* 82:190–200.

Abdala F, Jasinoski SC, Fernandez V. 2013. Ontogeny of the Early Triassic cynodont *Thrinaxodon liorhinus* (Therapsida): dental morphology and replacement. *Journal of Vertebrate Paleontology* 33:1408–1431.

Angielczyk KD, Schmitz L. 2014. Nocturnality in synapsids predates the origin of mammals by over 100 million years. *Proceedings of the Royal Society of London B: Biological Sciences* 281:20141642.

Bellary SS, Steinberg A, Mirzayan N, Shirak M, Tubbs RS, Cohen-Gadol AA, Loukas M. 2013. Wormian bones: a review. *Clinical Anatomy* 26:922–927.

Benoit J. 2019. Parental care or opportunism in South African Triassic cynodonts? *South African Journal of Science* 115:1–2.

Benoit J, Fernandez V, Manger PR, Rubidge BS. 2017a. Endocranial casts of pre-mammalian therapsids reveal an unexpected neurological diversity at the deep evolutionary root of mammals. *Brain, behavior and evolution* 90:311–333.

Benoit J, Manger PR, Fernandez V, Rubidge BS. 2016. Cranial Bosses of *Choerosaurus dejageri*

(Therapsida, Therocephalia): Earliest Evidence of Cranial Display Structures in Eutheriodonts. *PLoS One* 11:e0161457.
Benoit J, Manger PR, Fernandez V, Rubidge BS. 2017b. The bony labyrinth of late Permian Biarmosuchia: palaeobiology and diversity in non-mammalian Therapsida.
Boonstra LD. 1962. The dentition of the titanosuchian dinocephalians. *Annals of the South African Museum* 46:57–112.
Boonstra LD, Broom R. 1936. *The cranial morphology of some titanosuchid deinocephalians*. American Museum of Natural History.
Boos ADS, Kammerer CF, Schultz CL, Neto VP. 2015. A tapinocephalid dinocephalian (Synapsida, Therapsida) from the Rio do Rasto Formation (Paraná Basin, Brazil): taxonomic, ontogenetic and biostratigraphic considerations. *Journal of South American Earth Sciences* 63:375–384.
Broom R. 1913. On some new carnivorous therapsids. *Bulletin of the American Museum of Natural History* 32.
Broom R. 1942. Evidence of a new sub-order of mammal-like reptiles. *South African Museums Association Bulletin* 2:386.
Broom R. 1949. New fossil reptile genera from the Bernard Price collection. *Annals of the Transvaal Museum* 21:187–194.
de Buffrénil V, Rage J-C. 1993. La «pachyostose» vertébrale de *Simoliophis* (Reptilia, Squamata): données comparatives et considérations fonctionnelles [Pachyostosis of the vertebral column of *Simoliophis* (Reptilia: Squamata): comparative data and functional morphology]. *Annales de paléontologie* 79:315–335.
Cassini GH, Flores DA, Vizcaíno SF. 2015. Postnatal ontogenetic scaling of pampas deer (Ozotoceros bezoarticus celer: Cervidae) cranial morphology. *Mammalia* 79:69–79.
Day MO, Ramezani J, Bowring SA, Sadler PM, Erwin DH, Abdala F, Rubidge BS. 2015. When and how did the terrestrial mid-Permian mass extinction occur? Evidence from the tetrapod record of the Karoo Basin, South Africa. In: *Proc. R. Soc. B*. The Royal Society, 20150834.
Day MO, Rubidge BS. 2019. Biesiespoort revisited: a case study on the relationship between tetrapod assemblage zones and Beaufort lithostratigraphy south of Victoria West. *Palaeontologia Africana* 53:55–65.
Day MO, Rubidge BS, Abdala F. 2016. A new mid-Permian burnetiamorph therapsid from the Main Karoo Basin of South Africa and a phylogenetic review of Burnetiamorpha. *Acta Palaeontologica Polonica* 61:701–719.
Day MO, Smith RMH. 2020. Biostratigraphy of the Endothiodon Assemblage Zone (Beaufort Group, Karoo Supergroup), South Africa. *South African Journal of Geology* 123:165–180.
Day MO, Smith RMH, Benoit J, Fernandez V, Rubidge BS. 2018. A new species of Burnetiid (Therapsida, Burnetiamorpha) from the early Wuchiapingian of South Africa and implications for the evolutionary ecology of the family Burnetiidae. *Papers in Palaeontology*:1–23.
Duhamel A, Benoit J, Day MO, Rubidge BS. 2016. A new juvenile burnetiamorph (Therapsida: Biarmosuchia) skull from the Beaufort Group, South Africa and its role in a revision of *Lemurosaurus pricei* Broom, 1949. The Palaetolongical Association Annual Meeting with Program 54
Duhamel A, Benoit J, Rubidge BS. 2018. Juvenile Biarmosuchians from the Karoo Beaufort Group Shed New Light on Basal Therapsid Ontogeny. Palaontological Society of Southern Africa Annual Meeting
Ekdale EG. 2010. Ontogenetic variation in the bony labyrinth of *Monodelphis domestica*

(Mammalia: Marsupialia) following ossification of the inner ear cavities. *The Anatomical Record* 293:1896–1912.
Estes R. 1961. Cranial anatomy of the cynodont reptile *Thrinaxodon liorhinus*. *Bulletin of the Museum of Comparative Zoology at Harvard College*.
Fröbisch J. 2005. A double-tusked dicynodont therapsid-pathology, variability, or a new species? In: *Journal of Vertebrate Paleontology*. 61A-61A.
Fröbisch J, Reisz RR. 2008. A new species of *Emydops* (Synapsida, Anomodontia) and a discussion of dental variability and pathology in dicynodonts. *Journal of Vertebrate Paleontology* 28:770–787.
Gates TA, Organ C, Zanno LE. 2016. Bony cranial ornamentation linked to rapid evolution of gigantic theropod dinosaurs. *Nature communications* 7:1–10.
Giannini NP, Segura V, Giannini MI, Flores D. 2010. A quantitative approach to the cranial ontogeny of the puma. *Mammalian Biology-Zeitschrift für Säugetierkunde* 75:547–554.
Giere P, Möller L, Hilger A, Paulke A, Riesemeier H, Kuehbacher M. 2010. Modern and classic approaches towards revealing the orbital mosaic in the common shrew *Sorex araneus* Linnaeus, 1758 (Soricidae, Lipotyphla, Mammalia). *Zoosystematics and Evolution* 86:343–350.
Gregory WK, Broom R. 1926. *The skeleton of Moschops capensis broom: A Dinocephalian reptile from the Permian of South Africa*. The American Museum of Natural History.
Hall MI. 2008. The anatomical relationships between the avian eye, orbit and sclerotic ring: implications for inferring activity patterns in extinct birds. *Journal of Anatomy* 212:781–794.
Hanihara T, Ishida H. 2001. Os incae: variation in frequency in major human population groups. *Journal of Anatomy* 198:137–152.
Heesy CP, Hall MI. 2010. The nocturnal bottleneck and the evolution of mammalian vision. *Brain, behavior and evolution* 75:195–203.
Hoffman EA, Rowe TB. 2018. Jurassic stem-mammal perinates and the origin of mammalian reproduction and growth. *Nature* 561:104–108.
Hopson JA. 1964. Tooth replacement in cynodont, dicynodont and therocephalian reptiles. In: *Proceedings of the Zoological Society of London*. 625–654.
Hopson J, Barghusen H. 1986. An analysis of therapsid relationships. *The ecology and biology of mammal-like reptiles*:83–106.
Horner JR, Goodwin MB. 2009. Extreme cranial ontogeny in the Upper Cretaceous dinosaur *Pachycephalosaurus*. *PLoS One* 4:e7626.
Hrdlička A. 1903. *Divisions of the Parietal Bone in Man & Other Mammals*. order of the Trustees, American Museum of Natural History.
Huttenlocker AK, Abdala F. 2015. Revision of the first therocephalian, *Theriognathus* Owen (Therapsida: Whaitsiidae), and implications for cranial ontogeny and allometry in nonmammaliaform eutheriodonts. *Journal of Paleontology* 89:645–664.
Ivakhnenko MF. 1999. Biarmosuches from the Ocher faunal assemblage of eastern Europe. *Paleontological Journal* 33:289–296.
Ivakhnenko MF. 2003. Eotherapsids from the east European placket (Late Permian). *Paleontological Journal* 37.
Ivakhnenko MF. 2008. Cranial morphology and evolution of Permian Dinomorpha (Eotherapsida) of eastern Europe. *Paleontological Journal* 42:859–995.
Iwaniuk AN, Heesy CP, Hall MI. 2010. Morphometrics of the eyes and orbits of the nocturnal swallow-tailed gull (*Creagrus furcatus*). *Canadian journal of zoology* 88:855–865.
Jasinoski SC, Abdala F. 2017a. Cranial ontogeny of the Early Triassic basal cynodont

Galesaurus planiceps. *The Anatomical Record* 300:353–381.
Jasinoski SC, Abdala F. 2017b. Aggregations and parental care in the Early Triassic basal cynodonts *Galesaurus planiceps* and *Thrinaxodon liorhinus*. *PeerJ* 5:e2875.
Jasinoski SC, Abdala F, Fernandez V. 2015. Ontogeny of the Early Triassic cynodont *Thrinaxodon liorhinus* (Therapsida): cranial morphology. *The Anatomical Record* 298:1440–1464.
Jasinoski SC, Chinsamy-Turan A. 2012. Biological inferences of the cranial microstructure of the dicynodonts *Oudenodon* and *Lystrosaurus*. *Forerunners of Mammals—Radiation, Histology, Biology. Indiana University Press, Bloomington*:149–176.
Jasinoski SC, Cluver MA, Chinsamy A, Reddy BD. 2014. Anatomical plasticity in the snout of *Lystrosaurus*. In: *Early evolutionary history of the Synapsida*. Springer, 139–149.
Jeffery N, Spoor F. 2004. Prenatal growth and development of the modern human labyrinth. *Journal of Anatomy* 204:71–92.
Jinnah ZA, Rubidge B. 2007. A double-tusked dicynodont and its biostratigraphic significance. *South African Journal of Science* 103:51–53.
Kammerer CF. 2011. Systematics of the Anteosauria (Therapsida: Dinocephalia). *Journal of Systematic Palaeontology* 9:261–304.
Kammerer CF. 2016. Two unrecognised burnetiamorph specimens from historic Karoo collections. *Palaeontologia Africana* 50:64–75.
Kammerer CF, Sidor CA. 2021. A new burnetiid from the middle Permian of Zambia and a reanalysis of burnetiamorph relationships. *Papers in Palaeontology*.
Kemp TS. 2006. The origin and early radiation of the therapsid mammal-like reptiles: a palaeobiological hypothesis. *Journal of evolutionary biology* 19:1231–1247.
Kermack KA. 1956. Tooth replacement in mammal-like reptiles of the suborders Gorgonopsia and Therocephalia. *Philosophical Transactions of the Royal Society of London. Series B, Biological Sciences* 240:95–133.
Kermack D. 1984. New prosauropod material from South Wales. *Zoological Journal of the Linnean Society* 82:101–117.
Koyabu D, Maier W, Sánchez-Villagra MR. 2012. Paleontological and developmental evidence resolve the homology and dual embryonic origin of a mammalian skull bone, the interparietal. *Proceedings of the National Academy of Sciences* 109:14075–14080.
Koyabu D, Werneburg I, Morimoto N, Zollikofer CP, Forasiepi AM, Endo H, Kimura J, Ohdachi SD, Son NT, Sánchez-Villagra MR. 2014. Mammalian skull heterochrony reveals modular evolution and a link between cranial development and brain size. *Nature communications* 5:1–9.
Kraaijeveld K, Kraaijeveld-Smit FJ, Komdeur J. 2007. The evolution of mutual ornamentation. *Animal Behaviour* 74:657–677.
Krone IW, Kammerer CF, Angielczyk KD. 2019. The many faces of synapsid cranial allometry. *Paleobiology* 45:531–545.
Kruger A, Rubidge BS, Abdala F. 2017. A juvenile specimen of *Anteosaurus magnificus* Watson, 1921 (Therapsida: Dinocephalia) from the South African Karoo, and its implications for understanding dinocephalian ontogeny. *Journal of Systematic Palaeontology* 16:139–158.
Kruger A, Rubidge BS, Abdala F, Chindebvu EG, Jacobs LL. 2015. *Lende chiweta*, a new therapsid from Malawi, and its influence on burnetiamorph phylogeny and biogeography. *Journal of Vertebrate Paleontology* 35.
Kulik ZT, Sidor CA. 2019. The original boneheads: histologic analysis of the pachyostotic skull

roof in Permian burnetiamorphs (Therapsida: Biarmosuchia). *Journal of Anatomy*.
Lande R. 1980. Sexual dimorphism, sexual selection, and adaptation in polygenic characters. *Evolution*:292–305.
Lee AH. 2004. Histological organization and its relationship to function in the femur of *Alligator mississippiensis*. *Journal of Anatomy* 204:197–207.
Linton RG. 1906. On some anomalies in the skull of the dog. *The Veterinary Journal* 62:228–232.
Liu J. 2013. Osteology, ontogeny, and phylogenetic position of *Sinophoneus yumenensis* (Therapsida, Dinocephalia) from the Middle Permian Dashankou Fauna of China. *Journal of Vertebrate Paleontology* 33:1394–1407.
Liu J, Rubidge B, Li J. 2009. New basal synapsid supports Laurasian origin for therapsids. *Acta Palaeontologica Polonica* 54:393–400.
Marilao LM, Kulik ZT, Sidor CA. 2020. Histology of the prepariental: a neomorphic cranial element in dicynodont therapsids. *Journal of Vertebrate Paleontology*:e1770775.
Marti B, Sirinelli D, Maurin L, Carpentier E. 2013. Wormian bones in a general paediatric population. *Diagnostic and interventional imaging* 94:428–432.
da Mata JR, da Mata FR, Aversi-Ferreira TA. 2010. Analysis of bone variations of the occipital bone in man. *International Journal of Morphology* 28:243–248.
Mirone A, Brun E, Gouillart E, Tafforeau P, Kieffer J. 2014. The PyHST2 hybrid distributed code for high speed tomographic reconstruction with iterative reconstruction and a priori knowledge capabilities. *Nuclear Instruments and Methods in Physics Research Section B: Beam Interactions with Materials and Atoms* 324:41–48.
Neenan JM, Chapelle KE, Fernandez V, Choiniere JN. 2019. Ontogeny of the *Massospondylus* labyrinth: implications for locomotory shifts in a basal sauropodomorph dinosaur. *Palaeontology* 62:255–265.
Neumann S. 2020. Taxonomic revision of the short-snouted tapinocephalid dinocephalia (Amniota- Therapsida)- The key to understanding Middle Permian tetrapod biodiversity. University of the Witwatersrand.
Ngwenya A, Patzke N, Spocter MA, Kruger J-L, Dell L-A, Chawana R, Mazengenya P, Billings BK, Olaleye O, Herculano-Houzel S. 2013. The continuously growing central nervous system of the Nile crocodile (*Crocodylus niloticus*). *The Anatomical Record* 296:1489–1500.
Nikolova SY, Toneva DH, Yordanov YA, Lazarov NE. 2014a. Multiple Wormian bones and their relation with definite pathological conditions in a case of an adult cranium. *Anthropologischer Anzeiger* 71:169–190.
Nikolova S, Toneva D, Yordanov Y, Lazarov N. 2014b. Variations in the squamous part of the occipital bone in medieval and contemporary cranial series from Bulgaria. *Folia Morphologica* 73:429–438.
Norton L. 2020. Tooth replacement patterns in Eutheriodontia (Synapsida, Therapsida) from the South African Karoo Supergroup. University of the Witwatersrand.
Norton LA, Abdala F, Rubidge BS, Botha J. 2020. Tooth replacement patterns in the Early Triassic epicynodont *Galesaurus planiceps* (Therapsida, Cynodontia). *Plos one* 15:e0243985.
Paganin D, Mayo SC, Gureyev TE, Miller PR, Wilkins SW. 2002. Simultaneous phase and amplitude extraction from a single defocused image of a homogeneous object. *Journal of Microscopy* 206:33–40.
Reynoso V-H, Clark JM. 1998. A dwarf sphenodontian from the Jurassic La Boca formation of Tamaulipas, México. *Journal of Vertebrate Paleontology* 18:333–339.

Rieppel O. 1992. The skeleton of a juvenile *Lanthanotus* (Varanoidea). *Amphibia-Reptilia* 13:27–34.
Romer AS, Price LW. 1940. Review of the Pelycosauria. *Geological Society of America Special Papers* 28:1–534.
Rubidge BS, Kitching JW. 2003. A new burnetiamorph (Therapsida: Biarmosuchia) from the lower Beaufort Group of South Africa. *Palaeontology* 46:199–210.
Rubidge BS, Sidor CA. 2001. Evolutionary patterns among Permo-Triassic therapsids. *Annual Review of Ecology and Systematics* 32:449–480.
Rubidge BS, Sidor CA. 2002. On the cranial morphology of the basal therapsids Burnetia and Proburnetia (Therapsida: Burnetiidae). *Journal of Vertebrate Paleontology* 22:257–267.
Rubidge BS, Sidor CA, Modesto SP. 2006. A new burnetiamorph (Therapsida: Biarmosuchia) from the middle Permian of South Africa. *Journal of Paleontology* 80:740–749.
Sánchez-Villagra MR, Forasiepi AM. 2017. On the development of the chondrocranium and the histological anatomy of the head in perinatal stages of marsupial mammals. *Zoological letters* 3:1.
Schaefer M, Black SM, Schaefer MC, Scheuer L. 2009. *Juvenile osteology*. Elsevier.
Schmitz L, Motani R. 2011. Nocturnality in dinosaurs inferred from scleral ring and orbit morphology. *Science* 332:705–708.
Schmitz L, Wainwright PC. 2011. Nocturnality constrains morphological and functional diversity in the eyes of reef fishes. *BMC Evolutionary Biology* 11:338.
Schott RK, Evans DC, Goodwin MB, Horner JR, Brown CM, Longrich NR. 2011. Cranial ontogeny in *Stegoceras validum* (Dinosauria: Pachycephalosauria): a quantitative model of pachycephalosaur dome growth and variation. *PLoS One* 6:e21092.
Sekiya T, Dong Z. 2010. A New Juvenile Specimen of *Lufengosaurus* Huenei Young, 1941 (Dinosauria: Prosauropoda) from the Lower Jurassic Lower Lufeng Formation of Yunnan, Southwest China. *Acta Geologica Sinica-English Edition* 84:11–21.
Shapiro R. 1972. Anomalous parietal sutures and the bipartite parietal bone. *American Journal of Roentgenology* 115:569–577.
Shapiro R, Robinson F. 1976. The os incae. *American Journal of Roentgenology* 127:469–471.
Sidor CA. 2003. The naris and palate of *Lycaenodon longiceps* (Therapsida: Biarmosuchia), with comments on their early evolution in the therapsida. *Journal of Paleontology* 77:977–984.
Sidor CA, Hopson JA, Keyser AW. 2004. A new burnetiamorph therapsid from the Teekloof Formation, Permian, of South Africa. *Journal of Vertebrate Paleontology* 24:938–950.
Sidor CA, Rubidge BS. 2006. *Herpetoskylax hopsoni*, a new biarmosuchian (Therapsida: Biarmosuchia) from the Beaufort Group of South Africa. *Amniote paleobiology: Perspectives on the evolution of mammals, birds, and reptiles*:76–113.
Sidor CA, Smith RM. 2007. A second burnetiamorph therapsid from the Permian Teekloof Formation of South Africa and its associated fauna. *Journal of Vertebrate Paleontology* 27:420–430.
Sidor CA, Welman J. 2003. A second specimen of *Lemurosaurus pricei* (Therapsida: Burnetiamorpha). *Journal of Vertebrate Paleontology* 23:631–642.
Sigogneau D. 1970. *Révision systématique des Gorgonopsiens Sud-Africains [Systematic revision of the south african gorgonopsians]*. Éditions du Centre national de la recherche scientifique, Paris (in French).
Sigogneau-Russell D. 1989. *Theriodontia 1: Phthinosuchia, Eotitanosuchia, Gorgonopsia*. Gustav Fischer Verlag, Stuttgart.

Smith RM, Rubidge BS, Sidor CA. 2006. A new burnetiid (Therapsida: Biarmosuchia) from the Upper Permian of South Africa and its biogeographic implications. *Journal of Vertebrate Paleontology* 26:331–343.
Spiekman SN, Werneburg I. 2017. Patterns in the bony skull development of marsupials: high variation in onset of ossification and conserved regions of bone contact. *Scientific Reports* 7:43197.
Thanapaisal C, Duangthongpon P, Kitkuandee A, Chaiciwamongkol K, Morthong V. 2013. Incidence and variation of interpretably bone (os incae) in northeastern Thailand. *Journal of the Medical Association of Thailand* 96:S117–S123.
Van den Heever JA. 1980. On the validity of the therocephalian Family Lycosuchidae (Reptilia, Therapsida). South African Museum.
Van Heerden J. 1972. Interspecific variation and growth changes in the cynodont reptile *Thrinaxodon liorhinus*. *Navorsinge van die Nasionale Museum Bloemfontein* 2:307–347.
Whitney MR, Sidor CA. 2019. Histological and developmental insights into the herbivorous dentition of tapinocephalid therapsids. *PloS One* 14:e0223860.
Wu JK, Goodrich JT, Amadi CC, Miller T, Mulliken JB, Shanske AL. 2011. Interparietal bone (Os Incae) in craniosynostosis. *American Journal of Medical Genetics Part A* 155:287–294.

Figure 1

Holotype of *Rubidgina angusticeps*, here considered Biarmosuchia indet., RC 55.

Photograph (left) and 3D rendering (right). (**A**) Right lateral view. (**B**) Left lateral view. (**C**) Occipital view. (**D**) Dorsal view. (**E**) Ventral view. **Anatomical Abbreviations –ang**, angular; **art**, articular; **aso**, anterior extension of the supraoccipital; **bo**, basioccipital; **c**, caniniform tooth; **co**, occipital condyle; **cor**, coronoid; **d**, dentary; **ect**, ectopterygoid; **eo**, exoccipital; **f**, frontal; **fe**, temporal fenestra; **fm**, foramen magnum; **i**, incisiform tooth; **j**, jugal; **l**, lacrimal; **m**, maxilla; **n**, nasal; **o**, orbit; **op**, opisthotic; **p**, parietal; **pa**, anterior portion of the parietal; **pac**, caudal portion of the parietal; **pal**, palatine; **pal t**, palate teeth; **pao**, paroccipital process; **part**, pre-articular; **pbs**, parabasisphenoid; **pc**, postcanine; **pf**, postfrontal; **pif**, pineal foramen; **pl**, lateral portion of the parietal; **pm**, premaxilla; **po**, postorbital; **pp**, postparietal; **prf**, prefrontal; **pro**, prootic; **prp**, preparietal; **pt**, pterygoids; **ptf**, post-temporal fenestra; **q**, quadrate; **qj**, quadratojugal; **rt**, replacement tooth; **sb**, supraorbital boss; **scl**, sclerotic ring; **smx**, septomaxilla; **so**, supraoccipital; **spl**, splenial; **st**, stapes; **sq**, squamosal; **sur** surangular; **t**, tabular; **v**, vomer. Pictures by A. Duhamel. 3D reconstructions were made by A. Duhamel and belong to the University of the Witwatersrand. Scale bar=1cm.

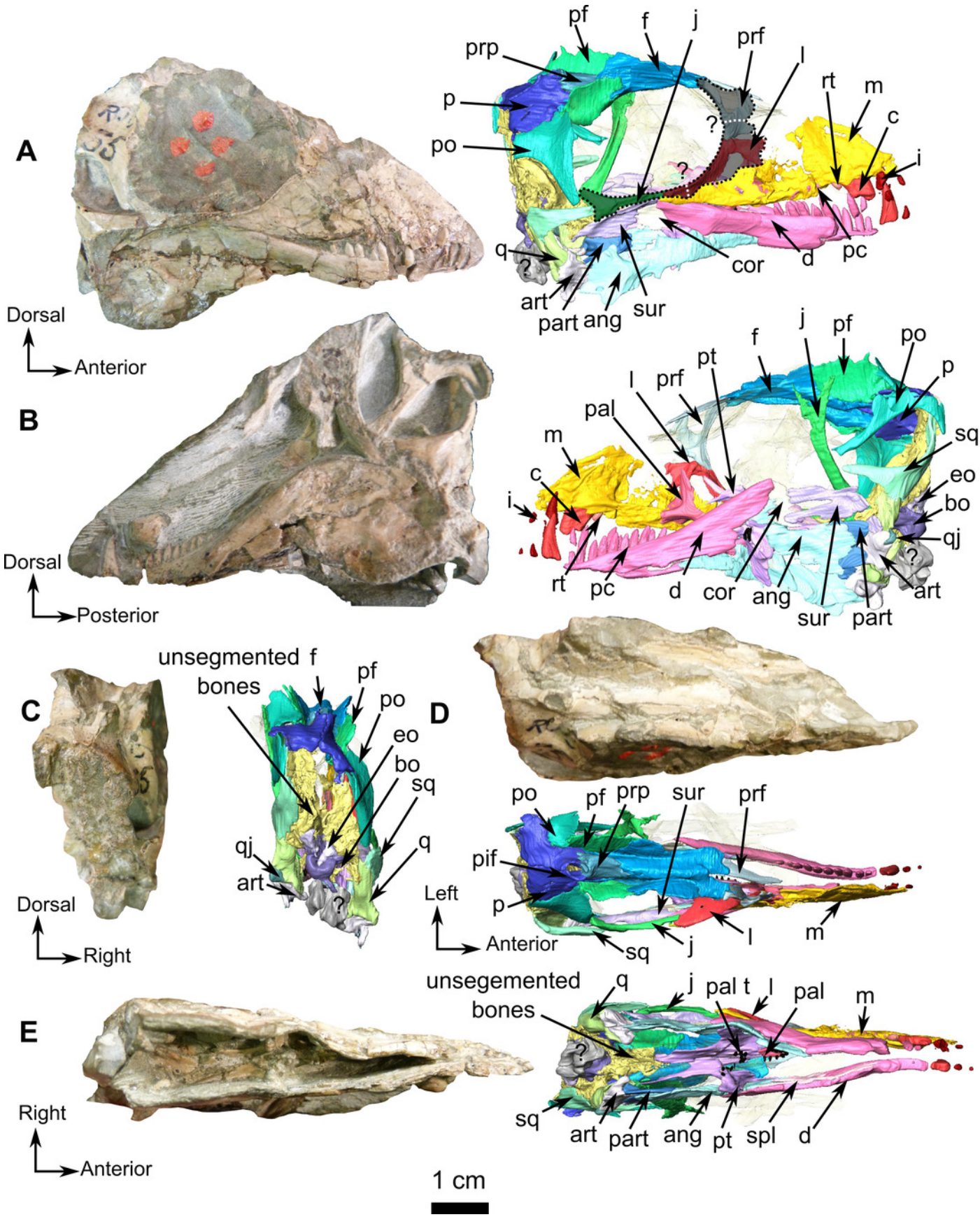
A
pf
f
j
prf
prp
l
p
rt
m
c
po
?
?
i
q
?
cor
d
pc
art
part
ang
sur
Dorsal
Anterior
B
f
j
pf
po
pt
l
prf
p
pal
sq
m
c
eo
i
bo
qj
?
rt
pc
d
cor
ang
art
sur
part
Dorsal
Posterior
C
unsegmented
bones
f
pf
po
eo
bo
sq
qj
q
art
?
Dorsal
Right
D
po
pf
prp
sur
prf
pif
p
Left
Anterior
sq
j
l
m
E
unsegemented
bones
q
j
pal
t
l
pal
m
?
sq
art
part
ang
pt
spl
d
Right
Anterior
1 cm

Figure 2

Holotype of *Rubidgina angusticeps*, here considered Biarmosuchia indet., RC 55.

3D rendering of the lateral portion of the skull. (**A**) Right lateral view. (**B**) Medial view. (**C**) Ventral view. (**D**) Dorsal view. (**E**) Anterior view. (**F**) Occipital view. **Anatomical Abbreviations –ang**, angular; **art**, articular; **aso**, anterior extension of the supraoccipital; **bo**, basioccipital; **c**, caniniform tooth; **co**, occipital condyle; **cor**, coronoid; **d**, dentary; **ect**, ectopterygoid; **eo**, exoccipital; **f**, frontal; **fe**, temporal fenestra; **fm**, foramen magnum; **i**, incisiform tooth; **j**, jugal; **l**, lacrimal; **m**, maxilla; **n**, nasal; **o**, orbit; **op**, opisthotic; **p**, parietal; **pa**, anterior portion of the parietal; **pac**, caudal portion of the parietal; **pal**, palatine; **pal t**, palate teeth; **pao**, paroccipital process; **part**, pre-articular; **pbs**, parabasisphenoid; **pc**, postcanine; **pf**, postfrontal; **pif**, pineal foramen; **pl**, lateral portion of the parietal; **pm**, premaxilla; **po**, postorbital; **pp**, postparietal; **prf**, prefrontal; **pro**, prootic; **prp**, preparietal; **pt**, pterygoids; **ptf**, post-temporal fenestra; **q**, quadrate; **qj**, quadratojugal; **rt**, replacement tooth; **sb**, supraorbital boss; **scl**, sclerotic ring; **smx**, septomaxilla; **so**, supraoccipital; **spl**, splenial; **st**, stapes; **sq**, squamosal; **sur** surangular; **t**, tabular; **v**, vomer. 3D reconstructions were made by A. Duhamel and belong to the University of the Witwatersrand. Scale bar=1cm.

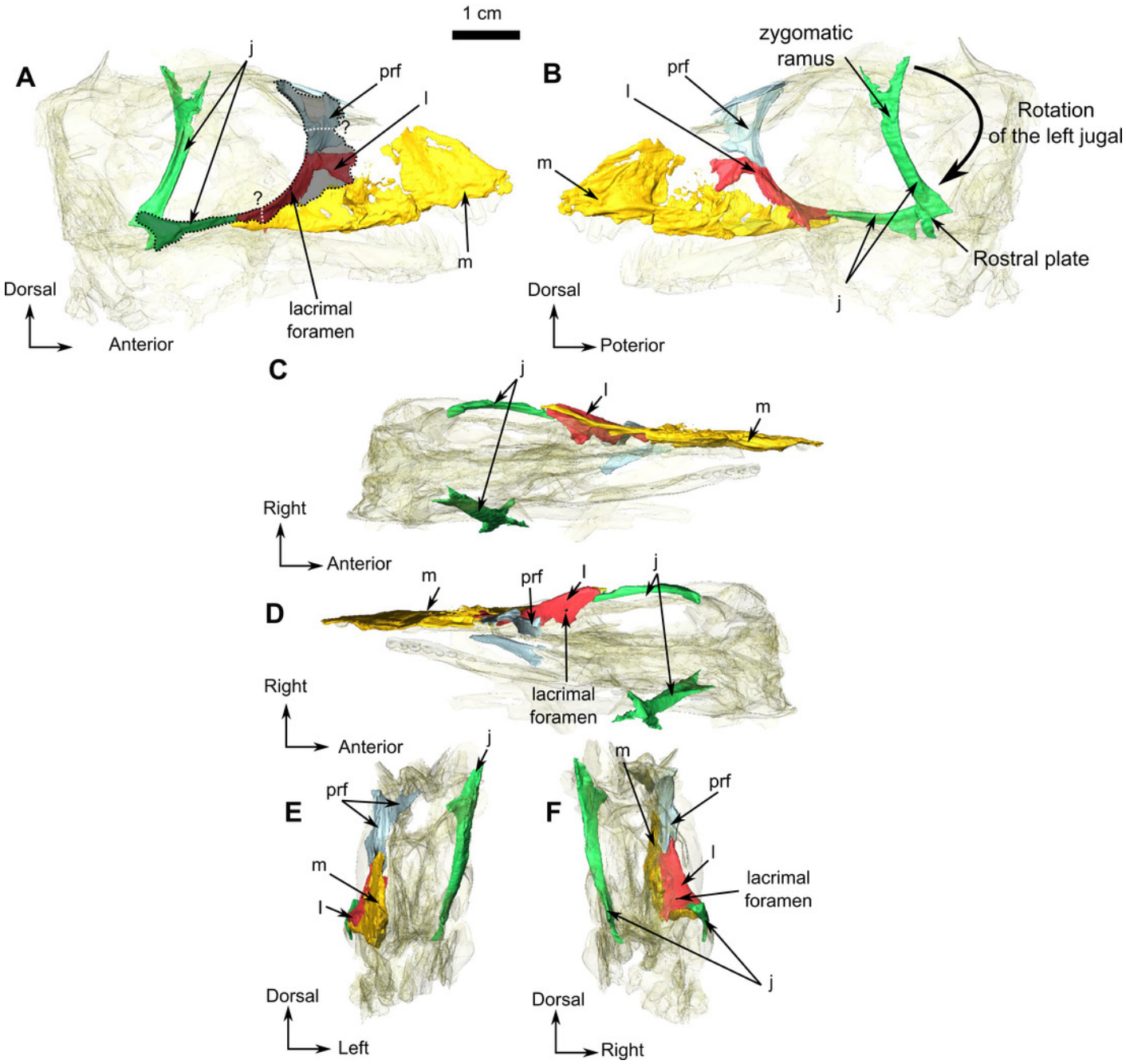
1 cm
A
j
prf
l
?
?
m
Dorsal
Anterior
lacrimal
foramen
B
zygomatic
ramus
prf
l
m
Rotation
of the left jugal
Rostral plate
j
Dorsal
Poterior
C
j
l
m
Right
Anterior
D
m
prf
l
j
lacrimal
foramen
Right
Anterior
E
j
prf
m
l
Dorsal
Left
F
m
prf
l
lacrimal
foramen
j
Dorsal
Right

Figure 3

Holotype of *Rubidgina angusticeps*, here considered Biarmosuchia indet., RC 55.

3D rendering of the dorsal portion of the skull roof of RC 55. (**A**) Right lateral view. (**B**) Left lateral view. (**C**) Dorsal view. (**D**) Ventral view. (**E**) Anterior view. (**F**) Occipital view. **Anatomical Abbreviations –ang**, angular; **art**, articular; **aso**, anterior extension of the supraoccipital; **bo**, basioccipital; **c**, caniniform tooth; **co**, occipital condyle; **cor**, coronoid; **d**, dentary; **ect**, ectopterygoid; **eo**, exoccipital; **f**, frontal; **fe**, temporal fenestra; **fm**, foramen magnum; **i**, incisiform tooth; **j**, jugal; **l**, lacrimal; **m**, maxilla; **n**, nasal; **o**, orbit; **op**, opisthotic; **p**, parietal; **pa**, anterior portion of the parietal; **pac**, caudal portion of the parietal; **pal**, palatine; **pal t**, palate teeth; **pao**, paroccipital process; **part**, pre-articular; **pbs**, parabasisphenoid; **pc**, postcanine; **pf**, postfrontal; **pif**, pineal foramen; **pl**, lateral portion of the parietal; **pm**, premaxilla; **po**, postorbital; **pp**, postparietal; **prf**, prefrontal; **pro**, prootic; **prp**, preparietal; **pt**, pterygoids; **ptf**, post-temporal fenestra; **q**, quadrate; **qj**, quadratojugal; **rt**, replacement tooth; **sb**, supraorbital boss; **scl**, sclerotic ring; **smx**, septomaxilla; **so**, supraoccipital; **spl**, splenial; **st**, stapes; **sq**, squamosal; **sur** surangular; **t**, tabular; **v**, vomer. 3D reconstructions were made by A. Duhamel and belong to the University of the Witwatersrand. Scale bar=1cm.

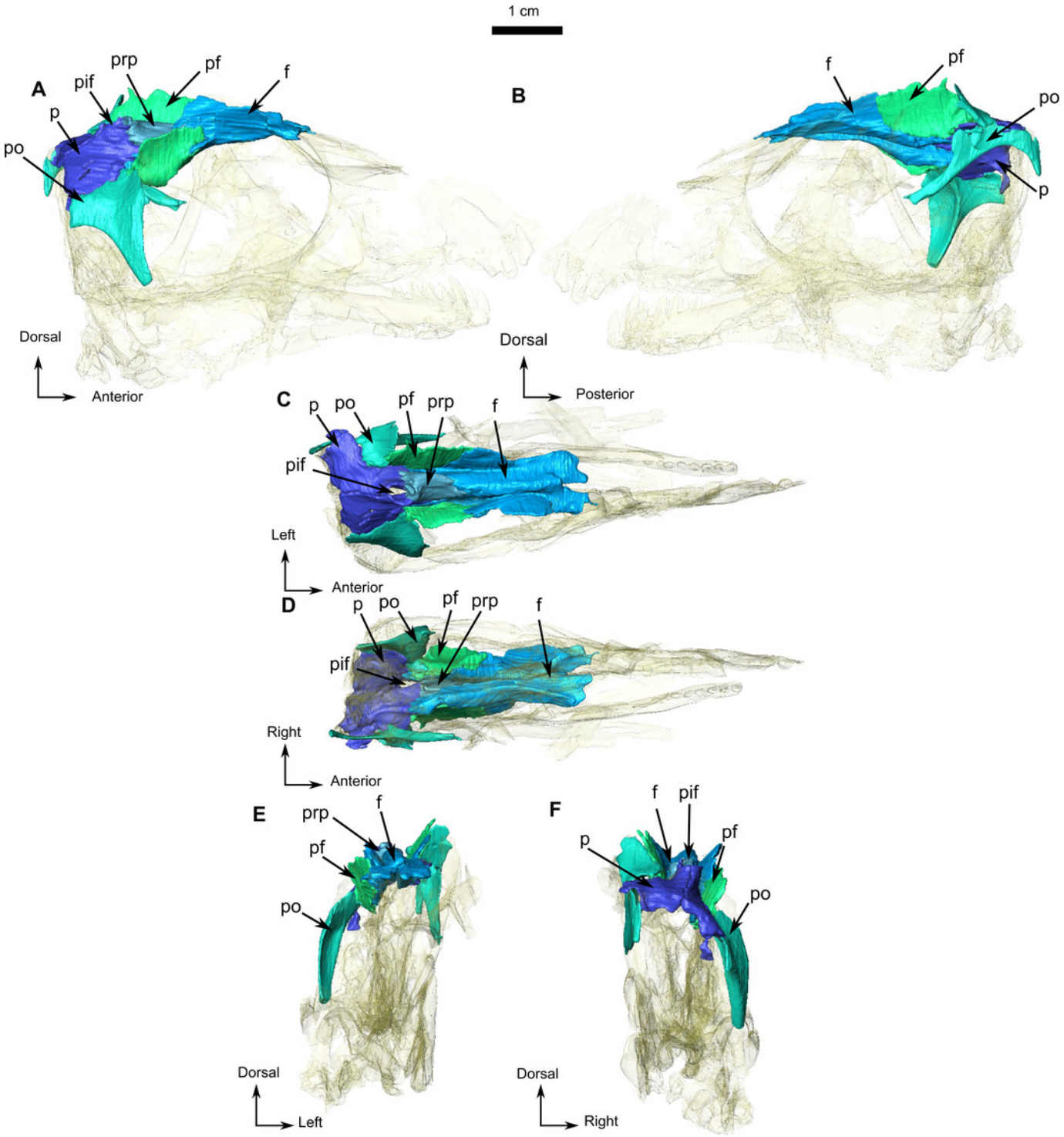
1 cm
A
prp
pf
f
pif
p
po
Dorsal
Anterior
B
f
pf
po
p
C
p
po
pf
prp
f
pif
Dorsal
Posterior
Left
Anterior
D
p
po
pf
prp
f
pif
Right
Anterior
E
prp
f
pf
po
Dorsal
Left
F
f
pif
p
pf
po
Dorsal
Right

Figure 4

Holotype of *Rubidgina angusticeps*, here considered Biarmosuchia indet., RC 55.

3D rendering of the occipital portion of the skull of RC 55. (**A**) Left lateral view. (**B**) Right lateral view. (**C**) Ventral view. (**D**) Dorsal view. (**E**) Occipital view. (**F**) Anterior view. **Anatomical Abbreviations –ang**, angular; **art**, articular; **aso**, anterior extension of the supraoccipital; **bo**, basioccipital; **c**, caniniform tooth; **co**, occipital condyle; **cor**, coronoid; **d**, dentary; **ect**, ectopterygoid; **eo**, exoccipital; **f**, frontal; **fe**, temporal fenestra; **fm**, foramen magnum; **i**, incisiform tooth; **j**, jugal; **l**, lacrimal; **m**, maxilla; **n**, nasal; **o**, orbit; **op**, opisthotic; **p**, parietal; **pa**, anterior portion of the parietal; **pac**, caudal portion of the parietal; **pal**, palatine; **pal t**, palate teeth; **pao**, paroccipital process; **part**, pre-articular; **pbs**, parabasisphenoid; **pc**, postcanine; **pf**, postfrontal; **pif**, pineal foramen; **pl**, lateral portion of the parietal; **pm**, premaxilla; **po**, postorbital; **pp**, postparietal; **prf**, prefrontal; **pro**, prootic; **prp**, preparietal; **pt**, pterygoids; **ptf**, post-temporal fenestra; **q**, quadrate; **qj**, quadratojugal; **rt**, replacement tooth; **sb**, supraorbital boss; **scl**, sclerotic ring; **smx**, septomaxilla; **so**, supraoccipital; **spl**, splenial; **st**, stapes; **sq**, squamosal; **sur** surangular; **t**, tabular; **v**, vomer. 3D reconstructions were made by A. Duhamel and belong to the University of the Witwatersrand. Scale bar=1cm.

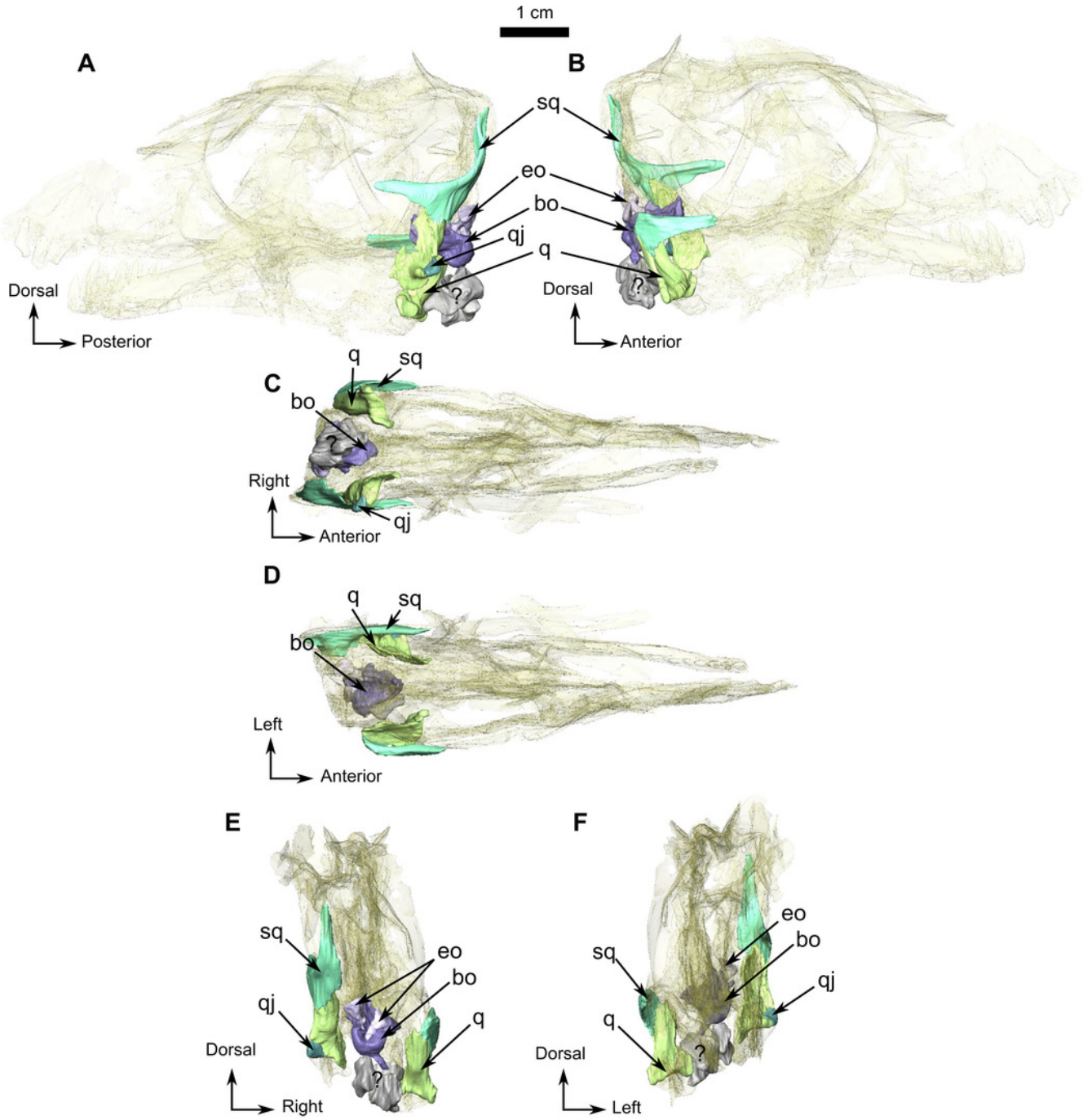
1 cm
A
B
sq
eo
bo
qj
q
?
Dorsal
Posterior
Dorsal
Anterior
C
q
sq
bo
?
Right
qj
Anterior
D
q
sq
bo
Left
Anterior
E
sq
eo
bo
qj
q
?
Dorsal
Right
F
eo
bo
sq
qj
q
?
Dorsal
Left

Figure 5

Holotype of *Rubidgina angusticeps*, here considered Biarmosuchia indet., RC 55.

3D rendering of the palatine portion of the skull of RC 55. (**A**) Right lateral view. (**B**) Left lateral view. (**C**) Ventral view. (**D**) Dorsal view. (**E**) Anterior view. (**F**) Occipital view. (**G**) Ventral view with lower jaw. (**H**) Dorsal view with lower jaw. **Anatomical Abbreviations –ang**, angular; **art**, articular; **aso**, anterior extension of the supraoccipital; **bo**, basioccipital; **c**, caniniform tooth; **co**, occipital condyle; **cor**, coronoid; **d**, dentary; **ect**, ectopterygoid; **eo**, exoccipital; **f**, frontal; **fe**, temporal fenestra; **fm**, foramen magnum; **i**, incisiform tooth; **j**, jugal; **l**, lacrimal; **m**, maxilla; **n**, nasal; **o**, orbit; **op**, opisthotic; **p**, parietal; **pa**, anterior portion of the parietal; **pac**, caudal portion of the parietal; **pal**, palatine; **pal t**, palate teeth; **pao**, paroccipital process; **part**, pre-articular; **pbs**, parabasisphenoid; **pc**, postcanine; **pf**, postfrontal; **pif**, pineal foramen; **pl**, lateral portion of the parietal; **pm**, premaxilla; **po**, postorbital; **pp**, postparietal; **prf**, prefrontal; **pro**, prootic; **prp**, preparietal; **pt**, pterygoids; **ptf**, post-temporal fenestra; **q**, quadrate; **qj**, quadratojugal; **rt**, replacement tooth; **sb**, supraorbital boss; **scl**, sclerotic ring; **smx**, septomaxilla; **so**, supraoccipital; **spl**, splenial; **st**, stapes; **sq**, squamosal; **sur** surangular; **t**, tabular; **v**, vomer. 3D reconstructions were made by A. Duhamel and belong to the University of the Witwatersrand. Scale bar=1cm.

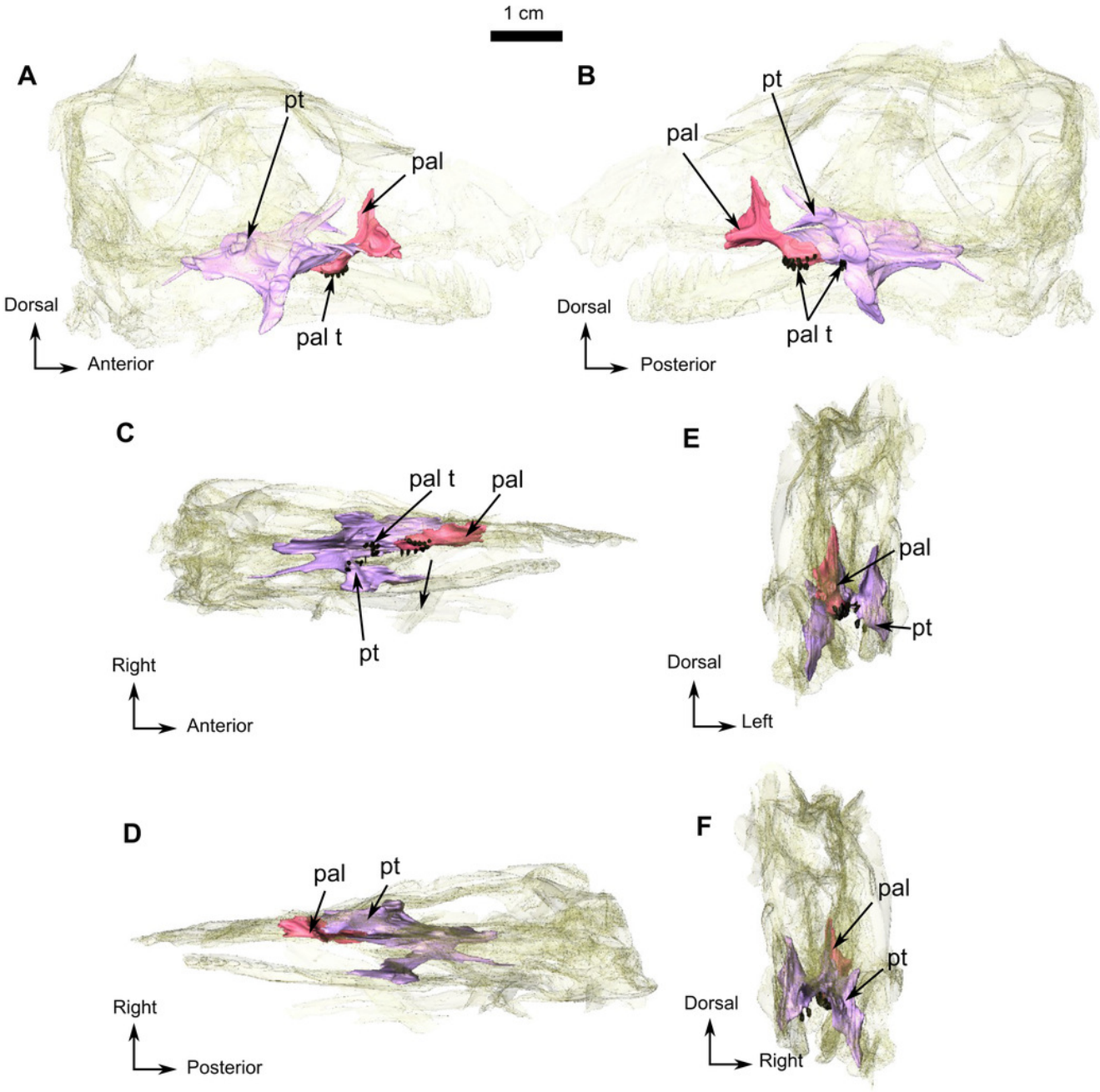
1 cm
A
pt
pal
pal t
Dorsal
Anterior
B
pt
pal
pal t
Dorsal
Posterior
C
pal t
pal
pt
Right
Anterior
D
pal
pt
Right
Posterior
E
pal
pt
Dorsal
Left
F
pal
pt
Dorsal
Right

Figure 6

Holotype of *Rubidgina angusticeps*, here considered Biarmosuchia indet., RC 55.

3D rendering of the lower jaw of RC 55. (**A**) Right lateral view. (**B**) Left lateral view. (**C**) Dorsal view. (**D**) Ventral view. (**E**) Occipital view. Black outlines denote bones situated in the first plan of the figure. **Anatomical Abbreviations –ang**, angular; **art**, articular; **aso**, anterior extension of the supraoccipital; **bo**, basioccipital; **c**, caniniform tooth; **co**, occipital condyle; **cor**, coronoid; **d**, dentary; **ect**, ectopterygoid; **eo**, exoccipital; **f**, frontal; **fe**, temporal fenestra; **fm**, foramen magnum; **i**, incisiform tooth; **j**, jugal; **l**, lacrimal; **m**, maxilla; **n**, nasal; **o**, orbit; **op**, opisthotic; **p**, parietal; **pa**, anterior portion of the parietal; **pac**, caudal portion of the parietal; **pal**, palatine; **pal t**, palate teeth; **pao**, paroccipital process; **part**, pre-articular; **pbs**, parabasisphenoid; **pc**, postcanine; **pf**, postfrontal; **pif**, pineal foramen; **pl**, lateral portion of the parietal; **pm**, premaxilla; **po**, postorbital; **pp**, postparietal; **prf**, prefrontal; **pro**, prootic; **prp**, preparietal; **pt**, pterygoids; **ptf**, post-temporal fenestra; **q**, quadrate; **qj**, quadratojugal; **rt**, replacement tooth; **sb**, supraorbital boss; **scl**, sclerotic ring; **smx**, septomaxilla; **so**, supraoccipital; **spl**, splenial; **st**, stapes; **sq**, squamosal; **sur** surangular; **t**, tabular; **v**, vomer. 3D reconstructions were made by A. Duhamel and belong to the University of the Witwatersrand. Scale bar=1cm.

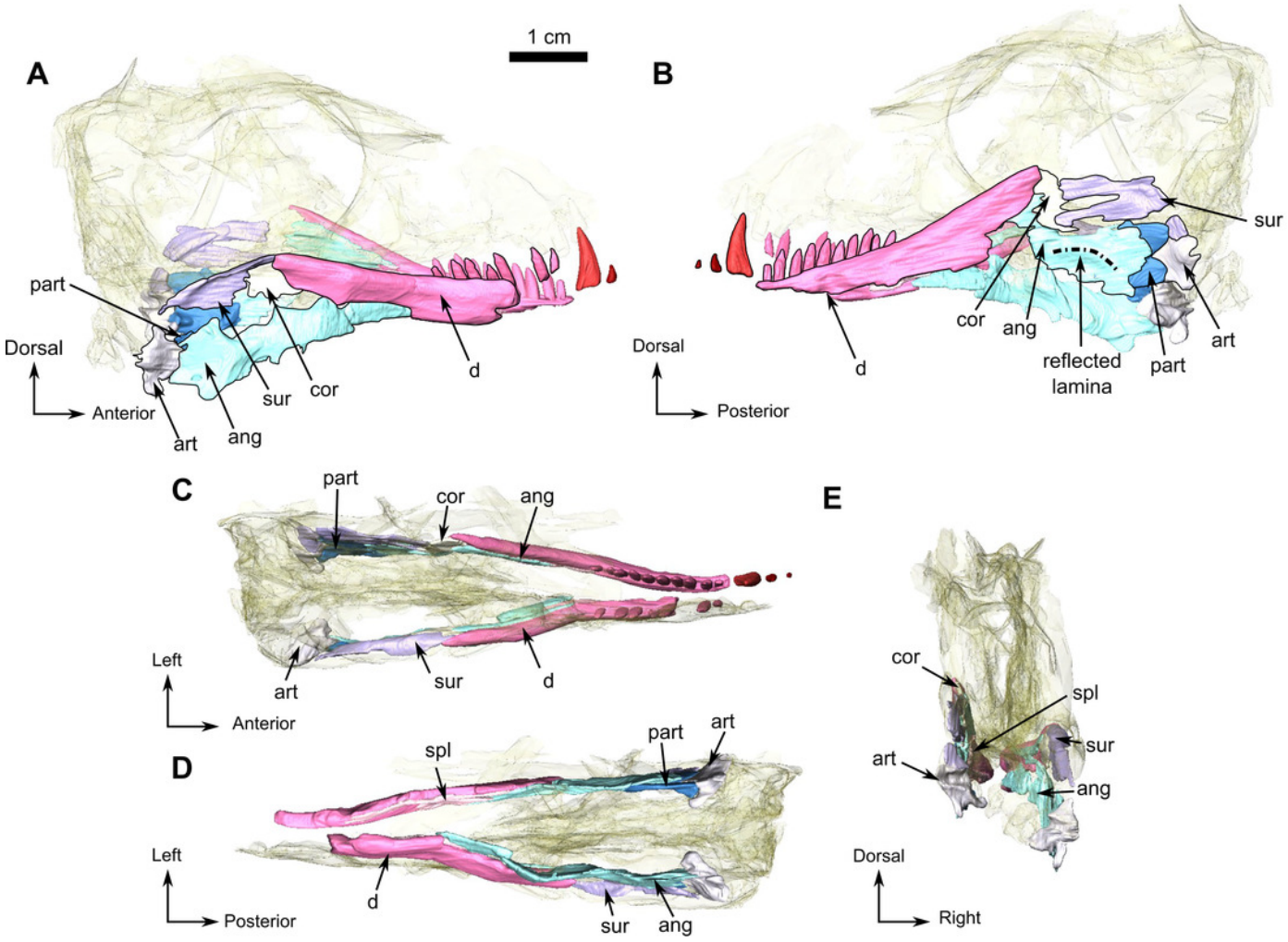
1 cm
A
part
Dorsal
Anterior
art
ang
sur
cor
d
B
sur
cor
ang
reflected
lamina
part
art
Dorsal
Posterior
d
C
part
cor
ang
Left
Anterior
art
sur
d
D
spl
part
art
Left
Posterior
d
sur
ang
E
cor
spl
art
sur
ang
Dorsal
Right

Figure 7

Holotype of *Rubidgina angusticeps*, here considered Biarmosuchia indet., RC 55.

3D rendering of the dentition of RC 55. (**A**) Right lateral view. (**B**) Left lateral view. **Anatomical Abbreviations–ang**, angular; **art**, articular; **aso**, anterior extension of the supraoccipital; **bo**, basioccipital; **c**, caniniform tooth; **co**, occipital condyle; **cor**, coronoid; **d**, dentary; **ect**, ectopterygoid; **eo**, exoccipital; **f**, frontal; **fe**, temporal fenestra; **fm**, foramen magnum; **i**, incisiform tooth; **j**, jugal; **l**, lacrimal; **m**, maxilla; **n**, nasal; **o**, orbit; **op**, opisthotic; **p**, parietal; **pa**, anterior portion of the parietal; **pac**, caudal portion of the parietal; **pal**, palatine; **pal t**, palate teeth; **pao**, paroccipital process; **part**, pre-articular; **pbs**, parabasisphenoid; **pc**, postcanine; **pf**, postfrontal; **pif**, pineal foramen; **pl**, lateral portion of the parietal; **pm**, premaxilla; **po**, postorbital; **pp**, postparietal; **prf**, prefrontal; **pro**, prootic; **prp**, preparietal; **pt**, pterygoids; **ptf**, post-temporal fenestra; **q**, quadrate; **qj**, quadratojugal; **rt**, replacement tooth; **sb**, supraorbital boss; **scl**, sclerotic ring; **smx**, septomaxilla; **so**, supraoccipital; **spl**, splenial; **st**, stapes; **sq**, squamosal; **sur** surangular; **t**, tabular; **v**, vomer. 3D reconstructions were made by A. Duhamel and belong to the University of the Witwatersrand. Scale bar=1cm.

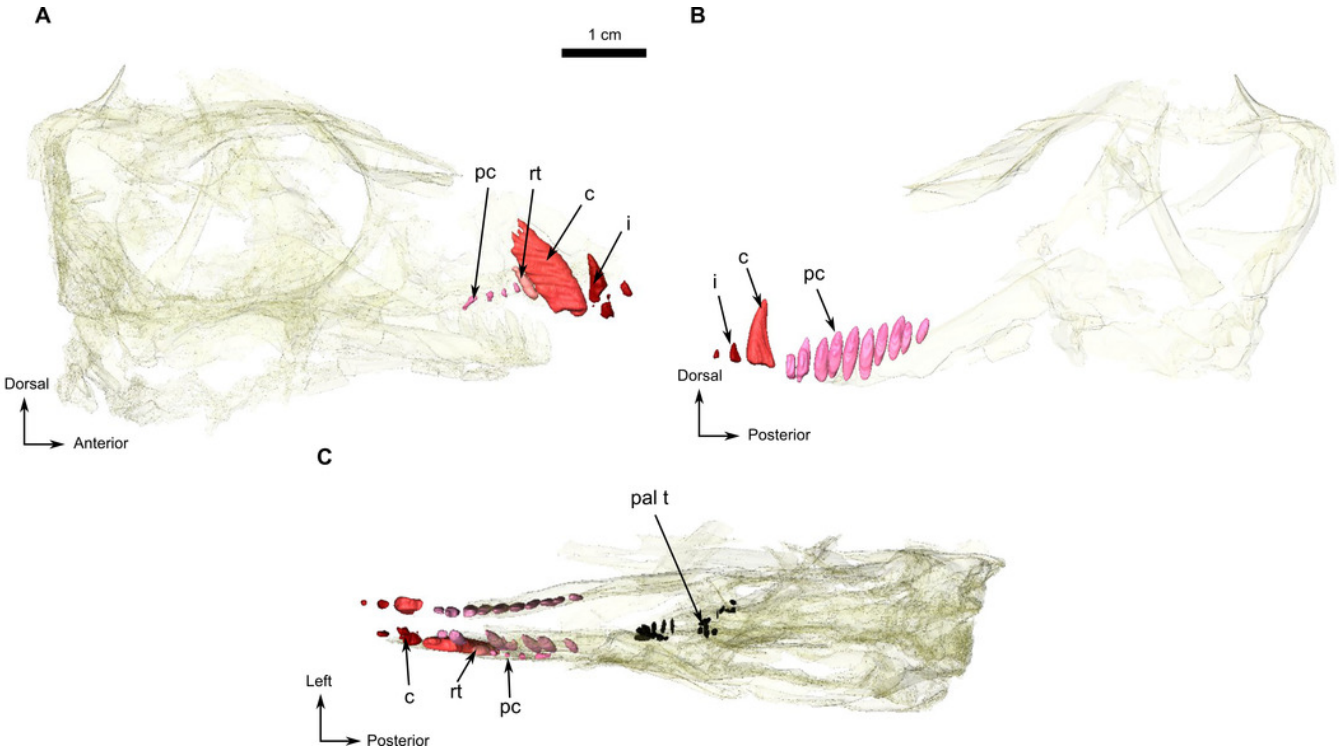
A
1 cm
pc
rt
c
i
Dorsal
Anterior
B
c
i
pc
Dorsal
Posterior
C
pal t
Left
c
rt
pc
Posterior

Figure 8

Burnetiamorpha indet., skull, CGP MJF 22.

(**A**) Lateral view, with a 3D rendering of the teeth (right). (**B**) Dorsal view with the bones of the pineal region segmented on the left; and the CT-image at the level of the supraorbital bosses and a diagram of the vasculature pattern found in the bosses (right). (**C**) Occipital view. (**D**) Ventral view. Questions mark denote unidentified bones. Short dotted line accentuates anatomical character; long dotted line indicates uncertainly about sutural pathway on bone. **Anatomical Abbreviations –ang**, angular; **art**, articular; **aso**, anterior extension of the supraoccipital; **bo**, basioccipital; **c**, caniniform tooth; **co**, occipital condyle; **cor**, coronoid; **d**, dentary; **ect**, ectopterygoid; **eo**, exoccipital; **f**, frontal; **fe**, temporal fenestra; **fm**, foramen magnum; **i**, incisiform tooth; **j**, jugal; **l**, lacrimal; **m**, maxilla; **n**, nasal; **o**, orbit; **op**, opisthotic; **p**, parietal; **pa**, anterior portion of the parietal; **pac**, caudal portion of the parietal; **pal**, palatine; **pal t**, palate teeth; **pao**, paroccipital process; **part**, pre-articular; **pbs**, parabasisphenoid; **pc**, postcanine; **pf**, postfrontal; **pif**, pineal foramen; **pl**, lateral portion of the parietal; **pm**, premaxilla; **po**, postorbital; **pp**, postparietal; **prf**, prefrontal; **pro**, prootic; **prp**, preparietal; **pt**, pterygoids; **ptf**, post-temporal fenestra; **q**, quadrate; **qj**, quadratojugal; **rt**, replacement tooth; **sb**, supraorbital boss; **scl**, sclerotic ring; **smx**, septomaxilla; **so**, supraoccipital; **spl**, splenial; **st**, stapes; **sq**, squamosal; **sur** surangular; **t**, tabular; **v**, vomer. Pictures by A. Duhamel. Scan of the specimen was performed by Kudakwashe Jakata and belongs to the University of the Witwatersrand. 3D reconstructions were made by A. Duhamel and belong to the University of the Witwatersrand. Scale bar=1cm.

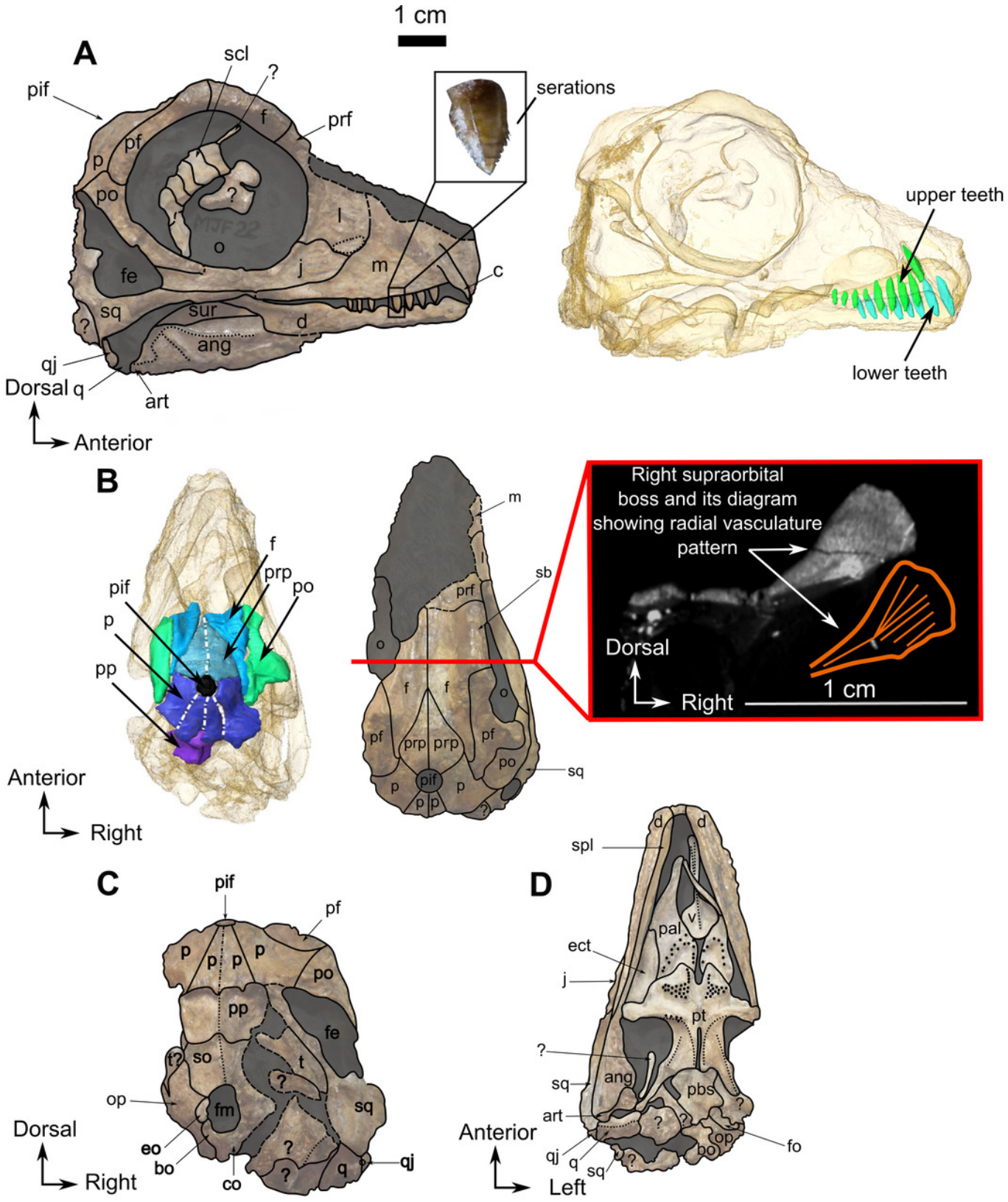
1 cm
A
scl
?
pif
f
prf
p
pf
po
?
l
o
fe
j
m
c
sq
sur
d
?
ang
qj
Dorsal
q
art
Anterior
serations
upper teeth
lower teeth
B
f
prp
po
pif
p
pp
Anterior
Right
m
l
sb
prf
o
f
f
o
pf
prp
prp
pf
po
sq
p
pif
p
p
p
?
Right supraorbital boss and its diagram showing radial vasculature pattern
Dorsal
Right
1 cm
C
pif
pf
p
p
p
p
po
pp
fe
t?
so
t
?
op
fm
sq
eo
bo
?
co
?
q
qj
Dorsal
Right
D
d
d
spl
v
pal
ect
j
pt
?
sq
ang
pbs
?
art
?
?
op
fo
qj
q
sq
bo
?
Anterior
Left

Figure 9

Burnetiamorph indet., snout, SAM-PK-K11126.

Photograph (left) and 3D rendering of SAM-PK-K11126 (right). (**A**) Left lateral view. (**B**) Ventral view. **Anatomical Abbreviations –ang**, angular; **art**, articular; **aso**, anterior extension of the supraoccipital; **bo**, basioccipital; **c**, caniniform tooth; **co**, occipital condyle; **cor**, coronoid; **d**, dentary; **ect**, ectopterygoid; **eo**, exoccipital; **f**, frontal; **fe**, temporal fenestra; **fm**, foramen magnum; **i**, incisiform tooth; **j**, jugal; **l**, lacrimal; **m**, maxilla; **n**, nasal; **o**, orbit; **op**, opisthotic; **p**, parietal; **pa**, anterior portion of the parietal; **pac**, caudal portion of the parietal; **pal**, palatine; **pal t**, palate teeth; **pao**, paroccipital process; **part**, pre-articular; **pbs**, parabasisphenoid; **pc**, postcanine; **pf**, postfrontal; **pif**, pineal foramen; **pl**, lateral portion of the parietal; **pm**, premaxilla; **po**, postorbital; **pp**, postparietal; **prf**, prefrontal; **pro**, prootic; **prp**, preparietal; **pt**, pterygoids; **ptf**, post-temporal fenestra; **q**, quadrate; **qj**, quadratojugal; **rt**, replacement tooth; **sb**, supraorbital boss; **scl**, sclerotic ring; **smx**, septomaxilla; **so**, supraoccipital; **spl**, splenial; **st**, stapes; **sq**, squamosal; **sur** surangular; **t**, tabular; **v**, vomer. Vertical jagging on the 3D rendering is an artefact of segmentation. Pictures by A. Duhamel. 3D reconstructions were made by A. Duhamel and belong to the University of the Witwatersrand. Scale bar=1cm.

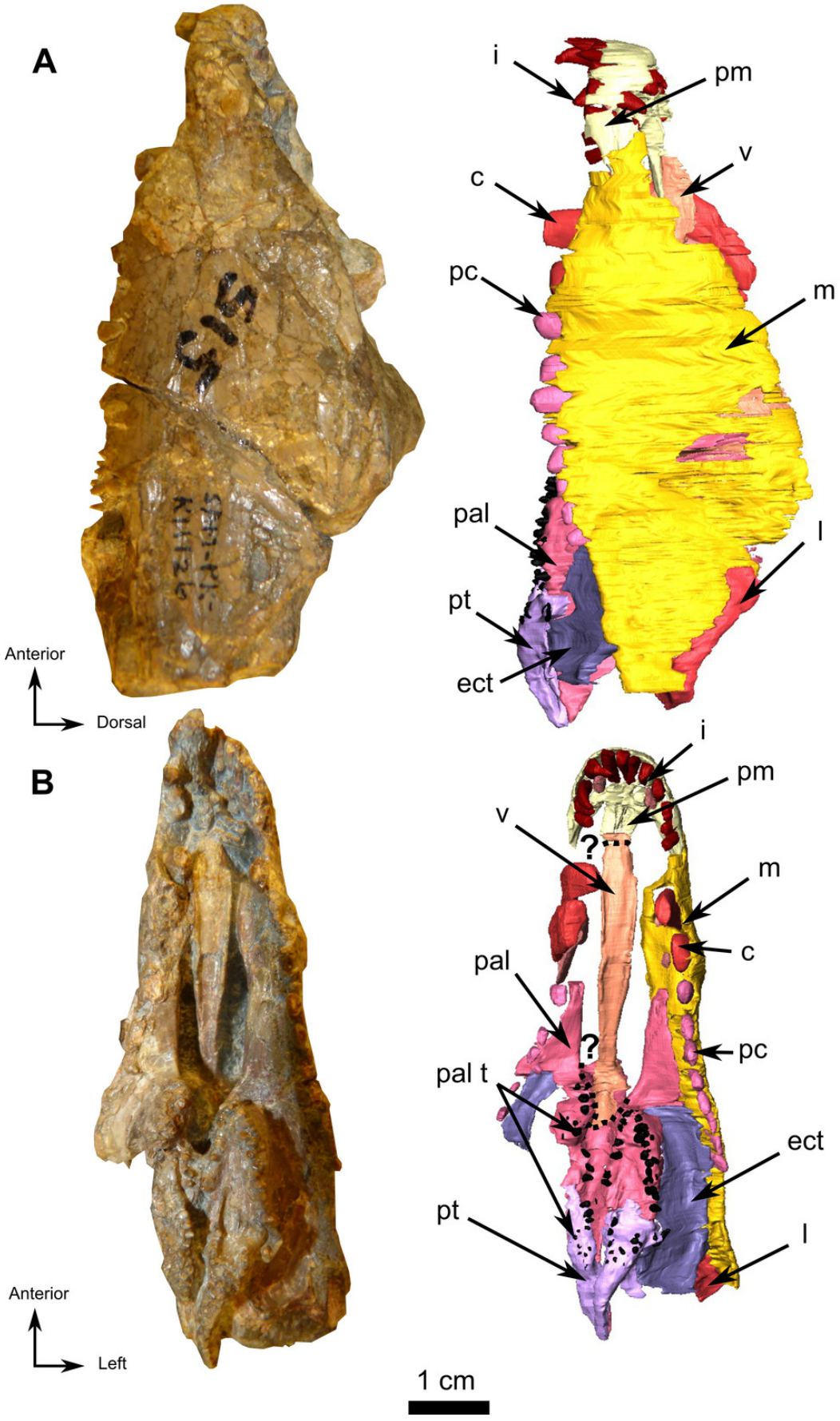
A
i
pm
v
c
pc
m
pal
l
pt
ect
Anterior
Dorsal
B
i
pm
v
?
m
c
pal
?
pc
pal t
ect
pt
l
Anterior
Left
1 cm

Figure 10

Burnetiamorph indet., palate, SAM-PK-K11126.

3D rendering of SAM-PK-K11126's palatine bones and teeth (right). (**A**) Ventral view. (**B**) Dorsal view. (**C**) Left lateral view. **Anatomical Abbreviations –ang**, angular; **art**, articular; **aso**, anterior extension of the supraoccipital; **bo**, basioccipital; **c**, caniniform tooth; **co**, occipital condyle; **cor**, coronoid; **d**, dentary; **ect**, ectopterygoid; **eo**, exoccipital; **f**, frontal; **fe**, temporal fenestra; **fm**, foramen magnum; **i**, incisiform tooth; **j**, jugal; **l**, lacrimal; **m**, maxilla; **n**, nasal; **o**, orbit; **op**, opisthotic; **p**, parietal; **pa**, anterior portion of the parietal; **pac**, caudal portion of the parietal; **pal**, palatine; **pal t**, palate teeth; **pao**, paroccipital process; **part**, pre-articular; **pbs**, parabasisphenoid; **pc**, postcanine; **pf**, postfrontal; **pif**, pineal foramen; **pl**, lateral portion of the parietal; **pm**, premaxilla; **po**, postorbital; **pp**, postparietal; **prf**, prefrontal; **pro**, prootic; **prp**, preparietal; **pt**, pterygoids; **ptf**, post-temporal fenestra; **q**, quadrate; **qj**, quadratojugal; **rt**, replacement tooth; **sb**, supraorbital boss; **scl**, sclerotic ring; **smx**, septomaxilla; **so**, supraoccipital; **spl**, splenial; **st**, stapes; **sq**, squamosal; **sur** surangular; **t**, tabular; **v**, vomer. 3D reconstructions were made by A. Duhamel and belong to the University of the Witwatersrand. Scale bar=1cm.

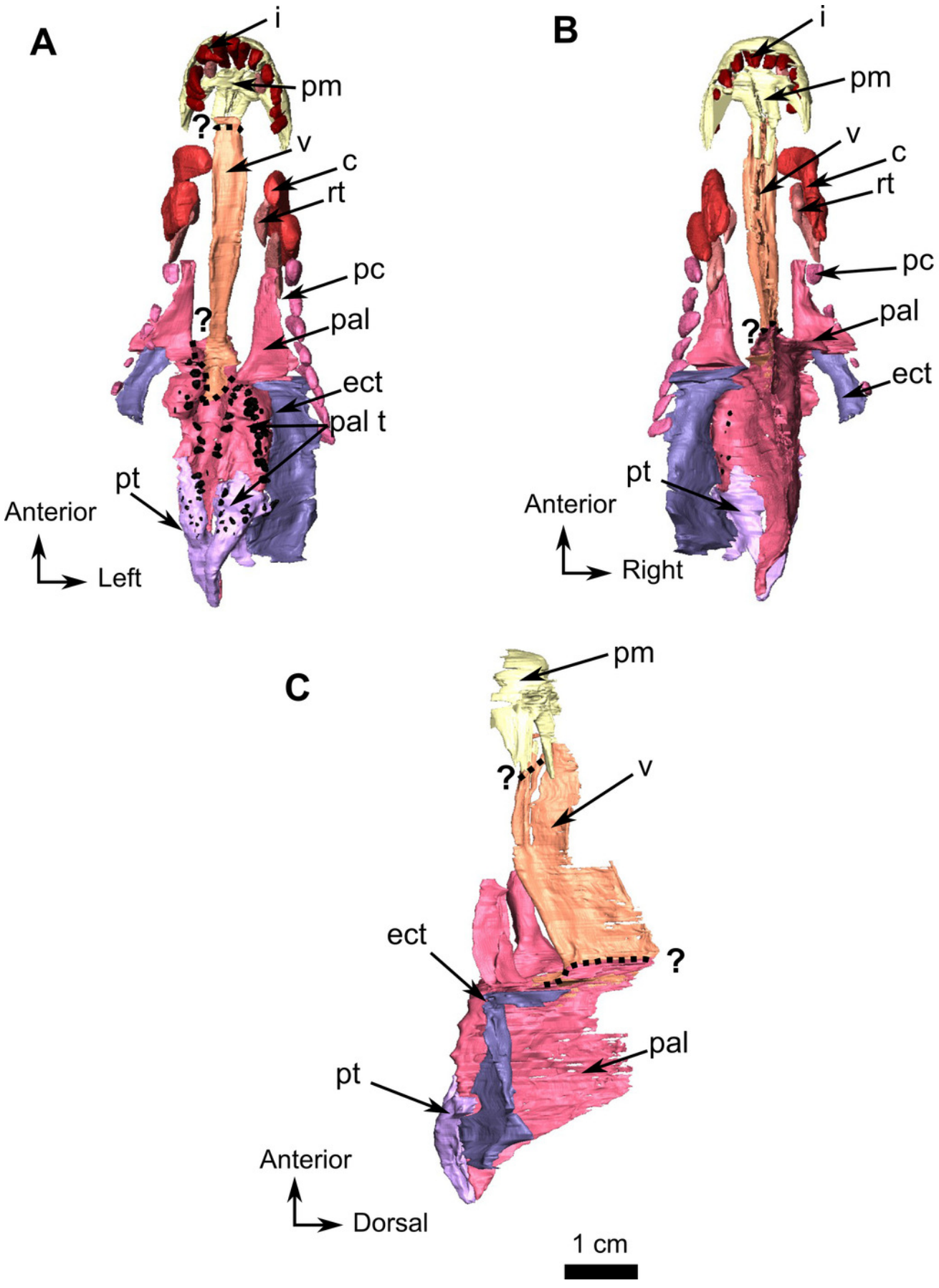
A
i
pm
?
v
c
rt
pc
?
pal
ect
pal t
pt
Anterior
Left
B
i
pm
v
c
rt
pc
?
pal
ect
pt
Anterior
Right
C
pm
?
v
ect
?
pal
pt
Anterior
Dorsal
1 cm

Figure 11

Burnetiamorph indet., occipital portion, SAM-PK-K11126.

Photograph (left) and 3D rendering of SAM-PK-K11126 (right). (**A**) Occipital view. (**B**) Right lateral view. (**C**) Dorsal view. (**D**) Ventral view. **Anatomical Abbreviations –ang**, angular; **art**, articular; **aso**, anterior extension of the supraoccipital; **bo**, basioccipital; **c**, caniniform tooth; **co**, occipital condyle; **cor**, coronoid; **d**, dentary; **ect**, ectopterygoid; **eo**, exoccipital; **f**, frontal; **fe**, temporal fenestra; **fm**, foramen magnum; **i**, incisiform tooth; **j**, jugal; **l**, lacrimal; **m**, maxilla; **n**, nasal; **o**, orbit; **op**, opisthotic; **p**, parietal; **pa**, anterior portion of the parietal; **pac**, caudal portion of the parietal; **pal**, palatine; **pal t**, palate teeth; **pao**, paroccipital process; **part**, pre-articular; **pbs**, parabasisphenoid; **pc**, postcanine; **pf**, postfrontal; **pif**, pineal foramen; **pl**, lateral portion of the parietal; **pm**, premaxilla; **po**, postorbital; **pp**, postparietal; **prf**, prefrontal; **pro**, prootic; **prp**, preparietal; **pt**, pterygoids; **ptf**, post-temporal fenestra; **q**, quadrate; **qj**, quadratojugal; **rt**, replacement tooth; **sb**, supraorbital boss; **scl**, sclerotic ring; **smx**, septomaxilla; **so**, supraoccipital; **spl**, splenial; **st**, stapes; **sq**, squamosal; **sur** surangular; **t**, tabular; **v**, vomer. Pictures by A. Duhamel. 3D reconstructions were made by A. Duhamel and belong to the University of the Witwatersrand. Scale bar=1cm.

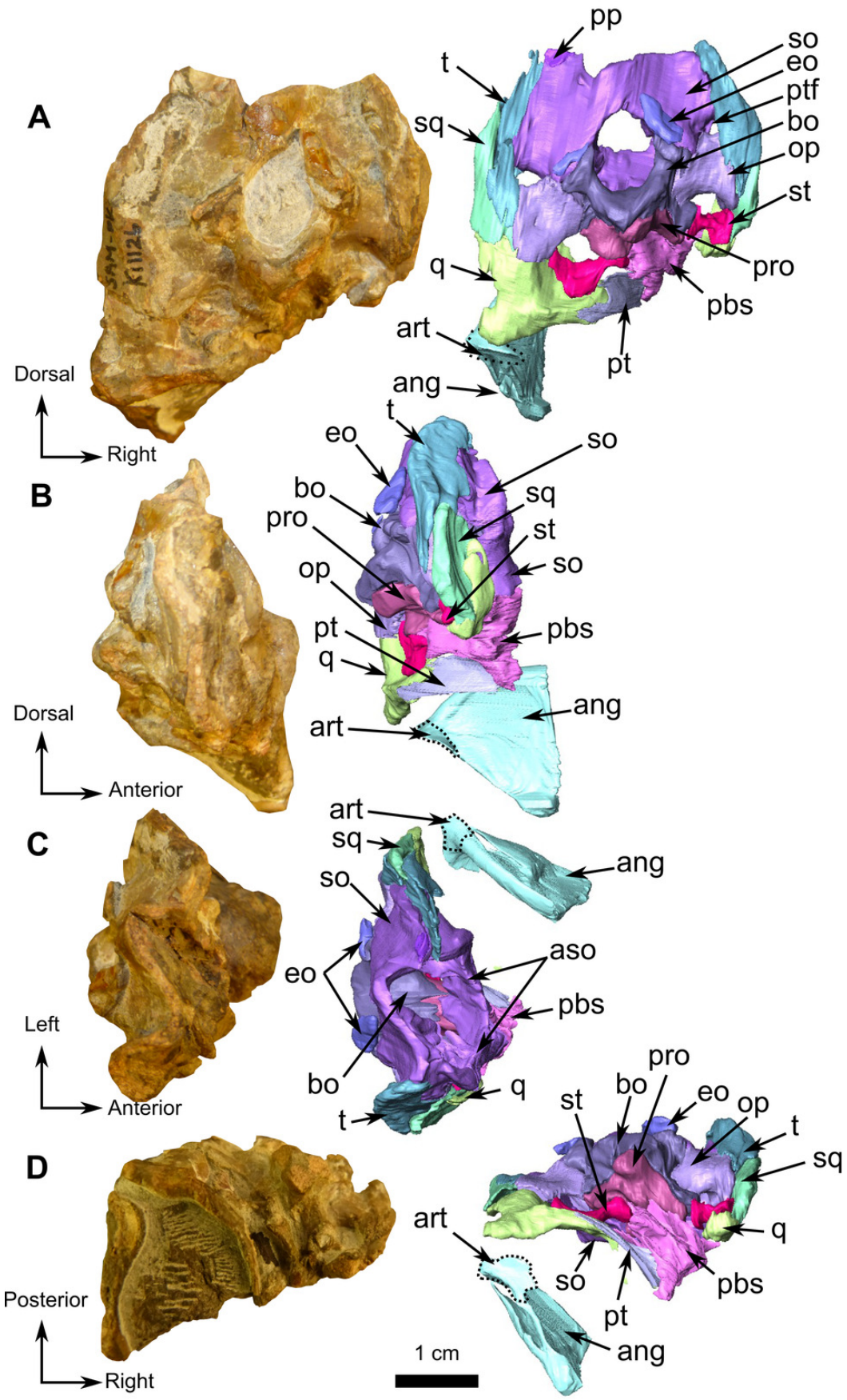
A
pp
t
sq
so
eo
ptf
bo
op
st
pro
q
pbs
art
pt
ang
Dorsal
Right
B
t
eo
so
bo
sq
pro
st
op
so
pt
pbs
q
ang
art
Dorsal
Anterior
C
art
sq
ang
so
aso
eo
pbs
bo
q
t
Left
Anterior
D
pro
bo
eo
st
op
t
sq
art
q
so
pbs
pt
ang
Posterior
Right
1 cm

Figure 12

Burnetiamorph indet., skull cap, SAM-PK-K11126.

Photograph (left) and 3D rendering of SAM-PK-K11126. (**A**) Dorsal view. (**B**) Ventral view. (**C**) Right lateral view. White dotted lines point out inner-bone sutures. **Anatomical Abbreviations –ang**, angular; **art**, articular; **aso**, anterior extension of the supraoccipital; **bo**, basioccipital; **c**, caniniform tooth; **co**, occipital condyle; **cor**, coronoid; **d**, dentary; **ect**, ectopterygoid; **eo**, exoccipital; **f**, frontal; **fe**, temporal fenestra; **fm**, foramen magnum; **i**, incisiform tooth; **j**, jugal; **l**, lacrimal; **m**, maxilla; **n**, nasal; **o**, orbit; **op**, opisthotic; **p**, parietal; **pa**, anterior portion of the parietal; **pac**, caudal portion of the parietal; **pal**, palatine; **pal t**, palate teeth; **pao**, paroccipital process; **part**, pre-articular; **pbs**, parabasisphenoid; **pc**, postcanine; **pf**, postfrontal; **pif**, pineal foramen; **pl**, lateral portion of the parietal; **pm**, premaxilla; **po**, postorbital; **pp**, postparietal; **prf**, prefrontal; **pro**, prootic; **prp**, preparietal; **pt**, pterygoids; **ptf**, post-temporal fenestra; **q**, quadrate; **qj**, quadratojugal; **rt**, replacement tooth; **sb**, supraorbital boss; **scl**, sclerotic ring; **smx**, septomaxilla; **so**, supraoccipital; **spl**, splenial; **st**, stapes; **sq**, squamosal; **sur** surangular; **t**, tabular; **v**, vomer. Pictures by A. Duhamel. 3D reconstructions were made by A. Duhamel and belong to the University of the Witwatersrand. Scale bar=1cm.

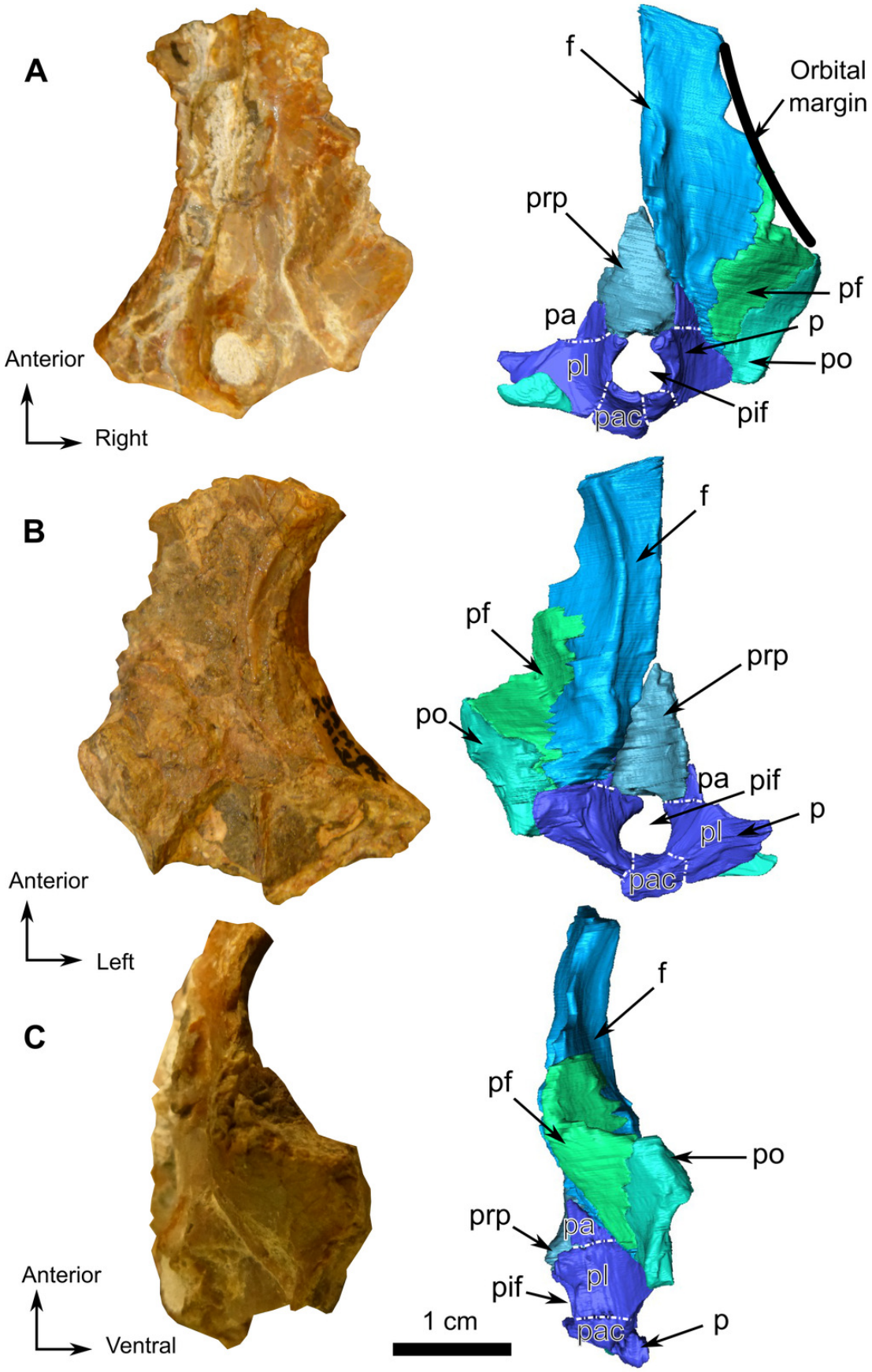
A
Anterior
Right
f
Orbital
margin
prp
pf
pa
p
po
pl
pif
pac
B
Anterior
Left
f
pf
prp
po
pa
pif
p
pl
pac
C
Anterior
Ventral
f
pf
po
prp
pa
pl
pif
p
pac
1 cm

Figure 13

Burnetiamorph indet., right lower jaw, SAM-PK-K11126.

Photograph (left) and 3D rendering of SAM-PK-K11126 (right). (**A**) Right lingual view. (**B**) Distal view. **Anatomical Abbreviations –ang**, angular; **art**, articular; **aso**, anterior extension of the supraoccipital; **bo**, basioccipital; **c**, caniniform tooth; **co**, occipital condyle; **cor**, coronoid; **d**, dentary; **ect**, ectopterygoid; **eo**, exoccipital; **f**, frontal; **fe**, temporal fenestra; **fm**, foramen magnum; **i**, incisiform tooth; **j**, jugal; **l**, lacrimal; **m**, maxilla; **n**, nasal; **o**, orbit; **op**, opisthotic; **p**, parietal; **pa**, anterior portion of the parietal; **pac**, caudal portion of the parietal; **pal**, palatine; **pal t**, palate teeth; **pao**, paroccipital process; **part**, pre-articular; **pbs**, parabasisphenoid; **pc**, postcanine; **pf**, postfrontal; **pif**, pineal foramen; **pl**, lateral portion of the parietal; **pm**, premaxilla; **po**, postorbital; **pp**, postparietal; **prf**, prefrontal; **pro**, prootic; **prp**, preparietal; **pt**, pterygoids; **ptf**, post-temporal fenestra; **q**, quadrate; **qj**, quadratojugal; **rt**, replacement tooth; **sb**, supraorbital boss; **scl**, sclerotic ring; **smx**, septomaxilla; **so**, supraoccipital; **spl**, splenial; **st**, stapes; **sq**, squamosal; **sur** surangular; **t**, tabular; **v**, vomer. Pictures by A. Duhamel. 3D reconstructions were made by A. Duhamel and belong to the University of the Witwatersrand. Scale bar=1cm.

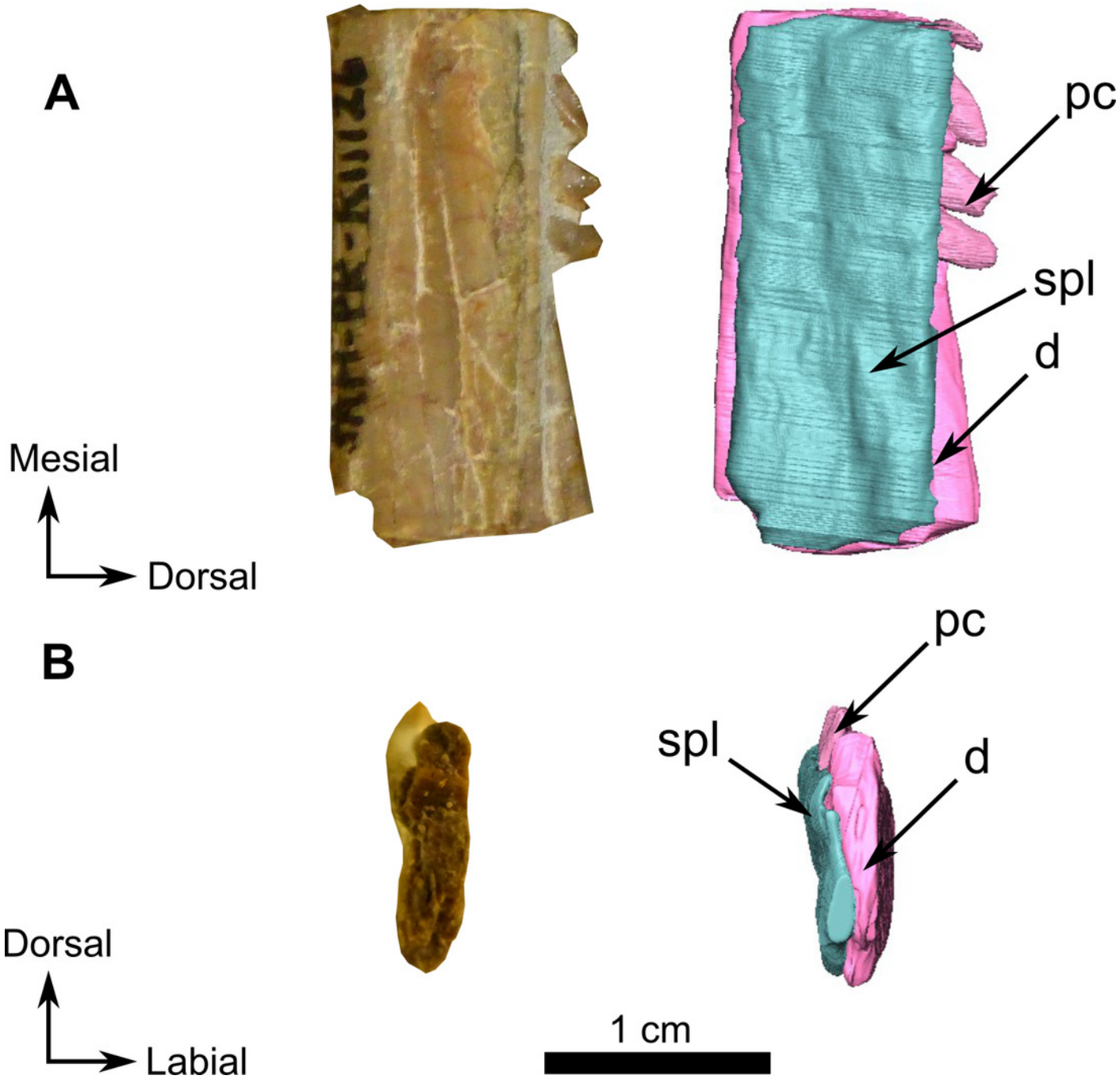
A
pc
spl
d
Mesial
Dorsal
B
pc
spl
d
Dorsal
Labial
1 cm

Figure 14

Burnetiamorph indet., upper dentition, SAM-PK-K11126.

3D rendering of the upper dentition of SAM-PK-K11126, with a photograph background of the snout. (**A**) Ventral view. (**B**) Left labial view. **Anatomical Abbreviation–ang**, angular; **art**, articular; **aso**, anterior extension of the supraoccipital; **bo**, basioccipital; **c**, caniniform tooth; **co**, occipital condyle; **cor**, coronoid; **d**, dentary; **ect**, ectopterygoid; **eo**, exoccipital; **f**, frontal; **fe**, temporal fenestra; **fm**, foramen magnum; **i**, incisiform tooth; **j**, jugal; **l**, lacrimal; **m**, maxilla; **n**, nasal; **o**, orbit; **op**, opisthotic; **p**, parietal; **pa**, anterior portion of the parietal; **pac**, caudal portion of the parietal; **pal**, palatine; **pal t**, palate teeth; **pao**, paroccipital process; **part**, pre-articular; **pbs**, parabasisphenoid; **pc**, postcanine; **pf**, postfrontal; **pif**, pineal foramen; **pl**, lateral portion of the parietal; **pm**, premaxilla; **po**, postorbital; **pp**, postparietal; **prf**, prefrontal; **pro**, prootic; **prp**, preparietal; **pt**, pterygoids; **ptf**, post-temporal fenestra; **q**, quadrate; **qj**, quadratojugal; **rt**, replacement tooth; **sb**, supraorbital boss; **scl**, sclerotic ring; **smx**, septomaxilla; **so**, supraoccipital; **spl**, splenial; **st**, stapes; **sq**, squamosal; **sur** surangular; **t**, tabular; **v**, vomer. Pictures by A. Duhamel. 3D reconstructions were made by A. Duhamel and belong to the University of the Witwatersrand. Scale bar=1cm.

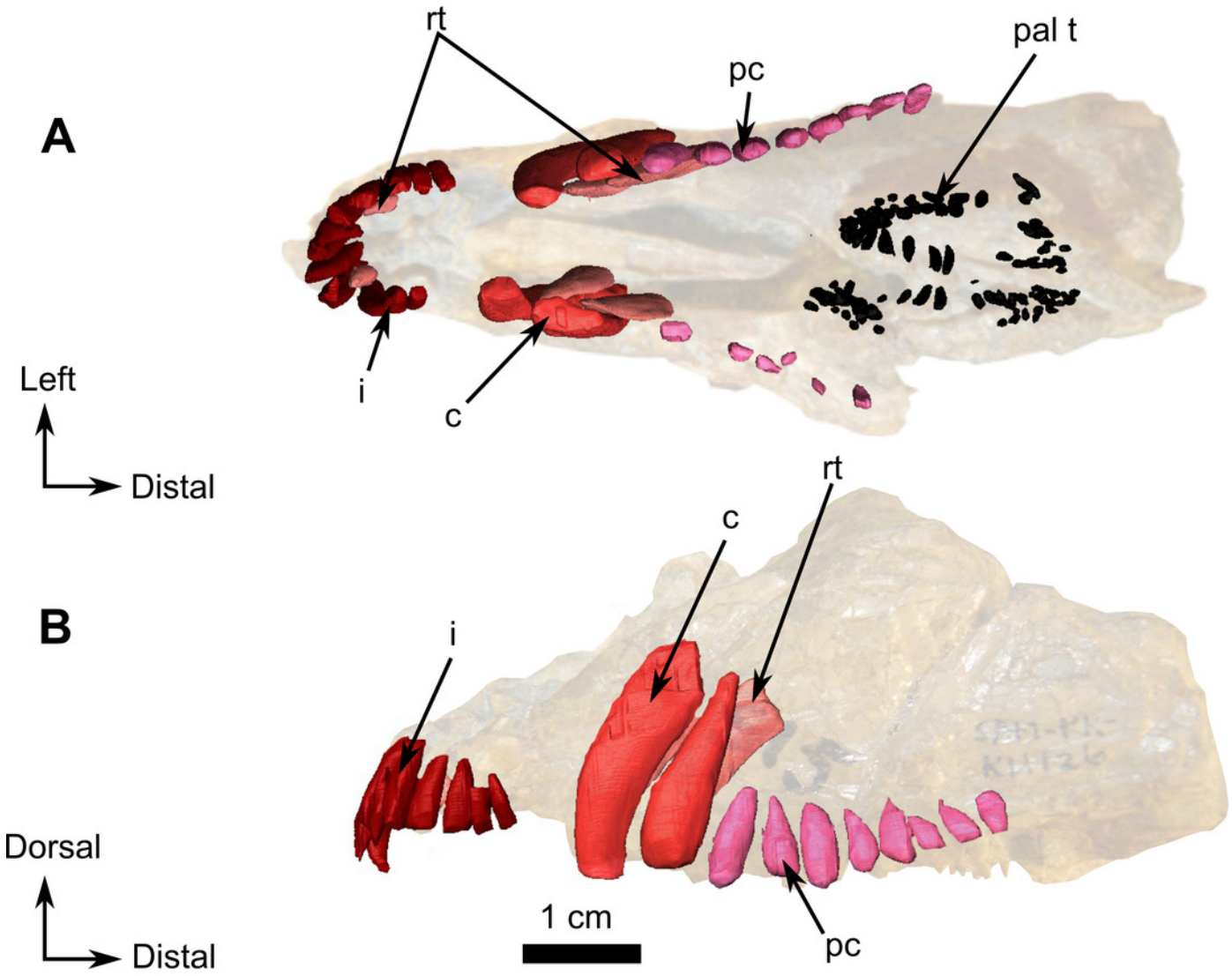
A
rt
pc
pal t
i
c
Left
Distal
B
rt
c
i
Dorsal
Distal
1 cm
pc

Figure 15

Holotype of *Lemurosaurus pricei*, skull, BP/1/816.

(**A**) CT image at the level of the supraorbital bosses and the braincase (**B**). Histology of supraorbital bosses, comprising thick and dense bone, and a well-ossified braincase, indicates that the specimen is an adult. (**B**) photograph of the right lateral view. Bright artefacts are caused by iron nodules. Pictures by A. Duhamel. Scan of the specimen was performed by Kudakwashe Jakata and belongs to the University of the Witwatersrand. Scale bar=1cm.

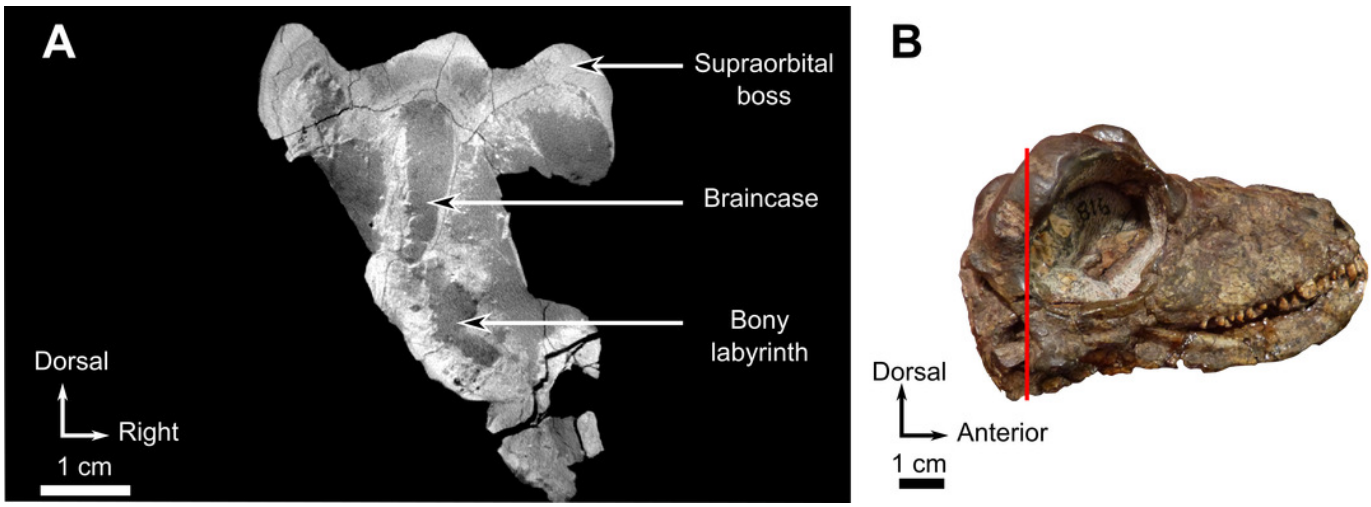

Figure 16

Anatomical comparison of BP/1/816 and NMQR 1702.

(**A**) holotype of *Lemurosaurus pricei*, skull, BP/1/816, from Dorsfontein farm, Graaff-Reinet District, Eastern Cape Province, South Africa; *Cistecephalus* AZ, Beaufort Group, Karoo Supergoup. **Left**: right lateral view; **right**: dorsal view. (**B**) NMQR 1702, from Petersburg farm, Graaff-Reinet District, Eastern Cape Province, South Africa; *Cistecephalus* AZ, Beaufort Group, Karoo Supergroup, South Africa. **Left**: right lateral view; **right**: dorsal view. Pictures by A. Duhamel. Scale bar=1cm.

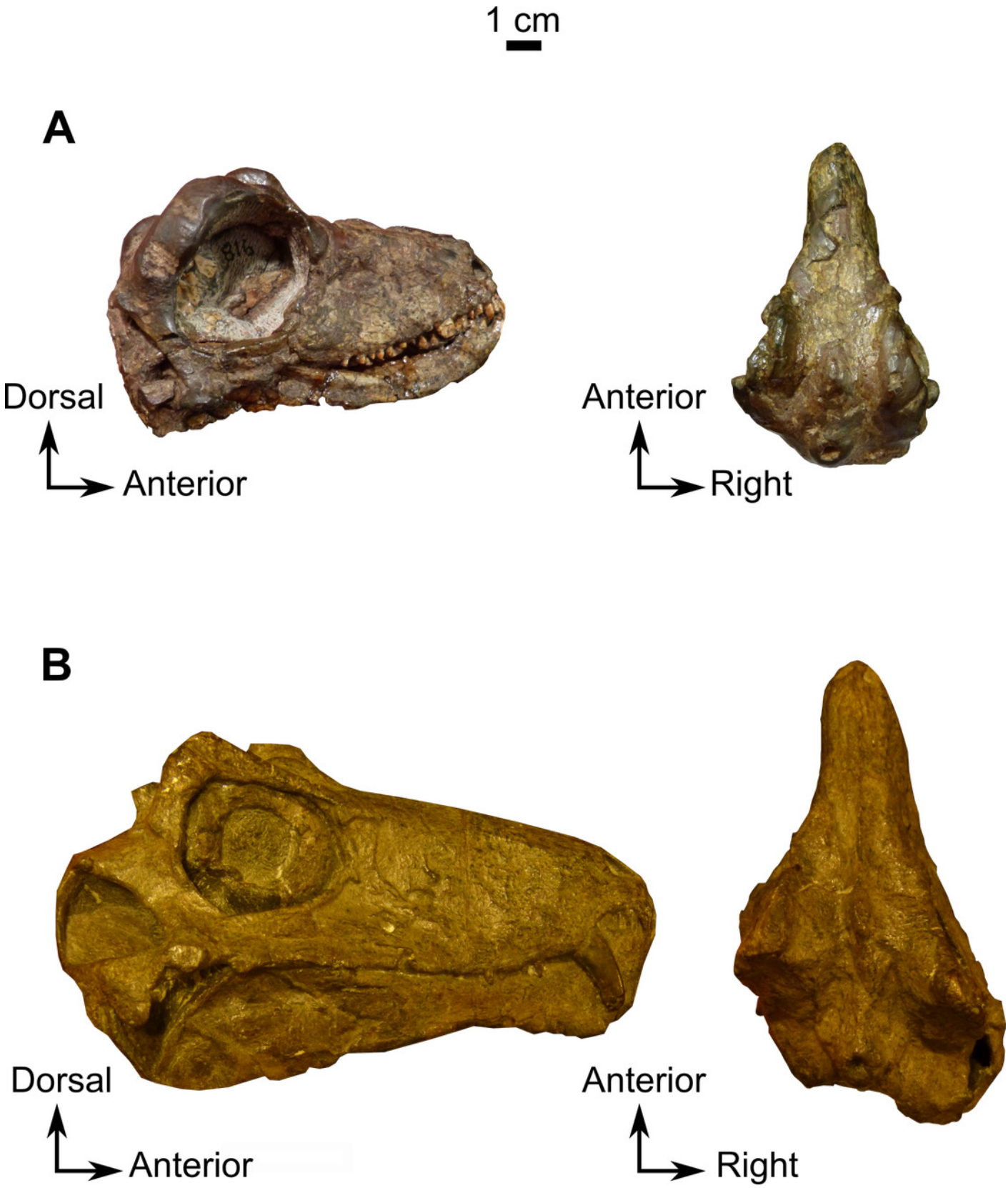
1 cm
A
Dorsal
Anterior
Anterior
Right
B
Dorsal
Anterior
Anterior
Right

Figure 17

Lende Chiweta, skull, MAL 290.

CT-images (**Left**) and lateral view (**Right**); (**A**) at the level of the supraorbital bosses, (**B**) braincase and (**C**) foramen magnum. Bright points are artefacts resulting from the presence of iron nodules. Pictures by A. Duhamel. Scan of the specimen was performed by Kudakwashe Jakata and belongs to the University of the Witwatersrand. Scale bar = 1cm.

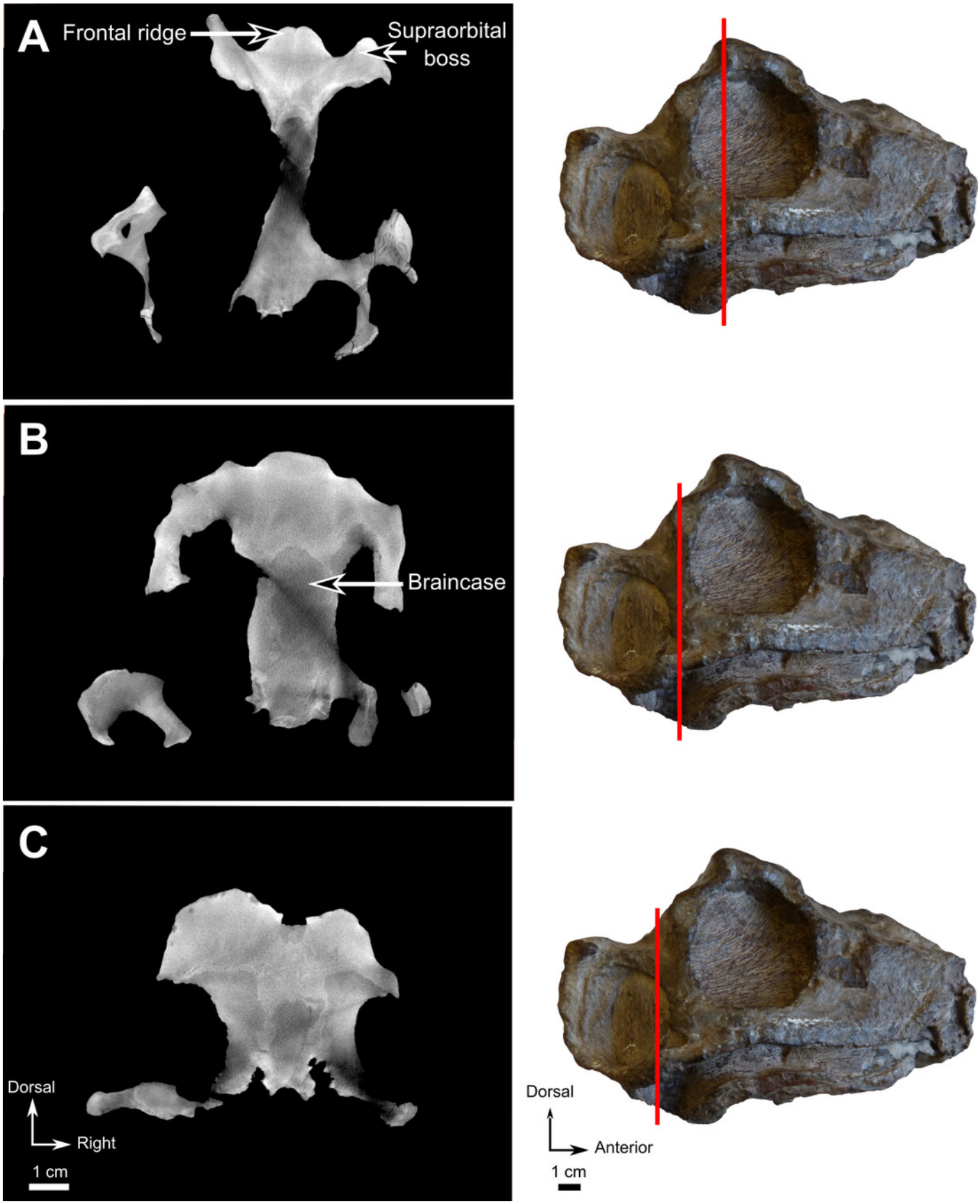
A
Frontal ridge
Supraorbital boss
B
Braincase
C
Dorsal
Right
1 cm
Dorsal
Anterior
1 cm

Figure 18

Lemurosaurus pricei, NMQR 1702.

CT image at the level of the supraorbital bosses and the braincase. Despite the quality of the scan, the thick supraorbital bosses, the well-ossified braincase, and absence of vasculature patterns in the supraorbital bosses, indicate that the specimen is an adult. Bright artefacts are caused by iron nodules. Scan of the specimen was performed by Vincent Fernandez and belong to the European Synchrotron Radiation Facility. Scale bar=1cm.

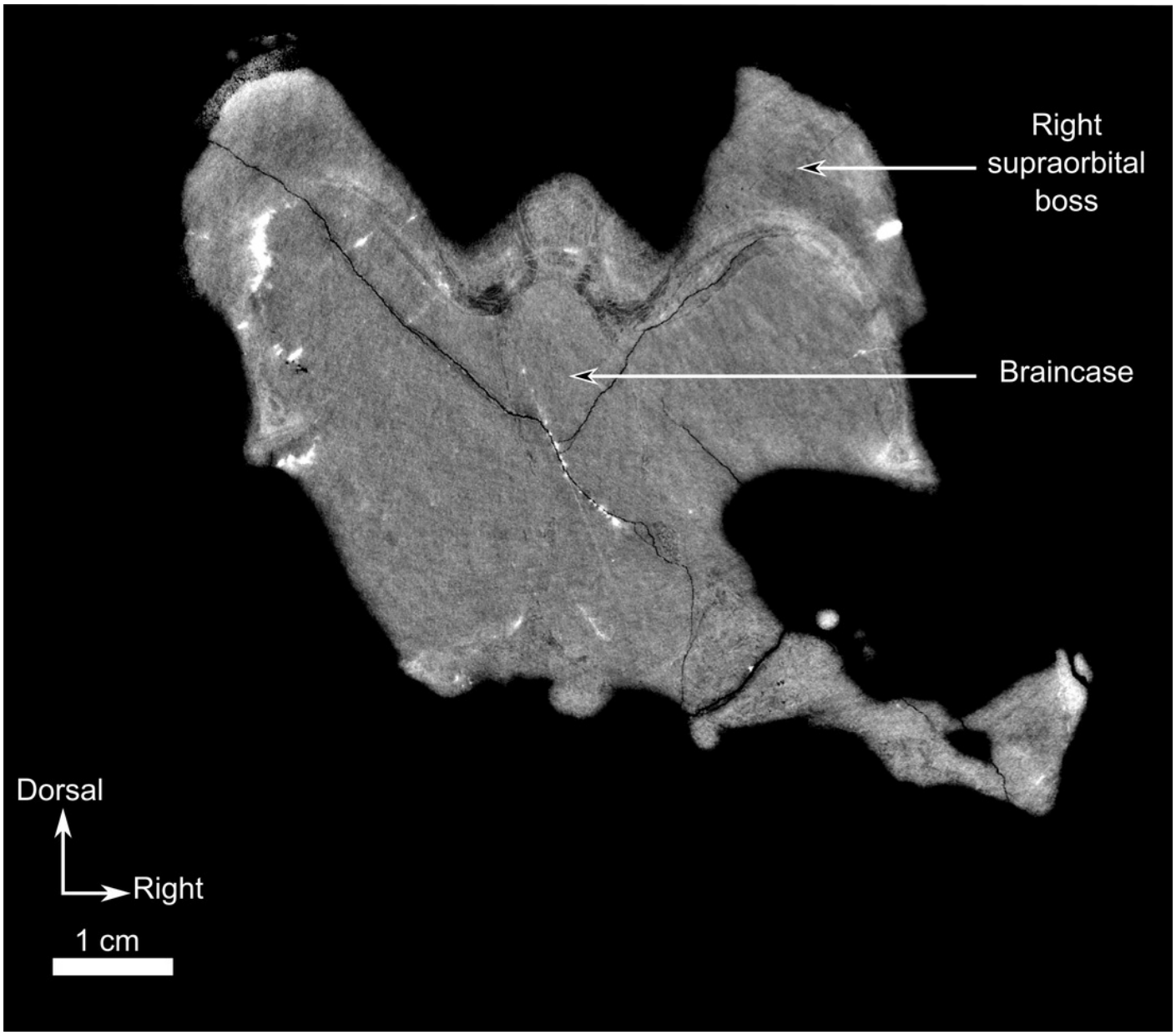
Right
supraorbital
boss
Braincase
Dorsal
Right
1 cm

Figure 19

Burnetiamorpha indet., skull, CGP MJF 22.

(**A**) CT image at the level of the braincase (**B**). Bony labyrinth is fused to the braincase (which itself is not ossified) which suggests incomplete ossification and juvenility. **(B**) Photograph of the specimen in right lateral view. Bright artefacts are caused by iron nodules. Pictures by A. Duhamel. Scan of the specimen was performed by Kudakwashe Jakata and belongs to the University of the Witwatersrand. Scale bar=1cm.

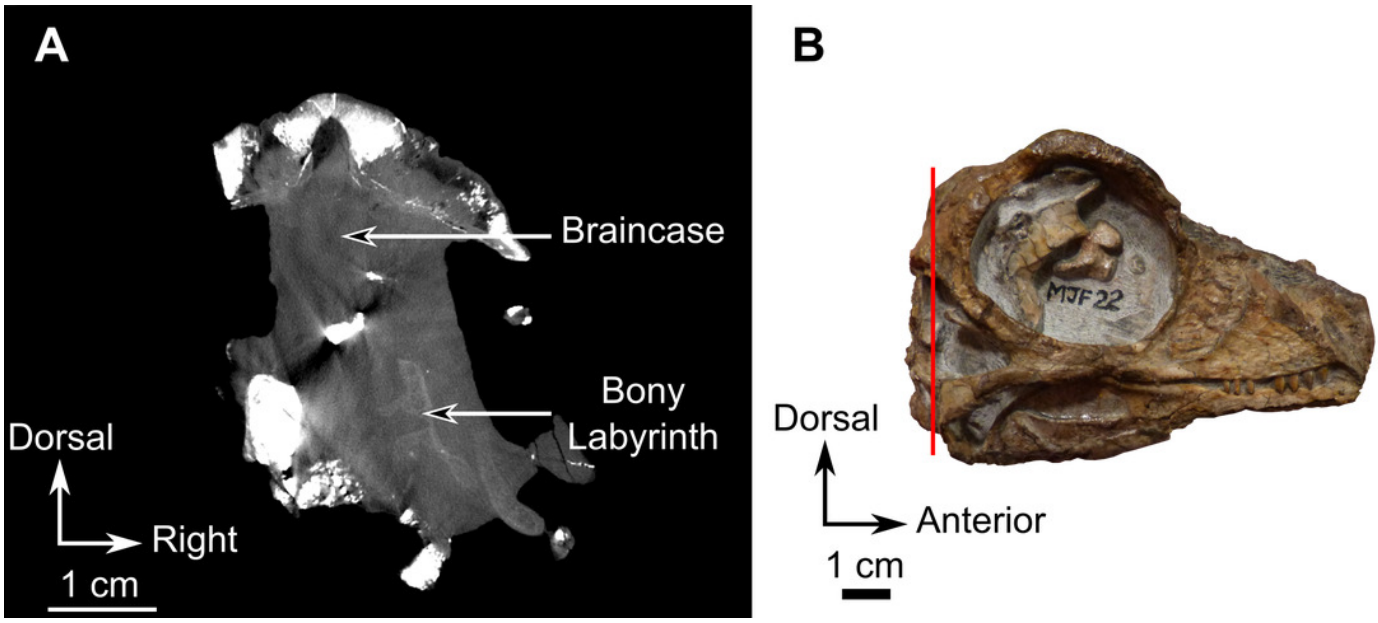

Figure 20

Burnetiamorpha indet., skull, CGP MJF 22.

(**A**) CT-image of a transverse section showing three symmetrical sutures, indicated by arrows, within the parietal. (**B**) Segmentation of the posterior part of the skull roof reveals the presence of extra-sutures in the prepariétal and the parietal. The black circle represents the pineal foramen. Bright points are artefacts resulting from the presence of iron nodules. Scan of the specimen was performed by Kudakwashe Jakata and belongs to the University of the Witwatersrand. 3D reconstruction was made by A. Duhamel and belongs to the University of the Witwatersrand. Scale bar=1cm.

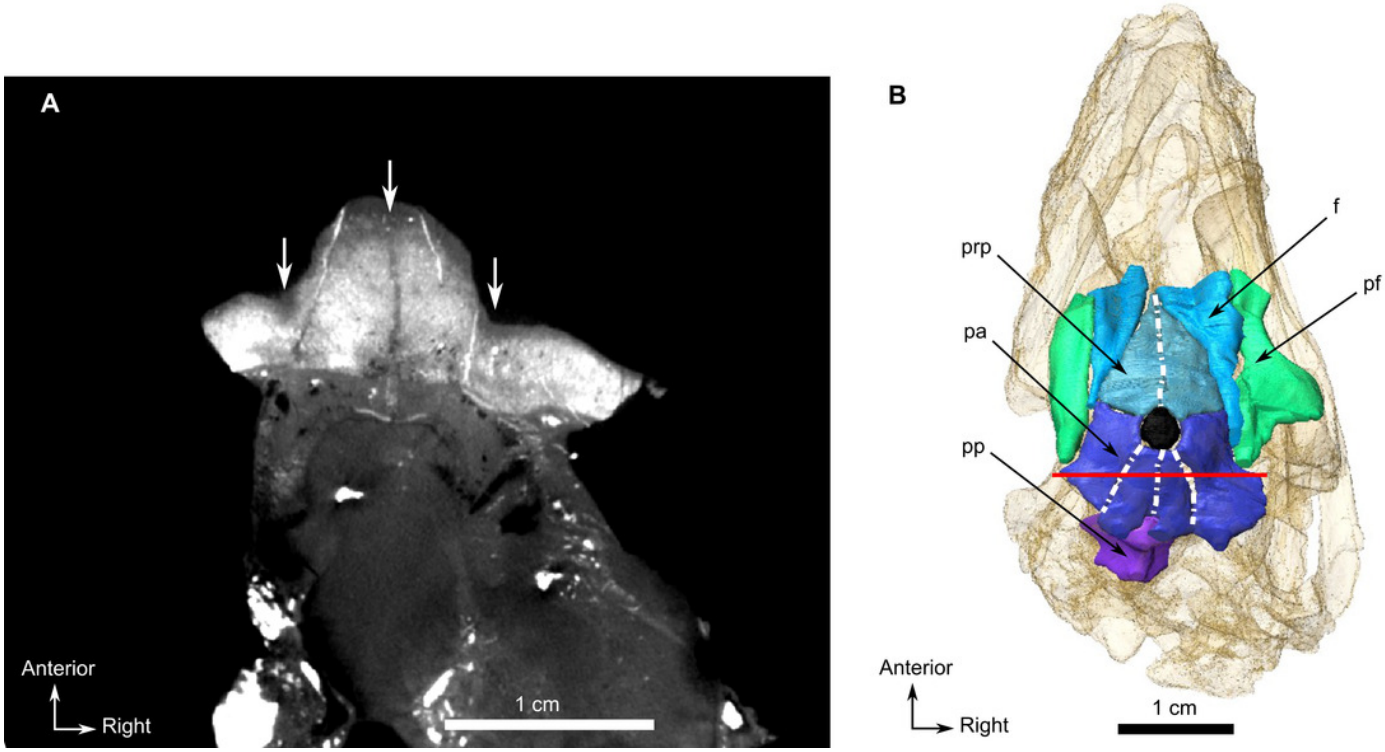

Figure 21

Burnetiamorph indet., dorsal piece, SAM-PK-K11126.

(**A**) CT-image of a transverse section showing three symmetrical sutures, indicated by arrows, within the parietal, at the level of the posterior border of the pineal foramen (**B**). (**B**) 3D rendering of the dorsal piece in dorsal view reveals the presence of extra-sutures in the parietal. Bright points are artefacts resulting from the presence of iron nodules. Scan of the specimen was performed by Kudakwashe Jakata and belongs to the University of the Witwatersrand. 3D reconstruction was made by A. Duhamel and belongs to the University of the Witwatersrand. Scale bar = 1cm.

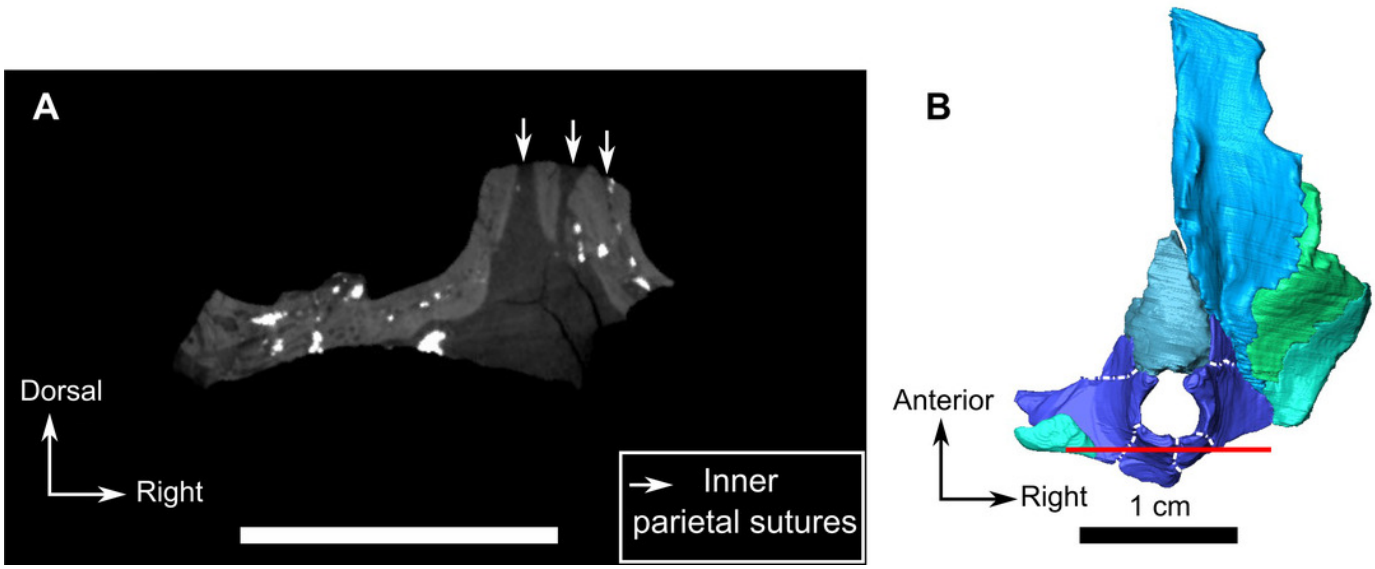

Figure 22

A hypothetical biarmosuchian ontogenetic series.
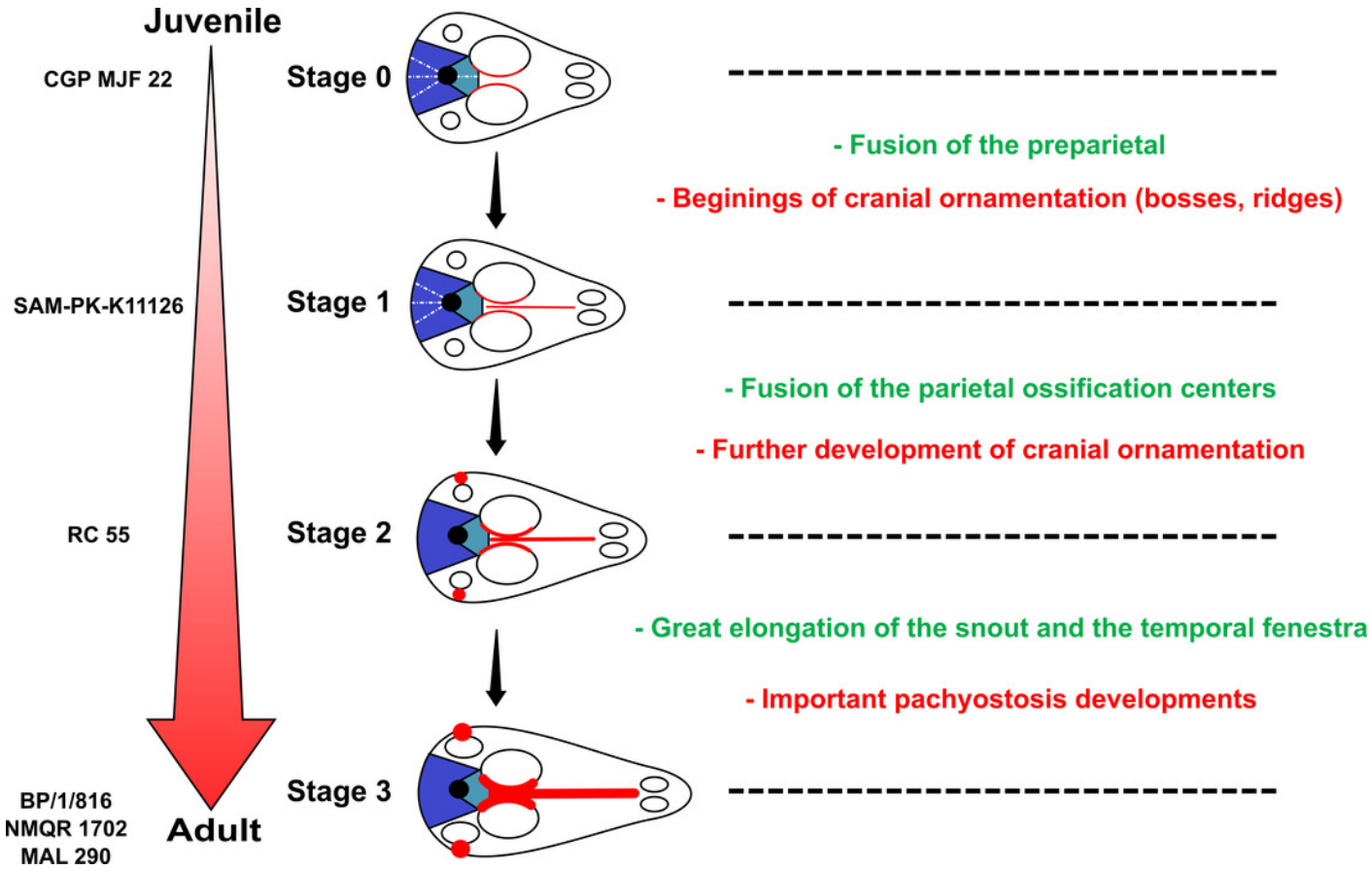
. Characters present in only Burnetiamorpha are written and drawn in red. Characters present in all biarmosuchian taxa are written in green. Figure by A. Duhamel.